UNIVERSITY OF CALIFORNIA,
IRVINE

Molecular Regulation of Cutaneous Skin Barrier and Inflammation and Relation to Whole Body Physiology

DISSERTATION

submitted in partial satisfaction of the requirements
for the degree of

DOCTOR OF PHILOSOPHY

in Biomedical Sciences

by

Morgan Ashley Dragan

Dissertation Committee:
Professor Xing Dai, Chair
Professor Bogi Andersen
Professor Selma Masri
Professor Armando Villalta
Professor Max Plikus

2022

DEDICATION

To

All work is dedicated to my family for always supporting me and my wild ideas. I would also like to make a special dedication in loving memory of my grandma "Popo" Alice Tang whose happy-go-lucky attitude despite hardships always inspired me.

A life is not important except in the impact it has on other lives.

Jackie Robinson

TABLE OF CONTENTS

LIST OF FIGURES

ABBREVIATIONS

IFE	Interfollicular epidermis
EMT	Epithelial to mesenchymal transition
EMP	Epithelial to mesenchymal plasticity
EpdSCs	Epidermal stem cells
K14	Keratin 14
K5	Keratin 5
K10	Keratin 10
K1	Keratin 1
ECM	Extracellular matrix
ER	Early response
GA	Growth Arrested
dWAT	Dermal white adipose tissue
iWAT	Inguinal white adipose tissue
LC	Langerhans cells
iDKO	Inducible *Ovol1/Ovol2* double knock-out
SSKO	*Ovol1* Skin-specific knock-out
TEWL	Trans-epidermal water loss
DETCs	Dermal γδT cells
AD	Atopic dermatitis

ACKNOWLEDGEMENTS

UC Irvine offered me the opportunity to work with many talented colleagues both within my lab and inter-departmentally. First, I would like to express the deepest appreciation to my committee chair, Xing Dai. She is a brilliant scientist who offered me excellent intellectual training that will allow me to be successful in my future endeavors. I would like to thank my Dai lab family both past and present, but especially Daniel, Remy, Jerry, Peng, Lupe, and Johnny for their training and assistance. Over the years all of your support and discussion inspired so many interesting scientific discoveries and made the lab a fun work environment.

I am very thankful to my collaborators and classmates over the years, namely, Jenna, Ghaidaa, Bridget, Michaela, Serena, David, Sharon, Sloan, Nam, Kevin, Suhas, Linzi and Kevin. I learned so much from all of you and appreciate your friendship and support.
I would also like to thank my thesis committee members Bogi, Armando, Selma, and Max for their suggestions, training, assistance and encouragement throughout my PhD. I am also very appreciative to Dr. Qing Nie and the NSF-Simons Center for Multiscale Cell Fate Research, as well as Dr. Eric Pearlman and the Institute for Immunology training grant for predoctoral fellowship support. I would also like to extend a special thank you to the Achievement Rewards for College Scientists (ARCSs) for the ARCS scholar award for believing in me and supporting my PhD endeavors. Finally, I would like to thank Dr. Dicki Hertel and Leora for selecting me to be a member of SOM grad council and offering me so much advice and assistance throughout the years.

I thank Elsevier for permission to include a copyrighted figure as part of Chapter 1 (Dai, X., and Segre, J.A. (2004). Transcriptional control of epidermal specification and

differentiation. Curr. Opin. Genet. Dev. *14*, 485.). Chapter 3 of this dissertation is a reprint of the material as it appears in *Epidermis-Intrinsic Transcription Factor Ovol1 Coordinately Regulates Barrier Maintenance and Neutrophil Accumulation in Psoriasis-Like Inflammation* (2022) Journal of investigative dermatology, 2022, Vol.142 (3, Part A), p.583-593.e5, used with permission from Elsevier. The coauthors listed in this publication are Peng Sun, Zeyu Chen, Xianghui Ma, Remy Vu, Yuling Shi, S. Armando Villalta, and Xing Dai. Financial support was provided by the University of California, Irvine, National Institutes of Health (NIH) grants R01-AR068074 and R01-GM123731, UCI National Science Foundation (NSF)-Simons Center for Multiscale Cell Fate Research through NSF grant DMS1562176 and Simons Foundation grant 594598, by the NIH T32 Immunology Research Training Grant (AI 060573).

VITA

Morgan Ashley Dragan

Education:

2022	Ph.D. in Biomedical Sciences, University of California, Irvine
2016	B.S. in Molecular Biology, University of California, San Diego

Professional Experience

2017-22	Graduate Student Researcher Xing Dai Laboratory, University of California, Irvine
2016-2017	Research Associate I Alan Saltiel Laboratory, University of California, San Diego
2015-16	Intern Ambrx Inc., San Diego, CA
2014-16	Research Assistant Richard Klemke Laboratory, University of California, San Diego

Fellowships and Honors:

2019-22	NSF Simons Graduate Fellowship NSF-Simons Center for Multiscale Cell Fate Research
2019-22	T32 Immunology Training Grant Trainee, UC Irvine; Institute of Immunology
2019-21	ARCS Foundation, Orange County Chapter, Scholar Award

Publications:

Dragan, M., Chen, Z.H., Li, Y., Lee, J., Sun, P., Verlande, A., Haensel, D., Pham, A., Vu, R., Gutierrez, G., Li, W., Jang, C., Masri, S., and Dai, X. Ovol loss-induced epidermal barrier dysregulation causes skin inflammation and metabolic adaptation. Manuscript submitted.

Dragan, M.*, Vu, R.*, Sun, P., Werner, S., and Dai, X. Epithelial-mesenchymal plasticity and endothelial-mesenchymal transition in cutaneous wound healing. In press, *Cold Spring Harbor Perspectives in Biology* (2022).

Ratitong, B., Marshall, M. E., **Dragan, M.,** Anunciado, C. M., Abbondante, S. & Pearlman, E. Differential Roles for IL-1a and IL-1b in Pseudomonas aeruginosa infection of the cornea. Manuscript in review, *J. Immunol.* (2022).

Vu, R., Jin, S., Sun, P., Haensel, D., Nguyen, Q.H., **Dragan, M.**, Kessenbrock, K., Nie, Q., and Dai, X. Wound healing in aged skin exhibits systems-level alterations in cellular composition and cell-cell communication. Manuscript in review, *Cell Reports* (2022).

Dragan, M.*, Sun, P.*, Chen, Z., Ma, X., Vu, R., Shi, Y., Villalta, S. A., & Dai, X. (2022). Epidermis-Intrinsic Transcription Factor Ovol1 Coordinately Regulates Barrier Maintenance and Neutrophil Accumulation in Psoriasis-Like Inflammation. ***J. Invest. Dermatol*ogy**, 142(3 Pt A), 583–593.e5.

Sun, P., Vu, R., **Dragan, M.,** Haensel, D., Gutierrez, G., Nguyen, Q., Greenberg, E., Chen, Z., Wu, J., Atwood, S., Pearlman, E., Shi, Y., Han, W., Kessenbrock, K., and Dai, X. (2021). OVOL1 Regulates Psoriasis-Like Skin Inflammation and Epidermal Hyperplasia. *J. Invest. Dermatol*ogy, S0022-202X(20)32392-7.

Greenberg, E. N., Marshall, M. E., Jin, S., Venkatesh, S., **Dragan, M.**, Tsoi, LC, Gudjonsson, JE., Nie, Q., Takahashi, JS., and Andersen, B. (2020). Circadian control of interferon-sensitive gene expression in murine skin. *PNAS*, 117(11), 5761–5771.

Haensel, D., Jin, S., Sun, P., Cinco, R., **Dragan, M.**, Nguyen, Q., Cang, Z., Gong, Y., Vu, R., MacLean AL., Kessenbrock, K., Gratton, E., Nie, Q., and Dai, X. (2020). Defining Epidermal Basal Cell States during Skin Homeostasis and Wound Healing Using Single-Cell Transcriptomics. *Cell Reports*, 30(11), 3932-3947.e6.

Skorobogatko, Y., **Dragan, M**., Cordon, C., Reilly, S., Hung, C., Xia, W., Zhao, P., Wallace, M., Lackey, D., Chen, X., Osborn, O., Bogner-Strauss, J., Theodorescu, D., Metallo, C., Olefsky, J. and Saltiel, A. (2018). RalA controls glucose homeostasis by regulating glucose uptake in brown fat. *PNAS*, 115(30), pp.7819-7824.

Presentations:
-2020-2022 CMCF Early Career Research Symposium. Oral presentation.
-2020 Society of Investigative Dermatology Meeting. Oral and Poster presentation. Published abstract.
-2019-21 CMCF Annual Symposium on Multiscale Cell Fate. Poster presentation.
-2018-21 UCI School of Medicine Grad Day & CMB recruitment. Poster Presentations & elevator pitches.
-2019-2020 UCI Immunology Fair. Oral and Poster presentation.
-2019 Society of Investigative Dermatology Meeting, Chicago. Poster Presentation. Published abstract.
-2019 La Jolla Immunology Conference. Poster presentation.
-2018-19 UCI Skin symposium. Poster Presentation.
-2018 UCI Immunology Fair. Poster Presentation.

Activities:
2019-2022 UCI School of Medicine Graduate Student Advisory Council
2018-2019 UCI Biological Chemistry Graduate Student Representative

ABSTRACT OF THE DISSERTATION

Molecular Regulation of Cutaneous Skin Barrier and Inflammation and Relation to Total Body Physiology

by

Morgan Ashley Dragan

Doctor of Philosophy in Biomedical Sciences

University of California, Irvine, 2022

Professor Xing Dai, Chair

The skin barrier has plethora of important functions including protection from and triggering the inflammatory response to mechanical, thermal and physical injury and provides insulation against moisture loss. Skin barrier is formed by the continuous proliferation and maturation of keratinocytes. The focus of this dissertation is to understand epithelial barrier regulation and immune crosstalk, and how dysfunctional barrier can cause systemic physiological response.

Chapter 3 expands upon a previous study and aims to understand the triggers and dynamics of neutrophil recruitment into skin during TLR7-induced skin inflammation. Previous work showed a protective role of Ovol1 in mediating the epidermal keratinocyte differentiation response and inflammatory response to psoriatic-like inflammation. However, the molecular mechanism by which Ovol1 mediates these responses, including the infiltration and migration of neutrophils was unknown. During development Ovol1 facilitates differentiation of keratinocytes through promoting growth arrest of progenitor cells; however, the skin-specific function of Ovol1, especially in adulthood and during

inflammation was unknown. This work showed a critical function of Ovol1 in regulating barrier and unraveled a novel function for Ovol1 in both directly and indirectly mediating inflammation. Using genetic mouse models and immunological assays, we show that loss of Ovol1 resulted in exacerbated barrier defects following imiquimod (IMQ) treatment of the back skin, followed by elevated neutrophil recruitment to the skin. We find that Ovol1 balances the extent of inflammation by repressing neutrophil recruitment through mitigating barrier-induced *Il1a* release, repression of *Cxcl1* transcription. Interestingly, we also found Ovol1 promotes epidermal hyperplasia by repressing of *Il33* suggesting Ovol1 is important for balancing epidermal maintenance with inflammation.

Chapter 4 utilizes multidisciplinary biological assays and high throughput sequencing technologies to understand Ovol1 and Ovol2 function in barrier maintenance during adult homeostasis and how barrier defects can affect total body physiology. The current work expands a previous study showing that Ovol1 and Ovol2 are important for the development of barrier during embryogenesis through modulating epithelial differentiation and adhesion. In the current work I take a wholistic and unbiased approach to focus on the biological and molecular function of Ovol1 and Ovol2 in adult homeostasis and established an epithelial-specific genetic knock out mouse model (*K14-CreER;Ovol1*$^{f/-}$*;Ovol2*$^{f/-}$) as a system to explore epidermal cross-talks and the contribution of barrier to physiological homeostasis. I show that inducible deletion of *Ovol1* and *Ovol2* in adulthood leads to spontaneous barrier defects, followed by activation of epidermal Langerhans cells, aberrant T cell response, reduced body weight, and altered metabolism. I find that Ovol1 and Ovol2 are important for regulating many genes associated with cytoskeletal structure and adhesion and loss of both results in increased epithelial to mesenchymal plasticity and

aged molecular signature in epidermis. Moreover, I show that that *Ovol1* and *Ovol2* knock out mice have increased immune cells, namely T cells in the skin-draining lymph nodes followed by increased energy expenditure and restricted fat accumulation over time. Importantly, inhibition of inflammation through continuous dexamethasone treatments partially rescues epidermal Langerhans cell activation and body weight phenotype suggesting that inflammation is partially instigating changes to whole body metabolism. This study suggests the importance of barrier in maintaining total body homeostasis through suppressing aberrant immune activation.

Overall, this thesis work combines multidisciplinary methods to broadly understand epidermal-immune cross talks and the role barrier plays in inflammation and in protecting total-body physiology, but also focuses on direct transcriptional regulation of gens involved in barrier that can trigger systemic responses.

CHAPTER 1: Introduction

Incorporates components from review article (in press) with Cold Spring Harbor (2022):

Article #1:

Epithelial-mesenchymal plasticity and endothelial-mesenchymal transition in cutaneous wound healing

Remy Vu*, Morgan Dragan*, Peng Sun, Sabine Werner, and Xing Dai
('*' denotes co-first authors)

Skin

Overview

Skin is the largest organ of the human body composing 15% of the total body weight. It is a complex and heterogeneous organ that plays many critical roles including regulation of body temperature and moisture and protection (Kolarsick et al., 2011; Natsuga, 2014). It provides a blockade against invading pathogens and physical and chemical damage (Natsuga, 2014).

The skin is a multi-layered, complex tissue containing appendages (e.g. hair follicles and sebaceous glands) and is comprised of the epidermis, dermis, dermal fats, muscle, and subcutaneous fat (Kolarsick et al., 2011). The outermost layer, the epidermis is an epithelial tissue primarily composed of keratinocytes with few resident immune cells (~10%) (Kabashima et al., 2018). Epidermal appendages like hair follicles, also composed of keratinocytes, extend into the underlying dermis (Gonzales and Fuchs, 2017). The dermis is a fibroblast-rich tissue that contains resident immune cells (e.g. T cells and macrophages) and is vascularized and enervated (Hsu and Fuchs, 2022; Kabashima et al., 2018). Fibroblasts in dermis are bound to one another via a dense network of collagen and elastin fibers (Kolarsick et al., 2011). Upon damage or wounding, the dermis is one of the main sites of immune cell infiltration into the skin through the extending vasculature network (Kabashima et al., 2018). The epidermis is bound to the dermis via the extracellular matrix (ECM)-rich basement membrane (Hsu and Fuchs, 2022). The adipocyte-rich dermal white adipose tissue (dWAT) layer is composed of adipocytes—or lipid storage cells, that provide and receive signals to promote epidermal maintenance, supply nutrients, and contributes to the regulation of hair follicle cycling and skin wound healing (Guerrero-Juarez and Plikus,

2018; Hsu and Fuchs, 2022). Lastly, skin contains a muscular layer followed by subcutaneous fats which provide insulation, thermoregulation, nutrients and structural support to the skin (Kolarsick et al., 2011). The subcutaneous fat can also contains immune cells and supply a variety of mediators (e.g., growth factors, adipokines, and cytokines) during wound healing and inflammation (Nguyen and Soulika, 2019). Collectively, the skin provides the first line of defense against the environment and each layer of the skin collaborates to maintain and return to skin homeostasis.

Mouse epidermis

Cutaneous epidermis is the outermost layer of the skin and provides a barrier against the external environment. The adult interfollicular epidermis (IFE) is a stratified squamous epithelium primarily composed of keratinocytes and contains multiple appendages, including hair follicles (HF) and sebaceous glands (SG). The epidermis is exposed to the harsh environment so it must constantly turnover (~one week in mice) to maintain the barrier and to respond to physical stress and wounding (Gonzales and Fuchs, 2017). Epidermal turnover is facilitated by the upward progression of differentiating keratinocytes towards the surface of the skin that can be visualized as the basal, spinous, granular, and stratum corneum layers (Wikramanayake et al., 2014) (Figure 1.1). In homeostasis IFE is maintained by distinct local stem cell lineages (Gonzales and Fuchs, 2017; Mascré et al., 2012). Epidermal stem cells (EpdSCs) that reside in the basal layer are capable of self-renewing to retain the pool of EpdSCs, and proliferating to give rise to the differentiated cell types (Gonzales and Fuchs, 2017). As keratinocytes differentiate, the morphology and biological composition of the cells changes which makes it easy to

differentiate the layers (Gonzales and Fuchs, 2017). Keratins are a group of intermediate filaments that provide structure to epithelial cells and are one of many types of proteins that can be used to mark differentiation in keratinocytes (Natsuga, 2014). The basal layer produces primarily keratin 14 (K14) and 5 (K5), followed by keratin 10 (K10) and 1 (K1) in the spinous layer, pro-filaggrin (Fil), loricrin (Lor) and keratohyalin granules in the granular layer, and finally loricrin (Lor) and involucrin (Inv) in the stratum corneum (Figure 1.1) (Wikramanayake et al., 2014).

Studies using techniques including lineage tracing, genetic labeling and transplantation were done to map the trajectory of these basal keratinocytes into differentiated cells (Hsu et al., 2014). These studies show that there are some cells that have more stem-like potential (i.e., live longer and slow dividing) (Mascré et al., 2012). However, until the advent of single cell high throughput sequencing technologies, understanding these changes on a cellular level was difficult and convoluted. Recently a study from our lab utilizing single cell RNA-sequencing (scRNA-seq), shows that four distinct basal cell states exist in homeostasis: *Col17a1*^{High}, early response (ER), growth arrested (GA), and proliferative states (Haensel et al., 2020). Using RNA velocity analysis, we find that *Col17a1*^{High} cells are the more stem-like population and that these basal cells progress through ER to either proliferative or GA states before the GA cells can differentiate into spinous cells (Haensel et al., 2020; Liu et al., 2019). This study provided interesting conceptual advances on the heterogeneity of adult epidermis and revealed a previously undefined molecular signature within cells that can designate their current activity level and state.

While the general structural framework of skin across the body is the same, epidermis adopts different characteristics based on the function of that region. For example, murine dorsal skin has dense numbers of HF to provide insulation and protection whereas mouse paw has no hair follicles, but contains a highly keratinized nail for protection and fine motor function, and a thicker stratum corneum to protect from abrasion (Ji et al., 2021; Saito et al., 2015). Studies have examined epidermal maintenance in various anatomical locations (e.g., tail, dorsal skin, or paw) and found them to have distinct proliferative dynamics or cellular trajectories (Gonzales and Fuchs, 2017). For example, the proximity to a HF can influence proliferation dynamics resulting in varied results between different skin anatomical locations (e.g. dorsal vs paw skin) (Gonzales and Fuchs, 2017). Moreover, nail epidermal stem cells present in the nail matrix, proliferate and differentiate superficially into the nail plate and distally into the nail bed as compared with the upward momentum of dorsal IFE (Lehoczky and Tabin, 2015; Leung et al., 2014; Nakamura and Ishikawa, 2008; Pulawska-Czub et al., 2021). Influencers of epidermal proliferation dynamics are also not limited to keratinocyte-intrinsic factors, as immune cells and associated factors also induce proliferation and differentiation of epidermal cells (Xiao et al., 2020) (see below)

Barrier

Maintaining a functional skin barrier is one of the most critical tasks of the epidermis. After proliferation, basal keratinocytes detach (delaminate) from the basement membrane and those daughter cells undergo many morphological and biochemical changes to transform into dead squames bound tightly to resist infection and hydrophobic to retain

moisture (Gonzales and Fuchs, 2017). As spinous cells transition to granular cells, profilaggrin—whose mature form (filaggrin or Flg) interacts with keratin filaments—accumulates in the cytoplasm to form keratohyalin granules (Freeman and Sonthalia, 2022). Keratohyalin granules help facilitate dehydration of the cell (Freeman and Sonthalia, 2022). Of note, Flg and its metabolites are critical for normal cornification which involves Flg to be broken down into free amnio acids that are converted into products such as urocanic acid and pyrrolidine carboxylic acid leaving these products as a readout for barrier defects (Egawa et al., 2016; Fluhr et al., 2010). Moreover, urocanic acid itself is important for normal acidification of the skin and pyrrolidine carboxylic acid is a major constituent of natural moisturizing factors leaving both metabolites essential for barrier function (Egawa et al., 2016; Fluhr et al., 2010). During terminal differentiation, keratinocytes de-nucleate and crosslink into corneocytes (Wikramanayake et al., 2014). Concomitantly, fatty acids, ceramides, and cholesterol esters that were accumulating in lamellar bodies within those keratinocytes exude into the intercellular space thus tightly adhering these corneocytes together creating a "brick and mortar" structure (Coderch et al., 2003; Feingold, 2007; Wikramanayake et al., 2014). This process also renders them water-resistant.

Defects in lipid metabolism and transport lead to severe barrier dysfunction in mammals. Transport of free fatty acids across cell membranes is facilitated by fatty acid transport proteins and defects in some of these proteins are associated with ichthyosis in humans (Natsuga, 2014). Fatty acid transport protein 4 (Fatp4) and ATP-binding cassette A12 (Abca12) facilitate the extension of very-long-chain fatty acids (VLFA) in epidermal ceramides and mediates lipid transport into extracellular spaces from lamellar bodies,

respectively, and germline deletion of these transporters leads to premature lethality due to defective barrier in mice (Natsuga, 2014). Ceramides are a complex group of sphingolipids and fatty acids are a major component of lamellar sheets which reside in the intercellular spaces of the stratum corneum (Coderch et al., 2003). Deficiencies in ceramides are associated with a plethora of skin diseases including psoriasis, atopic dermatitis (AD), some forms of ichthyosis, severe xerosis and acne (Coderch et al., 2003). Defects to the processing of ceramides, including hydrolysis, acylation, and fatty acid elongation all have been extensively studied and shown to lead to barrier defects in mice and have known mutations in human skin diseases. Of note, mutations in the fatty acid elongase (Elovl1-7) family, namely *Elovl1* and *4* lead to the loss of VLFA in both ceramides and free fatty acids, thus causing detrimental effects to the hydrophobic lipid bilayer between corneocytes (Natsuga, 2014). Beyond the functions of lipids within epidermal keratinocytes in the formation of barrier, lipid species are also important for protecting barrier through moisturizing and hydrating the epidermis. The sebaceous glands residing next to hair follicles secretes a mixture of triglycerides, wax esters and squalene, termed sebum, which covers the surface of the skin (Pappas, 2009). Stearoyl-CoA desaturase (*Scd1*) knock out mice show hair loss and hypoplastic to absent sebaceous glands that result in lower levels of triglycerides, wax esters in addition to the expected deficiency of monosaturated fatty acids in the skin (Pappas, 2009; Sampath et al., 2009).

The formation and maintenance of cellular architecture and cell adhesion in the epidermis is pertinent to establishing a water-tight epidermal barrier (Fuchs and Raghavan, 2002; Johnson et al., 2014). Basal keratinocytes in intact skin adhere to the underlying basement membrane and interact with the dermal ECM through integrins that

are organized in large adhesion complexes called hemidesmosomes (Fuchs et al., 1997; Margadant et al., 2010; Watt, 2002). Hemidesmosomes connect to the intermediate filaments, and focal adhesions, which connect to the actin cytoskeleton (Fuchs et al., 1997; Margadant et al., 2010; Watt, 2002). Keratinocytes tightly adhere to one another via desmosomes that are linked to the keratin intermediate filament cytoskeleton and via adherens junctions that are linked to the actin cytoskeleton (Fuchs and Raghavan, 2002). Adhering cells in the epidermal granular compartment also form tight junctions that seal intercellular space and form a functional barrier to regulate the diffusion of ions and solutes between cells (Rübsam et al., 2018; Yokouchi and Kubo, 2018). Alterations to desmosomes (losing hyper-adhesiveness and gaining calcium dependence) and reduction in adherens junctions between cells lead to the formation of intracellular gaps, and dampening adhesion between neighboring cells is detrimental to barrier function and wound re-epithelialization (Beaudry et al., 2010; Garrod et al., 2005; Nunan et al., 2015; Simpson et al., 2011; Thomason et al., 2012; Wang et al., 2018). Highlighting the importance of junction proteins, mice with *Desmocollin1*-deficiency show flaky skin and impaired epidermal barrier (Natsuga, 2014). Additionally, disrupting tight junction function, though *Claudin-1* deficient mice, shows both outside-in and inside-out barrier permeability (Natsuga, 2014).

Many things can cause a defective barrier such as physical breach, hyperplasia, and disruption to cell adhesion and organization (Natsuga, 2014; Proksch et al., 2006; Segre, 2006). Barrier integrity can be measured though a multitude of techniques including the non-invasive trans-epidermal water loss measurement (TEWL), and through using dyes and similar *in vivo* methods to test the penetrability of the skin (Natsuga, 2014).

Histological/ultrastructural techniques like H&E staining or transmission election microscopy of skin biopsies have also been utilized to uncover structural changes on a cellular level. Moreover, mutant mouse models affecting structural proteins, cell adhesions, and lipids have been tested for their contribution to maintaining barrier integrity. Besides the above-mentioned mutations in adhesion proteins, mutations in structural proteins like keratins can also cause barrier disruption(Natsuga, 2014). While some keratins can compensate for the loss of others (i.e., *Krt14* can compensate for loss of *Krt10*), *Krt1*-null mice show perinatal lethality and have elevated TEWL compared with wild type (Natsuga, 2014). In humans dominant-negative mutations in *KRT1* or *KRT10* (encoding K1 or K10) causes epidermolytic ichthyosis, which is characterized by erythroderma and widespread blister formation at birth (Cheng et al. 1992; Rothnagel et al. 1992). Additionally, mutations in *Claudin-1* in humans leads to ichthyosis hypotrichosis sclerosing cholangitis (IHSC syndrome), a disease characterized by peeling skin (Haftek et al., 2022).

Defective skin barrier has ties with various physiological defects, including some metabolic disorders. For instance, diabetes and obesity increases the risk of skin lesions and psoriasis, respectively (Ramos-e-Silva and Jacques, 2012). Consistent with human findings, studies in mice have shown a susceptibility for weakened barrier after diet induced obesity or in mouse mutants with diabetes (Aoki and Murase, 2019; Okano et al., 2016). However, studies have also found the opposite to be true: barrier defects induce weight loss or metabolic dysfunction. Skin-specific deletion of several genes in mice have led to changes in body weight (Binczek et al., 2007; Chen et al., 2019; Egawa et al., 2016; Oji et al., 2010; Sampath et al., 2009; Sano, 2015; Schmuth et al., 2015). *Elovl3*-deficient mice show defective skin barrier characterized by defective hair lipid content, and water

repulsion and increased TEWL along with resistance to diet induced obesity (Westerberg et al., 2004; Zach-Avec et al., 2010). Similarly, deletion of *Acer1*, a gene encoding alkaline ceramidase 1 which is important for ceramide synthesis, resulted in barrier defects, cyclic alopecia, and reduced fat content with age (Liakath-Ali et al., 2016). *K14-Cre*-driven deletion of *Scd1* causes reductions in fats and body weight due to lack of insulation and increased thermogenesis (Sampath et al., 2009). Moreover, a study performed on two mouse models that cause barrier defects— K14-ACBP$^{-/-}$ (acyl-CoA-binding protein) though lipid-defficient barrier defects, and *ma/ma Flg*$^{ft/ft}$ (filaggrin), though structural barrier defects— showed increased energy expenditure caused by augmented thermogenesis from browning of inguinal white adipose tissue (iWAT) (Neess et al., 2021). They find that browning is is driven by β-adrenergic signaling and that rescue of metabolic defects can be achieved by thermoeutraility and though blocking β-adrenergic signaling (Neess et al., 2021).

While the exact connection between skin, metabolism, and weight in mice may be complicated and situation-dependent, these studies collectively show an inherent link between the three. Importantly, keratinocytes are the workhorses that restore the broken barrier and coordinate other healing-associated cell types and events within the skin (Arwert et al., 2012; Belokhvostova et al., 2018; Dekoninck and Blanpain, 2019; Gonzales and Fuchs, 2017; Ito and Cotsarelis, 2008; Plikus et al., 2012; Rognoni and Watt, 2018). Therefore, understanding keratinocyte-regulatory mechanisms and inter-cross talk between keratinocytes and other tissues throughout the body is important for mediating skin-metabolic-associated complications.

Ovol1 and Ovol2 proteins in barrier development and epithelial fate maintenance

Ovol1 and Ovol2

Ovol1 and Ovol2 are two proteins expressed in epithelial tissues and are members of the Cys2/His2 zinc finger transcription factor family, Ovo (Mevel-Ninio et al., 1991). Ovol proteins are evolutionarily conserved (Mevel-Ninio et al., 1991). In Drosophila, *ovo/svb* is a molecular switch controlled by the competition between the Wingless and DER pathways where *ovo/svb* expression promotes denticle formation and thus epidermal differentiation (Payre et al., 1999). In mice, *Ovol1* and *Ovol2* encode transcriptional repressors and are expressed in multiple epithelial tissues including the epidermis and hair follicles. *Ovol2* is expressed in the progenitor-like epidermal basal layer and can inhibit genes such as *Zeb1*, *Vim*, and *Twist1* that are involved in epithelial-to-mesenchymal transition (EMT) (Lee et al., 2014; Watanabe et al., 2014) (see below). In mice and humans, *Ovol2/OVOL2* also appears to have relevant roles in cancer providing an example of Ovol2's contribution to EMT as cancerous cells lose their ability to differentiate and favor more stem-like and invasive characteristics similar to that of EMT (Saxena et al., 2022). *Ovol1* is expressed in the differentiated suprabasal layer and regulates the growth arrest of embryonic epidermal cells (Nair et al., 2006). Loss of *Ovol1* during development causes epidermal hyperproliferation and a delay in skin barrier formation (Nair et al., 2006; Teng et al., 2007), and loss of both *Ovol1* and *Ovol2* disrupts embryonic skin barrier development and keratinocyte adhesion/differentiation in a Zeb1-α-catenin dependent manner (Lee et al., 2014; Wells et al., 2009). Thus, Ovol1 and Ovol2 are important for maintaining an epithelial fate by suppressing undesired mesenchymal-like molecular traits.

In adulthood, *Ovol2* alone facilitates wound closure by dictating directionality of the epidermal migratory front (Haensel et al., 2019). Interestingly, adult *Ovol1*-deficient mice that are treated with a TLR7 agonist imiquimod (IMQ), have hyperplasia and exacerbated inflammation (Dragan et al., 2022; Sun et al., 2021). Moreover, human *OVOL1* has been identified as a susceptibility locus for inflammatory skin diseases such as AD and acne (Hirota et al., 2012; Marenholz et al., 2015; Paternoster et al., 2011) and its expression is elevated in patients with psoriasis (Sun et al., 2021). The embryonic lethality of *Ovol1/Ovol2* double knockout mice precluded the analysis of their possible redundant roles in maintaining epidermal fate and barrier function in adult skin as well as any potential impact on total body metabolism.

Epithelial to mesenchymal plasticity (EMP)

EMT is a fundamental cellular process in which epithelial cells lose or attenuate their epithelial traits and gain partial or complete mesenchymal characteristics (Nieto et al., 2016; Pastushenko and Blanpain, 2019; Sha et al., 2019; Thiery et al., 2009; Yang et al., 2020b). EMT occurs during embryonic development to enable morphogenesis and generation of cell lineages such as mesoderm or neural crest (Thiery et al., 2009). EMT is also believed to play a crucial role in cancer invasion, metastasis, and chemoresistance, as well as tissue fibrosis (Lamouille et al., 2014; Lim and Thiery, 2012; Nieto et al., 2016; Thiery et al., 2009; Vu et al.; Yang et al., 2020c). During EMT, epithelial cells lose their apical–basal polarity, destroy or destabilize cell–cell junctions such as adherens junctions, desmosomes, and tight junctions, reorganize cytoskeleton and shape, change interaction with the extracellular matrix (ECM), and acquire mesenchymal features including

fibroblast-like morphology, enhanced motility and invasiveness (Figure 1.2). These cellular events are triggered by microenvironmental signals, including different growth factors, and are driven by gene expression changes (e.g., downregulation of epithelial junctional proteins such as adherens junction component E-cadherin, and upregulation of mesenchymal-specific components such as the intermediate filament protein vimentin), as well as by post-translational regulatory mechanisms.

While past work often used morphological and cellular changes or expression of only a few markers (e.g., partial loss of E-cadherin, acquisition of vimentin expression) to identify and draw conclusions regarding EMT occurrence, an expanded view of EMT identification encompasses multiple layers of molecular changes including, but not limited to, transcription factors that are capable of inducing EMT (EMT-TFs), the chromatin changes they elicit, and their gene regulatory networks – all in conjunction with EMT-associated morphological, cellular, and functional changes (Nieto et al., 2016; Yang et al., 2020c). Core EMT-TFs include members of the Snail (e.g., Snail, Slug), Zeb (e.g., Zeb1), and Twist (e.g., Twist1) families, which transcriptionally repress genes encoding junctional proteins leading to the loss or decrease of adherens junctions and desmosomes (Nieto et al., 2016; Thiery et al., 2009; Yang et al., 2020c). TFs that inhibit EMT and promote the reverse process, mesenchymal-epithelial transition or MET, have also been identified and these include Ovol1, Ovol2, and Grhl2 (Lee et al., 2014; Nieto et al., 2016; Watanabe et al., 2014). Several growth factor signals, including transforming growth factor beta (TGF-b), epidermal growth factor (EGF) receptor ligands, hepatocyte growth factor (HGF), and certain members of the fibroblast growth factor (FGF) family, have been shown to induce EMT in diverse contexts, particularly in cancer cells and often through inducing the EMT-

TFs (Kalluri and Weinberg, 2009; Yang et al., 2020c). EMT regulation also occurs at the microRNA (miR), long noncoding RNA, alternative splicing, and post-translational levels (Nieto et al., 2016; Pradella et al., 2017; Xu et al., 2016; Yang et al., 2020c).

Rather than being a binary switch from a typical epithelial state to a typical mesenchymal state, EMT has been increasingly recognized as a continuum of states that cells can adopt between the stable epithelial and mesenchymal extremes (Haensel and Dai, 2018; Nieto et al., 2016; Sha et al., 2019; Yang et al., 2020c). The cells that possess characteristics of both epithelial and mesenchymal states are said to be in intermediate cell states, hybrid states, or in a partial EMT state. More recently, they are described by the EMT research community as possessing EMP (Nieto et al., 2016; Sha et al., 2019; Vu et al.; Yang et al., 2020c) (Figure 1.2). Importantly, EMP refers to the ability of epithelial cells to not only adopt mixed epithelial/mesenchymal (E/M) features, but also readily and reversibly convert between various states across the epithelial-mesenchymal spectrum, a type of plasticity believed to endow cells with enhanced fitness and flexibility (Yang et al., 2020c). Computational modeling and experimental evidence underscores the importance of mutual inhibitory loops, such as those between miR-200 and Zeb1, between miR-34 and Snail, or between Ovol2 and Zeb1, in generating stable or metastable intermediate E/M states (Nieto et al., 2016; Park et al., 2008; Sha et al., 2019).

Keratinocytes are inherently able to undergo EMP due to the required motility needed upon wounding. Importantly, parallels exist between the morphological, cellular, and molecular changes that occur as keratinocytes transit into a collective migratory phenotype during wound re-epithelialization and those that occur during the EMT process (Arnoux V., Come C., Kusewitt D., 2005; Haensel and Dai, 2018; Lambert and Weinberg,

2021). These include, as discussed above, the reductions in cell-cell and cell-matrix adhesions, reorganization of the cytoskeleton, alterations in cell shape and polarity. For example, keratinocytes most proximal to the wound site are alerted to the trauma and are activated to alter their adhesion, cytoskeleton, shape and polarity, leading to increased migratory potential (Aragona et al., 2017; Coulombe, 1997, 2003; Eming et al., 2014; Grinnell, 1992; Ross and Odland, 1968; Stone et al., 2016). Despite the morphological, cellular, molecular, biochemical, and regulatory parallels between wound re-epithelialization and EMT, the changes that occur in migrating epidermal cells are largely within the epithelial end of the EMT spectrum. Epidermal migration is also an integral part of epidermal morphogenesis and homeostatic tissue renewal, albeit it occurs here at a much smaller scale compared to that during wound re-epithelialization. Whether EMP regulators such as Ovol1/2 control EMP in the context of adult epidermal homeostasis and barrier maintenance had not been addressed.

Cutaneous inflammation and inflammatory disease:

Overview

As a tissue that has constant pathogen interactions, the skin is primed to mount an inflammatory response when damaged or dysregulated. To facilitate the process, immune, stromal, and epidermal cell cross talks exist to alert to danger and to facilitate the response (Kabashima et al., 2018; Pasparakis et al., 2014). Murine skin contains a plethora of resident immune cells that are part of both the innate and adaptive response. Within the epidermis, there mainly exists Langerhans cells, dendritic epidermal γδT cells (DETCs), and CD8+ resident memory T cells (Kabashima et al., 2018). The dermis contains resident dermal dendritic cells (DCs), macrophages, mast cells, dermal γδT cells , T regulatory cells (Tregs) and innate lymphoid cells (ILCs) while few neutrophils, monocytes, and αβT cells survey the area for pathogens (Kabashima et al., 2018). Complicating the study of immune cells in skin but highlighting the importance of keratinocyte-immune cross-talks, skin resident immune cells have functions in skin homeostasis. Both macrophages and Tregs affect hair follicle cycling in mouse dorsal skin (Ali and Rosenblum, 2017a; Ali et al., 2017; Castellana et al., 2014). During homeostasis and inflammation, immune cells enter into the skin via a dense network of blood vessels and navigate through the dermis using the ECM as a scaffold (Kabashima et al., 2018). Upon wounding or during skin inflammation, these blood vessels dilate to allow increased influx of immune cells into the dermis where they follow chemokine gradients to the afflicted site (Kabashima et al., 2018).

Keratinocytes as source and target of cytokines

Beyond supplying the barrier that prevents pathogens from entering, keratinocytes can act as members of the innate immune system, and trigger and respond to inflammation. Keratinocytes express several different pattern recognition receptors (PRRs) and can secrete cytokines and chemokines which are known for activating and recruiting immune cells (Kabashima et al., 2018). The cytokines and chemokines produced upon inflammation include members of the IL-1 family (IL-1α), IL-33, Cxcl1, thymic stromal lymphopoietin, and tumor necrosis factor (TNF) (Hänel et al., 2013). Notably, transcription factors involved in keratinocyte function (e.g., Jun and Fos) are also regulators of inflammation and dysregulation of these factors can initiate skin inflammation (Pasparakis et al., 2014; Zenz et al., 2008). Loss of *Junb* and *Jun* but increase in *Fos* expression has been shown to exacerbate psoriasis-like inflammation and trigger inflammation in mice, respectively (Briso et al., 2013; Chiang et al., 2013; Guinea-Viniegra et al., 2009; Pasparakis et al., 2014; Zenz et al., 2005). TNF and STAT3 signaling also have known functions in skin inflammation where ablation of *Ikbkb* (which encodes IKKβ) or the transgenic expression of a mutated super-repressor NF-κB inhibitor-α (also known as IκBα) resulted in psoriatic-like skin lesions (Pasparakis et al., 2014). Moreover, keratinocyte death has been implicated as an effective trigger of skin inflammation. Studies show that keratinocytes deficient in *Fadd* — a protein essential for caspase 8 activation and for apoptosis downstream of death receptor signaling—or caspase 8 alone, undergo RIPK3-dependent necroptosis (Bonnet et al., 2011; Cho et al., 2009; He et al., 2009; Pasparakis et al., 2014; Zhang et al., 2009). Necroptosis leads to release of damage associated molecular patterns (DAMPs) which activate TLRs to induce skin inflammation (Pasparakis et al., 2014). Moreover, skin specific mutations associated with NF-κB, TGFβ, SHARPIN and caspase 8

signaling showed increased apoptosis of keratinocytes followed by skin inflammation and in some cases dermatitis (Ikeda et al., 2011; Pasparakis et al., 2014; Tokunaga et al., 2011).

Not only are cytokines and chemokines important for amplifying and guiding a response in immune cells, but they also elicit responses in keratinocytes (Hänel et al., 2013; Kabashima et al., 2018). Keratinocytes become activated to proliferate or differentiate by numerous signaling molecules including growth factors, chemokines, and cytokines that are released by keratinocytes, immune cells, and fibroblasts in the wound microenvironment (Arnoux V., Come C., Kusewitt D., 2005; Rousselle et al., 2019). For example in an *in vitro* assay where calcium-induced differentiating keratinocytes were treated with recombinant IL-4/IL-13 or TNFα, they observed reduced gene expression of *FLG, LOR,* and/or *IVL* (Hänel et al., 2013). *In vitro* analysis of the effect of IL-1α on keratinocytes is more controversial due to differing methods. In general, *in vitro* stimulation of keratinocytes with IL-1α affects lipid composition and differentiation. *In vivo*, administration of IL-1α was able to improve barrier function in mice through enhancing lipid synthesis and though upregulation of genes associated with cell adhesion, proliferation and differentiation of epidermal cells whereas IL-1α overexpressing mice developed spontaneous skin lesions (Hänel et al., 2013). Consistently, IL-1 receptor type 1 knock out mice develop more profound barrier defects followed by increased IL-1α expression after barrier perturbation (Hänel et al., 2013). Overall, this suggests that IL-1α has effects on epidermal differentiation that must be modulated in physiological conditions and IL-1α seems to overall promote an inflammatory skin phenotype. IL-33 has also been implicated to have effects on keratinocytes but its effect can vary depending on the inflammatory situation. Studies predominantly suggest a pro-inflammatory role of IL-33 in

psoriasis (Balato et al., 2014; Duan et al., 2019; Miller et al., 2010; Sehat et al., 2018; Theoharides et al., 2010). However, it was recently reported that the introduction of recombinant IL-33 suppresses psoriatic inflammation and epidermal hyperplasia showing a protective role for IL-33 (Chen et al. 2020). While many of these studies reveal functions for these cytokines on keratinocytes, the upstream and downstream regulatory mechanisms by which these cytokines operate still has much room for exploration.

Innate immune cells

Innate immune cells are generally cells that respond rapidly to infection or damage, but that have less specificity towards the pathogen and can cause unintended damage to the surrounding tissue. While neutrophils, monocytes, macrophages, and innate lymphoid cells (ILCs) are classically considered innate immune cells, barrier tissues like skin also contain LCs and DETCs, among others, that are initial responders (Nguyen and Soulika, 2019; Pasparakis et al., 2014). Neutrophils are short-lived circulating innate lymphocytes responsible for sensing and rapidly responding to infection (Marzano et al., 2019). In homeostasis, neutrophil recruitment to skin is suppressed by repression of G-CSF; however after inflammation the release of IL-17 triggers G-CSF production and triggers neutrophils to produce IL-8, a potent neutrophil chemoattractant (Marzano et al., 2019). Neutrophils can be recruited to skin by a wide assortment of chemokines and signaling molecules (Su and Richmond, 2015). For example, neutrophil chemoattractants Cxcl4 and Cxcl12 released by the stroma during wounding to facilitate neutrophil recruitment during the early phase of wounding (Su and Richmond, 2015). Moreover IL-1α, which are released by damaged or stressed keratinocytes, can also recruit neutrophils which was shown in the context of

psoriasis-like inflammation (Rider et al., 2011, 2013; Sun et al., 2021). Cxcl1 is also a widely known neutrophil-attracting chemokine in various tissues (Rajarathnam et al., 2019; Sawant et al., 2015). While the function of these chemokines in recruiting leukocytes has been well-studied in a variety of contexts and models, less is known about the molecular regulators of these molecules beyond the canonical inflammatory signaling pathways (e.g., TNF and IFN signaling). Once neutrophils arrive to the afflicted site, they utilize respiratory burst and reactive oxygen species (ROS) generation, degranulation, and extrusion of neutrophils extracellular traps (NETs) to clear infection (Chiang et al., 2019). Moreover, neutrophils influence the local adaptive immunity by releasing signaling molecules and directly interacting with antigen presenting cells (APCs) and lymphocytes at the inflammatory site (Chiang et al., 2019). In inflammatory skin diseases like psoriasis, these processes become dysregulated and occur when there is no infection (Chiang et al., 2019). Neutrophils can also undergo swarm-like migration patterns, termed neutrophil swarming, which have been described in various tissue and disease contexts (Kienle and Lämmermann, 2016). However, less is known about neutrophil migratory patterns within tissues and the mediators of swarm-like events by neutrophils. Future studies investing these topics using *in vivo* live imaging could reveal interesting insight into neutrophil behavior and disease progression.

γδT cells are found the epidermis seeded between the junctions of keratinocytes (called DETCs) with dendrites that extend to the suprabasal layer, but are also present in the dermis (Nguyen and Soulika, 2019). In homeostasis, DETCs and keratinocytes have interdependencies where DETCs rely on keratinocytes to produce IL-7 to promote DETC survival and keratinocytes need DETC-derived IGF-1 (Nguyen and Soulika, 2019). To

exemplify this point, TCR $\delta^{-/-}$ mice have increased epidermal apoptosis due to loss of IGF-1 showing DETCs are important for homeostatic maintenance (MacLeod and Havran, 2011). When activated, DETCs retract their dendrites, and are signaling hubs for secreting many cytokines, cytotoxic effector molecules, chemokines and growth factors like IL-17 and can even travel to the lymph node in certain inflammatory settings (MacLeod and Havran, 2011). γδT cells in the dermis are distinct from epidermal γδT cells in that they express different chains. Namely dermal γδT cells express Vγ4 or 6 chain instead of 5 and they are also more mobile than keratinocyte-interacting γδT cells (Castillo-González et al., 2021; Nguyen and Soulika, 2019). Dermal γδT cells are also large producers of IL-17 so can be helpful to the skin in the case of certain pathogen infections (e.g., *Staphylococcus aureus*) but can also be detrimental in the case of autoinflammation and is associated with many skin diseases (Cai et al., 2011; Castillo-González et al., 2021; Cho et al., 2010; Nguyen and Soulika, 2019). γδT cells are not MHC-restricted and can recognize a diverse array of antigens including antigens that are soluble, released by damaged cells, or complexed with non-classical MHC molecules (Nguyen and Soulika, 2019). γδT cells also have roles in promoting skin wound healing, for example by releasing FGF9 to stimulate wound-induced HF neogenesis in large murine wounds, and tumor immunity where they are speculated to secrete cytolytic effector molecules to directly kill tumor cells (Gay et al., 2013; MacLeod and Havran, 2011).

Langerhans cells

One of the first responders to disrupted skin barrier are Langerhans cells (LCs). LCs are epidermal-resident, dendritic-like, APC that maintain tolerance in homeostasis but

instigate an inflammatory response after perturbation (Doebel et al., 2017; Merad et al., 2008). Lineage tracing experiments have revealed that LCs are bone marrow-derived monocytes formed mainly from the fetal liver and minorly the yolk sac that migrate to the epidermis during embryonic development where they remain as resident immune cells (Kolarsick et al., 2011; Merad et al., 2008; Pasparakis et al., 2014). LCs rest in the suprabasal layers of the epidermis and extend dendrites towards the surface to constantly surveil for damage or infection. In homeostasis LCs depend on keratinocytes to secrete IL-34 for their survival in epidermis (Yan et al., 2020). LCs constantly travel to the skin draining lymph nodes to promote tolerance in homeostasis (Nguyen and Soulika, 2019). Upon barrier breach, LCs dissolve inter-keratinocyte junctions so their dendrites can extend to the stratum corneum and engulf pathogens. They then migrate to lymph nodes to present antigen on MHC II receptors for T cell activation (Doebel et al., 2017). Interestingly, recent work that analyzes the transcriptional profile and activation of migrating human LCs speculated that loss of contact with epidermal cells may drive transcriptional changes that activate LCs to promote tolerogenic T cell response and immune homeostasis (Sirvent et al., 2020). The abundance and morphology of LCs have also been shown to depend on neighboring epidermal cells (Park et al., 2021). Intravital imaging of LCs cells show that LCs can adjust their shape to their surrounding keratinocytes (Park et al., 2021). Unsurprisingly, many skin inflammatory diseases such as psoriasis and AD are linked with barrier defects and elicit a LC response (Cumberbatch et al., 2006; Deckers et al., 2018; Eidsmo and Martini, 2018; Kunz et al., 1991).

Adaptive immune cells

Adaptive immune cells are generally highly specialized T and B cells to target specific peptides through antigen receptor gene recombination (Murphy et al., 2000). During trauma or infection, mature APCs bearing antigen traffic through the lymphatics to the draining lymph nodes where they can activate naïve or recirculating central memory T cells (Ho and Kupper, 2019). This process of T cell activation and proliferation causes lymph nodes to swell to accommodate the increase in T cell numbers (Yang et al., 2014). There are different subsets of T cells that can be produced depending on the class of MHC it interacts with including $CD8^+$ cytotoxic T cells, generally known for efficient killing, and $CD4^+$ helper cells that have a myriad of responsibilities (Xiong and Bosselut, 2012). Interestingly, $CD8^+$ T cells are implicated in cachexia-associated weight loss in a cytokine independent manner where $CD8^+$ T cells interact with adipocytes and cause morphologic and molecular changes to the adipose tissue that leads to depletion of lipid stores (Baazim et al., 2019). $CD4^+$ T cells have been implicated in many inflammatory skin diseases (Ho and Kupper, 2019). In AD mutations in Flg predispose the skin to barrier defects and damage to the skin results in dysregulated T cell function, of note allergic $CD4^+$ T cells (including Th2 type cells) (Ho and Kupper, 2019; Yang et al., 2020a). Moreover, *Ccl22* can recruit $CD4^+$ T cells to skin in mouse models of AD (Wang et al., 2010). One subset of $CD4^+$ cells are called regulatory T cells (Tregs) known for their immunosuppressive activities and functions in mediating skin homeostatic events (Ali and Rosenblum, 2017b; Nguyen and Soulika, 2019). Once an effector T cell with a specific receptor is generated, it hyper-proliferates and begins to express proteins that allow it to home to skin. Some of these proteins include cutaneous lymphocyte antigen (CLA) and various chemokines receptors including CCR4, CCR8, and CCR10 where, once expressed, they can then tether, traverse,

and extravasate from blood vessels into the dermis (Ho and Kupper, 2019). These newly deposited effector T cells can then follow chemokine gradients to the afflicted site (Ho and Kupper, 2019). There are different classes of T cells that express different markers based on the response they need to mount.

DCs in the skin can also activate recruited or tissue resident T cells (Ho and Kupper, 2019). αβT cells including $CD4^+$, $CD8^+$, and Tregs can be resident in the skin as memory T cells which are long-lived and distinct from their circulating and effector counterparts in that they express lower levels of CD28 but can still mount a robust local recall response (Nguyen and Soulika, 2019). Moreover, circulating and skin-resident memory T cells provide immunosurveillance and allow for rapid response to a reoccurring event. As mentioned before, Tregs are resident T cells that have important function in skin to facilitate hair follicle stem cell activation in mice leading to the possibility that other resident T or immune cells have important functions in mediating immune-autonomous events (Ali and Rosenblum, 2017b). Overall, the components of the adaptive immune response exhibit high selectivity for specific target pathogens depending on the trigger for inflammation but show they can be strong mediators of inflammation. T cells dysfunction contributes to many skin inflammatory diseases, and the complexity and diversity of T cells make it difficult to use one treatment or target as a solution to all problems. Understanding the composition of T cells in a given inflammatory setting has helped immensely with discovering existing treatments and further investigation into these fields will provide insights to further treatments.

Skin inflammatory diseases and models

Epidermal barrier defects underlie common inflammatory skin diseases such as psoriasis and AD which are also characterized by dysregulated inflammation (Kim and Leung, 2018; Sano, 2015; Sun et al., 2021). AD is an allergic-type skin inflammatory disease affecting 10-20% of children in industrialized countries and is characterized by highly itchy eczematous erythematous plaques (Hänel et al., 2013; Kim and Leung, 2018). Predispositions for barrier defects (i.e., mutations in *Flg*) coupled with barrier breach allows allergens (e.g., house dust mite) to enter the skin and leads to an allergic, namely Th2, type of T cell inflammatory response in skin (Kim and Leung, 2018; Kortekaas Krohn et al., 2022). Of note, dysregulation of both keratinocyte and barrier response along with dysregulation of T cell responses is believed to facilitate the disease (Kim and Leung, 2018). AD is associated with other comorbidities that share similar pathological mechanisms termed the "atopic march" where children with AD see the progression of this disease to other areas of the body like developing asthma (lungs) and rhinitis (eyes, nose, and throat) as they age (Brunner et al., 2017; Oliveira and Torres, 2019; Zheng, 2014). There is more mounting evidence to support AD as a systemic disease due to its links with autoimmune and inflammatory diseases, cardiovascular risk, risk for cutaneous infections and ties with sleep and metal health disorders (Oliveira and Torres, 2019). AD shows that a disease that begins in the skin can have whole body detrimental effects. Understanding how this develops may help with treating AD and preventing its "spread" throughout the body.

Contrastingly, psoriasis affects roughly 3% of the population and is characterized by dry, red plaques and white non-adherent scales, and hyperproliferation and abnormal differentiation of the epidermis (Griffiths, 2003; Roberson and Bowcock, 2010). Psoriasis is

classically regarded as a T cell-mediated disease due to elevated levels of Th1/Th17 markers including IL-1 family members, TNFα, IFNγ, IL-17, IL-20, and IL-22; however, the importance of fibroblasts, keratinocytes and other immune cells in facilitating this disease are beginning to be recognized (Benhadou et al., 2019; Roberson and Bowcock, 2010). For example, dermal γδT cells can to produce IL-23 receptor so are triggered to release IL-17, a key cytokine involved in the pathogenesis of psoriasis, and in humans Tregs can display a deficiency in their immunosuppressive capabilities that allows effector T cell functions to go unchecked exacerbating disease (Benhadou et al., 2019; Cai et al., 2011). Moreover, emerging roles for mast cells, pDCs and neutrophils are becoming more apparent in psoriasis (Benhadou et al., 2019; Chiang et al., 2019).

Neutrophil accumulation in differentiated layers of the epidermis (Munro's abscesses) distinguishes a subset of human psoriasis patients, namely pustular psoriasis, and is a key feature of psoriasis-like skin inflammation in mice (Chiang et al. 2019; Pinkus and Mehregan 1966; Sumida et al. 2014; Uribe-Herranz et al. 2013). Pustular psoriasis is characterized by excessive presence of neutrophils, especially in the form of Munro's abscesses, and many patients with this form of psoriasis do not respond well to conventional treatments (Chiang et al., 2019). Much is known about the function of neutrophils that can exacerbate psoriasis in this tissue. For example, neutrophils and blood samples acquired from patients with psoriasis exhibit elevated levels of ROS, degranulation markers like MPO and NETs in circulation and in tissue, which are hallmark highly proinflammatory functions of neutrophils, and are known for causing tissue damage and worsened pathology (Chiang et al., 2019). However, much less is known about the mechanisms that regulate neutrophil recruitment and trafficking in this subset of psoriasis.

While there are many treatments for general psoriasis, these treatments are not as effective for all patients and some have secondary unwanted side effects (Chiang et al., 2019). Since neutrophils are largely understudied in the context of psoriasis, continued work to understand the regulatory mechanisms of keratinocytes and role of neutrophils could provide much needed insights to improving medicines for these patients. While much work has been done on both barrier defects and skin inflammatory diseases, the mechanisms linking epidermal-immune cross talks remains to be fully understood. Illuminating the molecular pathways that promote barrier maintenance and the subsequent inflammatory response especially under stressful conditions, such as abrasion, are important for effective disease prevention and treatment.

Inflammation is also linked with metabolically related diseases such as obesity (Duff et al., 2015; Hirt et al., 2019; Kunz et al., 2019) and some studies also link this inflammation to skin dysregulation. For example, skin that was disrupted with *Gasdermin-A3* can trigger thermogenesis in brown adipose through releasing the IL-6 inflammatory cytokine (Chen et al., 2019). Additionally, overexpression of *Tslp*, a cytokine involved in T helper cell 2 immune response associated with atopic dermatitis-like inflammation, protects against weight gain and fat accumulation (Choa et al., 2021). However, the drivers and regulators of the communication between skin and distal organs are still largely unknown; unraveling them would provide much needed insights into disease prevention and treatment for both metabolic diseases and inflammatory skin diseases. Moreover, many immune studies take a narrow approach asking questions about isolated inflammatory responses or immune cells. Due to limitations in technology and the complexity of the experiments, less work has been done to characterize local mechanisms that cause systemic responses. Understanding these

mechanisms, while highly challenging, is critical to better understand how local treatments can have global effects, and what methods or treatments can be used to minimize this effect.

Thesis work

My thesis research aimed to use genetic mouse models to ask fundamental questions about epidermal barrier maintenance and epidermal-immune cross talk in homeostasis and disease, and how perturbations to this system can cause systemic effects. Chapter 3 examines the function of Ovol1 in adult skin psoriatic-like inflammation and its regulation of neutrophil response. My findings contributed to the identification of multiple mechanisms of epidermal-neutrophil cross-talks. Specifically, Ovol1 can both directly regulate genes involved in neutrophil recruitment (e.g., *Cxcl1*), and it can initiate neutrophil recruitment through maintaining a robust barrier against environmental perturbations, thereby preventing the release of *Il1α* that in turn recruits neutrophils (Dragan et al., 2022).

Chapter 4 examines the redundant and unique functions of Ovol1 and Ovol2 in regulating barrier function in homeostasis. I then sought to use Ovol1 and Ovoll2 inducible knock out mice as a model system to study how skin barrier defects affect the whole-body physiology. I found that inducible Ovol1 and Ovol2 epithelial-specific knock out (iDKO) mice develop spontaneous barrier defects through Ovol1/2 repression of genes involved in cytoskeletal structure and adhesion. These perturbations to the epidermis cause aberrant changes in local skin immune cell composition (e.g. epidermal LC activation and increased dermal $CD4^+$ and γδT cells) and increased size and immune presence of skin draining lymph nodes in iDKO mice compared with control. This inflammation in part then affects iDKO fat accumulation likely caused by elevated baseline energy expenditure. Together this work highlights the importance of an epidermally-derived transcription factor and how changes to the epidermis can alter total-body metabolism.

Figure 1.1: Epidermal structure and TFs regulating specification, maintenance and differentiation of interfollicular epidermis (Dai and Segre, 2004). Shown are the stages of differentiation color coded to match the schematic diagram of epidermis, shown below. The lower basal layer contains progenitor cells that then proliferate and differentiate to form the suprabasal layers of the epidermis. The top most layer, the stratum corneum is the result of keratinocytes undergoing denucleation, protein cross-linking, and secretion of fatty acids, carbohydrates and esters to bind the cells together creating a strong and hydrophobic "brick and mortar" structure.

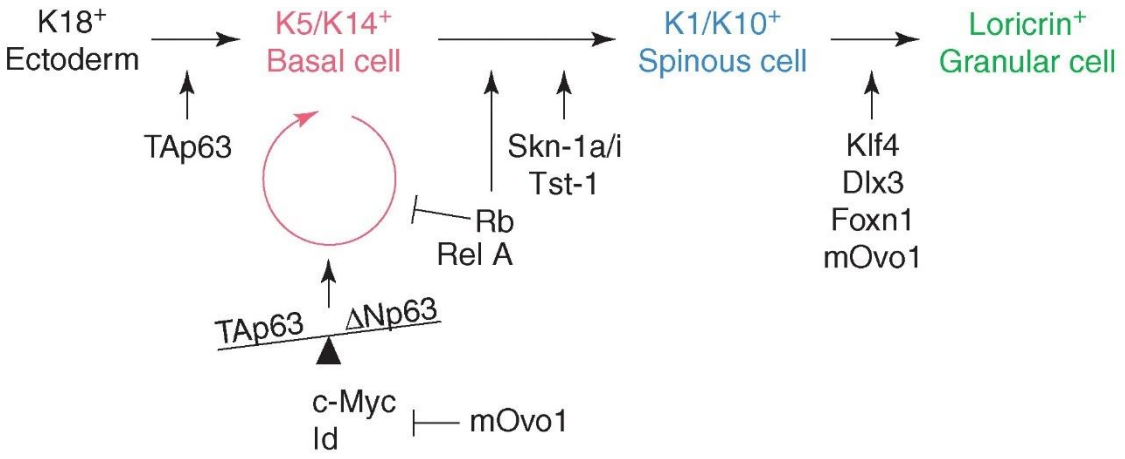

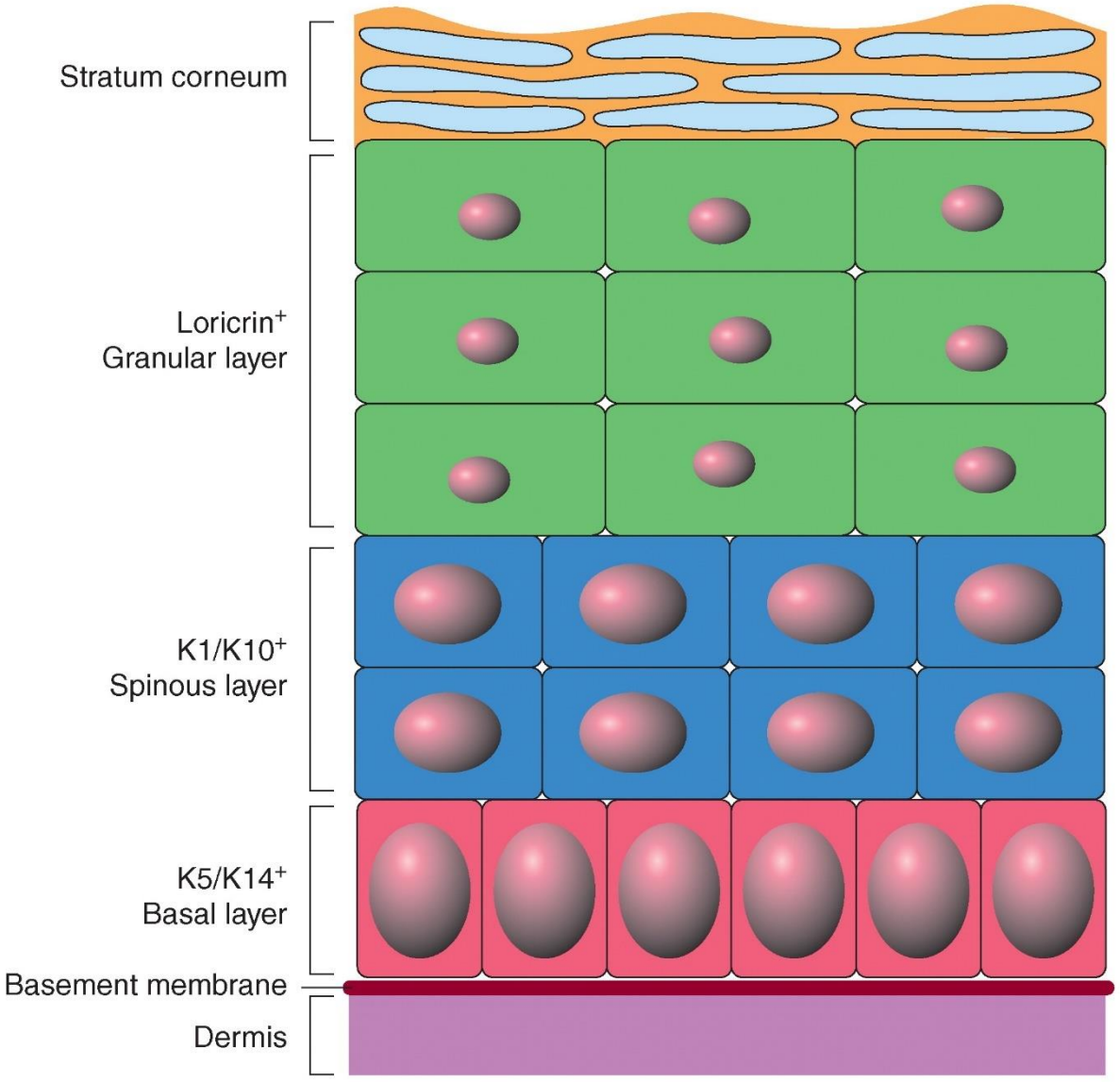

Current Opinion in Genetics & Development

Figure 1.2: EMT/MET and EMP in epithelial cells. (a) Static epithelial cells, marked by tight adhesion to the basement membrane and between neighboring cells, gain migratory function and become mesenchymal cells by undergoing EMT. Examples of markers of, and regulators that promote, epithelial (left) or mesenchymal (right) fates are provided. (b) EMP emphasizes the existence of multiple intermediate E/M states that that can readily interconvert. EMT is a cell type transition, whereas EMP is a functional state transition. EMT is unidirectional, whereas EMP is bi-directional.

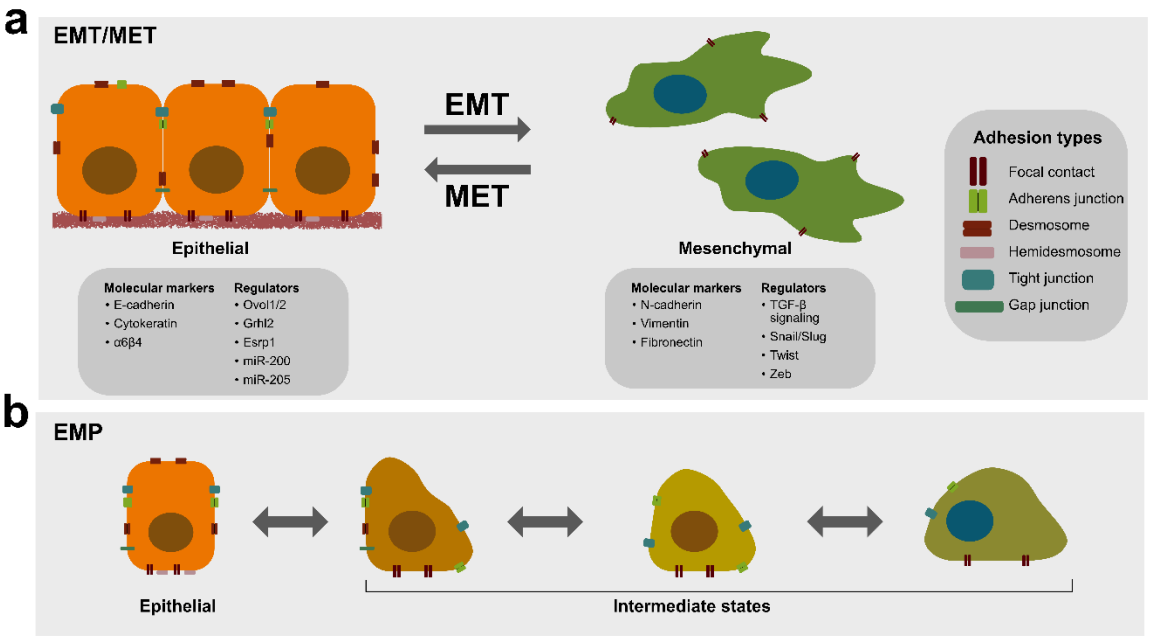

CHAPTER 2: Materials and Methods

Mice

B6N-*Ovol1*$^{tm1a(KOMP)Wtsi/J}$ mice, where a cassette composed of an FRT site, a *LacZ* sequence, and loxP sites is inserted into the *Ovol1* locus, were purchased from UC Davis KOMP Repository. These mice were crossed with B6.Cg-Tg(ACTFLPe)9205Dym/J (Rodriguez et al., 2000) mice to generate a "floxed" (f) *Ovol1* allele. *Ovol1*$^{+/-}$; *K14-Cre* males were crossed with *Ovol1*$^{f/f}$ females to generate *Ovol1* SSKO (*Ovol1*$^{f/-}$; *K14-Cre*) mice, which were then analyzed along with their sex- and weight-matched control littermates. Genotyping primers are provided in Table S1. All animal studies have been approved and abide by regulatory guidelines of the Institutional Animal Care and Use Committee (IACUC) of the University of California, Irvine.

Ovol1$^{+/-}$ mice are maintained in a CD1 strain background (Sun et al. 2021) and intercrossed to produce homozygous mutant (*Ovol1*$^{-/-}$) progeny for study. CD1-*Ovol1*$^{-/-}$ mice survive to adulthood but are sometimes smaller than control littermates, so sex- and weight-matched control and mutant littermates were used for all analysis.

Ovol1 and *Ovol2* floxed alleles were previously described (Dragan et al., 2022; Haensel et al., 2019; Unezaki et al., 2007) and intercrossed to generate *Ovol1*$^{fl/fl}$; *Ovol2*$^{fl/fl}$ breeders. *Ovol1*$^{fl/fl}$; *Ovol2*$^{fl/fl}$ females were crossed with *Ovol1*$^{+/-}$; *Ovol2*$^{+/-}$; *K14*-CreER mice (Haensel et al., 2019; Sun et al., 2021; Vasioukhin et al., 1999) to generate *Ovol1*$^{fl/-}$; *Ovol2*$^{fl/-}$; *K14*-CreER (iDKO) mice that were injected with 75 mg tamoxifen/kg body weight for 5 consecutive days at 7 weeks-old. All controls used are sex-matched littermates. Information for all genotyping primers is provided in Table S1. All animal studies have

been approved and abide by regulatory guidelines of the Institutional Animal Care and Use Committee (IACUC) of the University of California, Irvine.

IMQ-induced psoriasis model

Mice at 7~8 weeks of age received a daily topical dose of 62.5 mg 5% IMQ cream (Perrigo) on shaved backs for one to five consecutive days or as indicated. Based on a previously described objective scoring system called Psoriasis Area and Severity Index (van der Fits et al. 2009), erythema (redness of skin) and scaling (approximated by dry, white cracks and patches on the skin surface) were blindly scored independently by one or more investigators, on a score from 0 (none) to 4 (most severe). The cumulative score (erythema plus scaling) served as a measure of the severity of clinical signs (score 0–8).

Tape stripping and TEWL measurement

Tape stripping was performed as described in (Bruhs et al., 2018). In brief, hairs were removed from the mouse back by shaving. Three days later, shaved back skin was stripped with adhesive cellophane tape for 20 times. For each stripping, a fresh piece of tape was lightly pressed onto the back and gently pulled off.

TEWL was measured on shaved mouse back skin using the Delfin VapoMeter (SWL4400) under basal conditions (untapped or untreated), after tape stripping, or after two-time IMQ applications. TEWL values are output as g/m^2h.

Flow cytometry

For the IMQ model: T cells were isolated as described in (Ali et al., 2017). Whole

skin was digested in 2% collagenase, 0.5 mg/ml hyaluronidase and 0.1 mg/ml DNase in RPMI with 1% HEPES, 1% penicillin-streptomycin and 10% fetal calf serum) at 37^{o}C for 45 minutes. Cells were filtered through 70- and 40-μm filters, rinsed in 5% FBS/1xPBS, and stained for 10 minutes with Zombie NIR (Biolegend, 423105). Cells were stained with cell surface markers and anti-mouse CD16/32 (Biolegened, 101320) in FACS buffer (5%FBS/1xPBS) on ice for 30 minutes. Cells were fixed with the Transcription Factor Staining Buffer Set (eBioscience, 00-5523-00), and stained for eFluor450 anti-Foxp3 (eBioscience, 48-5773-82) for 1 hour at room temperature then analyzed on a FACS Aria Fusion™. Surface markers include APC anti-CD45 (Biolegend, 103112), PerCP/Cy5.5 anti-CD3 (Biolegend, 100218) and anti-CD90.2 (Biolegend, 140322), FITC anti-CD8a (Biolegend, 100705), BV605 anti-CD4 (Biolegend, 100548), and PE anti-ST2 (Biolegend, 145303). Additional details are described in the Supplementary Materials and Methods.

To obtain single cell suspension, minced samples were digested with 10 ml of a solution containing 0.25% collagenase (Sigma, C9091), 0.01 M HEPES (ThermoFisher, BP310), 0.001 M sodium pyruvate (ThermoFisher, BP356), and 0.1 mg/mL DNase (Sigma, DN25) at 37 ^{o}C for 1 hour with rotation, and then filtered through a 70-μm filter, spun down, and resuspended in 2% fetal bovine serum (Alphabioregen, Alpha FBS). Five x 10^5 cells were stained by incubation for 30 min at room temperature with the following antibodies diluted in 2% FBS/1xPBS: Alexa Fluor 488-conjugated anti-CD11b (Biolegend, 101217), PE-conjugated anti-F4/80 (Biolegend, 123110), APC-conjugated anti-CD45 (Tonbo biosciences, clone 30-F11, 20-0451), APC-Cy7-conjugated anti-Ly6G (Tonbo biosciences, clone 1A8, 25-1276), and 7-AAD (BD, 559925).

Lymph nodes, back skin, and paw skin (removed from bone) were dissected. Lymph nodes were crushed in FACS buffer (5% fetal bovine serum in 1xPBS), filtered through a 70-µm filter, rinsed, and resuspended in FACS buffer.

Epidermis and dermis were separated using incubation with 0.25% trypsin (Sigma; T4799) for 30 min to 1.5 hours at 37°C. Epidermis was minced, filtered through a 40-µm filter, rinsed, and resuspended in FACS buffer. Minced dermis and whole paw skin were digested with 10 ml of a solution containing 0.25% collagenase (Sigma, C9091), 0.01 M HEPES (ThermoFisher, BP310), 0.001 M sodium pyruvate (ThermoFisher, BP356), and 0.1 mg/mL DNase (Sigma, DN25) at 37 °C for 30 min (dermis) or 1 hour (paw) with rotation, and then filtered through a 40-µm filter, spun down, and resuspended in FACS buffer. Cells were stained by incubation for 30 min on ice with the antibodies listed in Table S6.

Histology and immunostaining

Sections from paraformaldehyde-fixed, paraffin-embedded back skin were stained with H/E, and epidermal thickness was measured at over 30 positions per section and values were averaged.

Sections from 4% paraformaldehyde-fixed, paraffin-embedded back skin were stained with H/E as previously described (Dragan et al., 2022). Sections from mouse toe were fixed in 4% paraformaldehyde for 8 hours followed by decalcification in 2% paraformaldehyde/0.4 M EDTA for 2-3 weeks at 4˚C followed by paraffin-embedding and staining with H/E.

For indirect immunofluorescence, mouse back skin and toe pads were trimmed and freshly frozen in optimum cutting temperature (OCT) compound (Tissue-Tek) and stained

using the appropriate antibodies. The primary antibodies used were: K1, K14, and loricrin (rabbit or chicken, gifts of Julie Segre, National Institutes of Health, Bethesda, 1:1000), Ki67 (Cell Signaling, rabbit, clone #D3B5, catalog # 9129; 1:1000), CD207 (Fischer, 12-2075-82). The following secondary antibodies were used: FITC-conjugated goat anti-rabbit (Vector Laboratories, FI-1000; 1:1000), rhodamine-conjugated donkey anti-goat (Jackson ImmunoResearch Laboratories, 711-025-147; 1:1000), rhodamine-conjugated goat anti-chicken (Jackson ImmunoResearch Laboratories, 103-295-155; 1:1000), and Alexa Fluor 488-conjugated donkey anti-rat (ThermoFisher, A-21208; 1:1000). Slides were mounted in Antifade medium (Vectashield H-1000; Vector Laboratories). Images were quantified using Fiji/ImageJ software (Schindelin et al., 2012).

For indirect immunofluorescence, mouse back skins were freshly frozen in optimum cutting temperature (OCT) compound (Tissue-Tek) and stained using the appropriate antibodies. The primary antibodies used were: K1, K14, and loricrin (rabbit or chicken, gifts of Julie Segre, National Institutes of Health, Bethesda, 1:1000), Ki67 (Cell Signaling, rabbit, clone #D3B5, catalog # 9129; 1:1000), and Ly6G (eBioscience, rat, clone 1A8; 1:200). The following secondary antibodies were used: FITC-conjugated goat anti-rabbit (Vector Laboratories, FI-1000; 1:1000), rhodamine-conjugated goat anti-chicken (Jackson ImmunoResearch Laboratories, 103-295-155; 1:1000), and Alexa Fluor 488-conjugated donkey anti-rat (ThermoFisher, A-21208; 1:1000). Slides were mounted in Antifade medium (Vectashield H-1000; Vector Laboratories).

RNA extraction and RT-qPCR

Back skin was collected, and epidermis separated from dermis following incubation in a 1:1 dilution of dispase in Epilife media (Cascade Biologics, M-EPICF-500) at 37 °C for 1 hour. The epidermis was then lysed in TRIzol (ThermoFisher, 15596018), followed by chloroform extraction and RNA purification from the aqueous phase using Zymo Research's Quick-RNA MiniPrep per manufacturer's protocol.

For RT-qPCR, 2 μg of RNA was used to generate cDNA (Applied Biosystems, 4368814) as per manufacturer's protocol. qPCR was performed using a Bio-Rad CFX96 Real-Time System and SsoAdvanced Universal SYBR® Green Supermix (Bio-Rad, 172-5271). *Gapdh* was used as a loading control. Information for gene-specific primers used is provided in Table S1

Transmission electron microscopy

TEM was processed as previously reported (Kashgari et al., 2020; Lee et al., 2014). Briefly, mouse back skin was isolated, trimmed and fixed in 2% paraformaldehyde and 2.5% glutaraldehyde in 0.2 M sodium cacodylate buffer and incubated at 4˚C for 2-3 days. Samples were then rinsed in 0.1 M sodium cacodylate buffer and post fixed for 2 hours at room temperature in 1% aqueous osmium tetra oxide in 0.1 M sodium cacodylate buffer. The samples were then dehydrated, processed and imaged at the UC Irvine Materials Research Institute core by Dr. Li Xing.

Metabolomics analysis

Metabolites were extracted from trypsin-isolated back skin epidermis. Nine hundred microliters of ice-cold 80% MeOH (extraction solvent) containing 0.5% formic acid was added to each well and the plate was gently nutated for 10 seconds. NH_4HCO_3 [15% (w/v); 80 µl for 900 µl of an 80% MeOH solution] was added to every well to neutralize pH. Plates were placed in −80°C for 1 hour. Cells were scraped and the entire content of the well was transferred to an Eppendorf tube. The well was rinsed with a small amount of ice-cold 80% MeOH and the remaining cells were added to the tube. Samples were vortexed for 10 seconds and centrifuged at 16,000 g for 15 min at 4°C. The supernatant was transferred to a new tube (first extraction), and 100 µl of extraction solvent was added to resuspend the pellet, followed by vortexing and centrifugation at 16,000 g for 5 min at 4°C. The resulting supernatant that represents the second extraction was combined with the first extraction. The extract was dried down with nitrogen to concentrate metabolites 10 times. The samples were centrifuged at 16,000 g for 10 min at 4°C, and 30 µl of supernatant was transferred to vials for mass spectrometry analysis.

Metabolite abundance and labeling was measured by quadrupole-orbitrap mass spectrometer (Q Exactive Plus Hybrid Quadrupole-Orbitrap Mass Spectrometer, ThermoFisher), operating in a negative ion mode via electrospray ionization and used to scan from mass/charge ratio 70 to 830 and 140,000 resolution. Liquid chromatography separation was on an Xbridge BEH Amide column (2.1 mm by 150 mm, 2.5-µm particle size, 130-Å pore size; Waters) at 25°C using a gradient of solvent A (5% acetonitrile in water with 20 mM ammonium acetate and 20 mM ammonium hydroxide) and solvent B (100% acetonitrile). Flow rate was 350 µl/min. The liquid chromatography gradient was as follows: 0 min, 75% B; 3 min, 75% B; 4 min, 50% B; 5 min, 10% B; 7 min, 10% B; 7.5 min,

75% B; and 11 min, 75% B. The injection volume of the sample was 3 µl. Data were analyzed using the MAVEN software, and natural isotope correction was performed with the AccuCor R code (https://github.com/XiaoyangSu/AccuCor).

Indirect calorimetry and Echo magnetic resonance imaging (MRI)

Oxygen consumption (ml/h), carbon dioxide release (ml/h), RER, locomotor activity (counts), and food intake (grams) were monitored for individually housed mice using the Phenomaster metabolic cages (TSE Systems Inc., Chesterfield, MO). The climate chamber was set to 21°C, 50% humidity with a 12-hour light-dark cycle as the home cage environment. Animals were entrained for two days in the metabolic cages before the start of each experiment to allow for environmental acclimation. Data were collected at 40 minutes intervals and each cage was recorded for 3.25 minutes before time point collection.

Body composition was measured using EchoMRI™ Whole Body Composition Analyzer (Houston, TX) which provides whole body fat and lean mass measurements.

Measurement of oxygen consumption rate and extracellular acidification rate

Basal oxygen consumption rate and extracellular acidification rate were measured using Seahorse XF Cell Energy Phenotype Assay on Seahorse XFp Flux Analyzer (Agilent Technologies) following manufacturer's instructions. Briefly, 150,000 isolated epidermal cells (see Flow Cytometry for details) processed in Keratinocyte SFM (1X) media (Thermo Fisher, 17005042) were resuspended in Seahorse assay medium (114 mM NaCl, 4.7 mM KCl, 1.2 mM KH_2PO_4, 1.16 mM $MgSO_4$, 2.5 MM $CaCl_2$, and 2.8 mM glucose) and seeded in

triplicate on Cell-Tak (Corning) coated 8-well culture plates. Seeded plates were incubated for 1 hour at 37^{o}C without CO_2 then run on the XFp for 5 cycles of basal measurements, followed by acute injection of oligomycin (50 uM) and FCCP (50 uM). Data were analyzed on Seahorse Wave desktop software (Agilent Technologies). Aggregate differences were compared using an unpaired t-test with Welch's correction.

RT-qPCR and RNA-sequencing

Tissues were collected ad libitum for gene expression analysis. iWAT, BAT, dWAT, and single-cell suspension of epidermis (see below) were homogenized in Trizol (ThermoFisher, 15596018), followed by chloroform extraction and RNA purification from the aqueous phase using ZYMO RESEARCH Quick-RNA MiniPrep per manufacturer's protocol. RNA was quantified using the NanoDrop ND-1000 spectrophotometer (ThermoFisher) and quality checked using the Agilent Bioanalyzer 2100 (Agilent). For RT-PCR, 2 µg of RNA was used to generate cDNA (Applied Biosystems, 4368814) per manufacturer's protocol. qPCR was performed using a Bio-Rad CFX96 Real-Time System and SsoAdvanced Universal SYBR® Green Supermix (Bio-Rad, 172-5271). *Gapdh* was used as a loading control. Information for gene-specific primers used is provided in Table S6.

Library construction was performed according to the Illumina TruSeq® Stranded mRNA Sample Preparation Guide. One µg of total RNA was used and mRNA was enriched using oligo dT magnetic beads. The enriched mRNA was chemically fragmented for three minutes, followed by reverse transcription to make cDNA. The resulting cDNA was cleaned using AMPure XP beads, end repaired, and the 3' ends were adenylated. Illumina barcoded adapters were ligated on the ends and the adapter-ligated fragments were enriched by nine

cycles of PCR. The resulting libraries were validated by qPCR and sized by Agilent Bioanalyzer DNA high sensitivity chip. The barcoded cDNA libraries were multiplexed on the Illumina HiSeq 4000 platform to yield 100-bp paired-end reads. FASTQ files were trimmed using Trimmomatic version 0.35 (Bolger et al. 2014) and aligned to the mm10 genome and counted using STAR version 2.5.2a (Dobin et al. 2013). Differential expression analysis was performed using DESeq2 version 1.24.0 (Love et al. 2014) on R version 3.6.1.

ChIP-seq and ChIP-qPCR

ChIP-seq analysis was performed on skin harvested at 6 hours after imiquimod treatment, such that the level of Ovol1 protein expression was sufficiently high to enable ChIP-seq success (Dragan et al., 2022). To separate epidermis from dermis, back skin was collected and digested with 0.25% trypsin for 1 hour at 37°C, scraped, minced, resuspended in 5% fetal bovine serum in PBS, and filtered through 70-μm and then 40-μm filters. Epidermal cells in single-cell suspension were then cross-linked in 1% formaldehyde, followed by ChIP assay using rabbit anti-Ovol1 antibody (Dai *et al*, 1998) and SimpleChIP® Enzymatic Chromatin IP Kit Magnetic Beads (9006, Cell Signaling) according to manufacturer's instructions. DNA was then purified and NexteraPE adapters were ligated on the ends and the adapter-ligated fragments were enriched by nine cycles of PCR. The resulting libraries were validated by Agilent Bioanalyzer dsDNA high sensitivity chip. The barcoded DNA libraries were multiplexed on the Illumina HiSeq 4000 platform to yield 100-bp paired-end reads. FASTQ files were trimmed using Trimmomatic version 0.35 (Bolger et al. 2014), aligned to the mm10 genome using Bowtie2 version 2.2.3 (Langmead and Salzberg, 2012), sorted/removed duplicates using Samtools version 1.3 (Danecek et al.,

2021) and Picard tools version 1.87 (http://broadinstitute.github.io/picard.). Finally, peaks were called with MACS2 version (Zhang et al., 2008).

The back skin of B6 mice was shaved and treated with IMQ for 2-6 hours. To separate epidermis from dermis, back skin was collected and digested with 2.5 U/mL dispase (Stem Cell Technologies, 07913) for 1 hour at 37°C, scraped, minced, resuspended in 5% FBS/1xPBS, and filtered through 70-μm and 40-μm filters. Epidermal cells in single-cell suspension were then cross-linked in 1% formaldehyde, followed by ChIP assay using rabbit anti-Ovol1 antibody (Dai et al., 1998) and SimpleChIP® Enzymatic Chromatin IP Kit (Agarose Beads) (Cell Signaling, 9002) according to manufacturer's instructions. DNA was then purified, and qPCR performed using SYBRgreen reagent (QIAGEN, Hilden, Germany) and gene-specific primers (Table S1).

In vivo administration of IL-33 neutralizing and anti-Ly6G antibodies

For IL-33 neutralization experiments, same-sex/same-weight *Ovol1* SSKO littermates were i.p. injected with 15 μg of goat anti-mouse IL-33 Affinity Purified Polyclonal antibody (R&D Systems, AF3626) or goat IgG (R&D Systems, AB0108-C) 30 minutes before the two IMQ applications and at the same time of day for 6 total applications. For neutrophil depletion studies, same-sex/same-weight *Ovol1*$^{-/-}$ littermates were i.p. injected with 500 μg rat anti-mouse Ly-6G antibody (eBioscience, clone 1A8) or rat IgG2a (eBioscience, clone eBR2a) once at 24 hours before IMQ application. In separate control experiments, same-sex/same-weight wild-type littermates were also treated and analyzed. Skin was harvested either 6 days after the first IMQ treatment (IL-33 neutralizing) or 24 hours after the third IMQ treatment (for Ly6G), and fixed in 4%

paraformaldehyde for H/E staining, embedded in OCT and frozen for immunostaining, or single cells were isolated for flow cytometry analysis.

In vivo administration of Dex and anti-□□TCR antibody

For Dex experiments, same-sex/same-weight control and iDKO littermates were intraperitoneally injected with either PBS or 1 mg Dex (in PBS) per kg body weight for 14 days on and off starting at 30 DPI and ending at 4-5 MPI. For □□TCR blocking (Koenecke et al., 2009)/depletion (Sandrock et al., 2018) experiments, same-sex/same-weight control and iDKO mice were intraperitoneally injected with 0.5 mg of hamster anti-mouse TCR γ/δ Antibody (UC7-13D5, Biolegend) or hamster IgG control (HTK888, Biolegend) on 30 DPI and then 0.2 mg every 3 days starting at 31 DPI and ending at 4 MPI. Mouse tissue samples were then collected for either flow cytometry or histology.

***OVOL1* knockdown in NHEKs and *Ovol1* deletion in primary mouse keratinocytes**

NHEK cells were cultured in Keratinocyte SFM (Gibco™, 17005042). *OVOL1* siRNA was purchased from Thermo Fisher Scientific (siRNA ID 115544) and transfected into NHEK cells on 6-well plates using Lipofectamine® RNAiMAX Transfection Reagent (Invitrogen™, 13778030) according to manufacturer's instructions. One day after transfection, the medium was replaced and NHEK cells were treated with Ca^{2+} (1.8 mM) for 24 hours.

Primary mouse keratinocytes were isolated from newborn *Ovol1*$^{f/f}$ mice as described in (Haensel et al. 2019) with minor modification. Briefly, the epidermis was separated from the dermis by overnight incubation with dispase. The epidermis was

dissociated on a drop of TrypLE™ Express Enzyme (Gibco™, 12604013) for 30 minutes at room temperature. Keratinocytes were cultured in Epidermal Keratinocyte Medium (CELLNTEC, CnT-07). For acute deletion of *Ovol1*, 50,000 keratinocytes were infected with adenoviruses expressing Cre recombinase (MOI = 100) or control adenoviruses, centrifuged at 500g at room temperature for 2 hours, followed by incubation for 24 hours on 12-well plates. Keratinocytes were treated with Ca^{2+} (1.8 mM) in fresh medium for 24 or 48 hours.

Statistics and reproducibility

Nearly all experiments were performed on at least three biological replicates or repeated at least twice. The sample size and number of independent experiments are indicated in the relevant figure legends. Disease pathology scoring was performed blindly. No data were excluded. For analysis of differences between groups, Student's unpaired *t*-test was performed with 2-tailed in Excel unless otherwise indicated. *p* values of 0.05 or less were considered statistically significant and are indicated in the figures/legends. Those where *p* values are not indicated are not statistically significant.

CHAPTER 3: Epidermis-Intrinsic Transcription Factor Ovol1 Coordinately Regulates Barrier Maintenance and Neutrophil Accumulation in Psoriasis-Like Inflammation

Morgan Dragan, Peng Sun, Zeyu Chen, Xianghui Ma, Remy Vu, Yuling Shi, S. Armando Villalta, and Xing Dai; Journal of Investigative Dermatology 2021

Journal of Investigative Dermatology 142, 583-593.e5
(https://doi.org/10.1016/j.jid.2020.10.025)

ABSTRACT

Skin epidermis constitutes the exterior barrier that protects the body from dehydration and environmental assaults. Barrier defects underlie common inflammatory skin diseases, but the molecular mechanisms that maintain barrier integrity and regulate epidermal-immune cell cross-talk in inflamed skin are not fully understood. Here we show that skin epithelia-specific deletion of *Ovol1* (ovo-like 1), which encodes a skin disease-linked transcriptional repressor, impairs the epidermal barrier and aggravates psoriasis-like skin inflammation in mice in part through enhancing neutrophil accumulation and abscess formation. Through molecular studies, we identify *Cxcl1,* a neutrophil-attracting chemokine, and *Il33*, a cytokine with known pro- and anti-inflammatory activities, as potential strong and weak direct targets of Ovol1, respectively. Furthermore, we provide functional evidence that elevated *Il33* expression reduces, whereas persistent accumulation and epidermal migration of neutrophils exacerbates, disease severity in imiquimod-treated *Ovol1*-deficient mice. Collectively, our study uncovers the importance of an epidermally expressed transcription factor that regulates both the integrity of the epidermal barrier and the behavior of neutrophils in psoriasis-like inflammation.

INTRODUCTION

Skin epidermis is a self-renewing epithelium composed of stem/progenitor cells that terminally differentiate to produce stratum corneum, which constitutes a physical barrier at the skin's outmost surface against myriad external assaults (Gonzales and Fuchs, 2017). Common inflammatory skin diseases such as psoriasis and atopic dermatitis are

associated with disruption of this epidermal barrier either as a trigger for disease or as a secondary consequence of immune cell dysregulation (Harden et al., 2015; Ring et al., 2012; Schmuth et al., 2015; Segre, 2006). Moreover, disease progression is facilitated by epidermal cell regulation of, and response to, immune cells (Kobayashi et al., 2019; Pasparakis et al., 2014; Zhang et al., 2019). However, the molecular mechanisms that regulate epidermally-driven communication between epidermal and immune cells in coordination with barrier maintenance remain largely unknown.

Previously, we reported that germline deletion of *Ovol1*, which encodes a transcription factor known to regulate epidermal development (Dai et al., 1998; Lee et al., 2014; Nair et al., 2006; Teng et al., 2007), leads to exacerbated skin inflammation and epidermal hyperplasia in response to imiquimod (IMQ), an agent widely used to induce psoriasis-like symptoms in mice (van der Fits et al., 2009; Sun et al., 2021). Moreover, human *OVOL1* is upregulated in psoriatic lesions (Sun et al., 2021). Neutrophil accumulation in differentiated layers of the epidermis (Munro's abscesses) distinguishes a subset of human psoriasis patients and is a key feature of psoriasis-like skin inflammation in mice (Chiang et al., 2019; Pinkus and Mehregan, 1966; Sumida et al., 2014; Uribe-Herranz et al., 2013). Epidermal keratinocytes play an important role in neutrophil recruitment by secreting cytokine/chemokines such as IL-1α, CXCL1, CXCL8, and LTB_4 (Milora et al., 2015; Olaru and Jensen, 2010; Sumida et al., 2014; Sun et al., 2021). Although we found elevated levels of IL-1α in IMQ-treated *Ovol1* null epidermis (Sun et al., 2021), it remains unclear whether Ovol1 functions within the epidermis to directly regulate epidermal-neutrophil cross-talk and whether it promotes barrier integrity.

In this work, we generated and analyzed mice with skin epithelia-specific knockout (SSKO) of *Ovol1* and examined their responses to IMQ. We found that epidermal loss of *Ovol1* dramatically aggravates IMQ-induced barrier disruption, epidermal hyperplasia, and neutrophil accumulation. In contrast, there was a reduction of lymphocytes, except for regulatory T cells (Tregs). We detected upregulated expression of *Il33* - the human counterpart of which is suppressed by OVOL1 overexpression (Furue et al., 2019; Tsuji et al., 2020) - in the skin of *Ovol1* SSKO mice but found IL-33 antibody neutralization to further enhance the psoriasis-like skin phenotypes of these mice. We showed that Ovol1 protein binds weakly to the *Il33* promoter but strongly to the promoter of *Cxcl1*, and indeed *Cxcl1* expression was elevated in *Ovol1*-deficient epidermis. Finally, we obtained evidence that *Ovol1* loss facilitates neutrophil accumulation near, and migration through, the epidermis, and that neutrophil depletion partially mitigates the psoriasis-like phenotypes of *Ovol1*-deficient mice. Together, our findings uncover an epidermal-intrinsic transcription factor that both promotes barrier integrity and directly suppresses neutrophil accumulation in psoriasis-like inflammation.

RESULTS

Ovol1 acts in the epidermis to promote robust barrier maintenance and to suppress IMQ-induced epidermal hyperplasia

Skin of *Ovol1*$^{-/-}$ mice exhibit elevated *Il1a* expression in response to IMQ (Sun et al., 2021). Since barrier disruption increases *Il1a* transcription (Wood et al., 1992), we asked whether *Ovol1*$^{-/-}$ skin is barrier-defective by performing TEWL measurements, a widely used

method to assess epidermal barrier function (Alexander et al., 2018). During homeostasis (Day 0), TEWL values were the same between *Ovol1*$^{-/-}$ and control littermates (Figure 1a-b). However, following IMQ treatment, which is known to induce transient barrier disruption (Barland et al., 2004), the *Ovol1*$^{-/-}$ mutants displayed significantly higher and longer-lasting TEWL increases than their control littermates (Figure 1a). Similarly, enhanced barrier disruption was observed in *Ovol1*$^{-/-}$ mice after tape stripping (Figure 1b).

To ask if *Ovol1* functions within the epidermis to regulate barrier maintenance, we generated *Ovol1* SSKO (*Ovol1*$^{-/f}$; *K14-Cre*, where *Ovol1* is deleted in epithelial cells of the skin) mice in a congenic C57BL/6 (B6) background. Like *Ovol1*$^{-/-}$ mice, during homeostasis TEWL values in *Ovol1* SSKO mice showed no deviation from their control littermates (Figure 1c). Consistently, expression of epidermal terminal differentiation markers appeared largely normal in *Ovol1* SSKO skin (Figure S1a). Upon IMQ treatment, *Ovol1* SSKO mice displayed significantly more dramatic and persistent TEWL increases compared to control littermates (Figure 1c). Therefore, *Ovol1* expression in the epidermis is required for maintaining a robust barrier when skin is under external physical or chemical assaults.

We also asked whether *Ovol1* suppression of IMQ-induced inflammation is intrinsic to the epidermis. Compared with weight- and gender-matched littermate controls, *Ovol1* SSKO mice showed dramatically more severe psoriasis-like phenotypes that included erythema, scaling, and epidermal hyperplasia after five consecutive days of IMQ treatments (Figure 1d-e). Exacerbated phenotypes of *Ovol1* SSKO mice could also be observed after only two consecutive days of IMQ treatments (Figure S1b). Interestingly, under identical IMQ treatment conditions, the psoriatic-like symptoms including epidermal hyperplasia of *Ovol1* SSKO mice appeared more remarkable than the *Ovol1*$^{-/-}$ mice, with the SSKO - but not *Ovol1*$^{-}$

$^{/-}$ - skin presenting finger-like projections reminiscent of the elongated rete ridges in psoriasiform hyperplasia of human patients (Murphy et al., 2007) (Figure 1e; Figure S1c-d). Together, our findings show that *Ovol1* is required in the epidermis to suppress IMQ-induced epidermal hyperplasia and associated skin phenotypes.

Acute immune responses in IMQ-treated *Ovol1* SSKO skin feature increased neutrophil abundance and decreased T cell presence

Next, we performed flow cytometry to compare the immune cell compositions in IMQ-treated control and *Ovol1* SSKO mice. At 24 hours after the second IMQ treatment, we detected a ~3.7-fold increase in neutrophils ($CD45^+/Ly6G^+/CD11b^+$) in *Ovol1* SSKO skin compared to control littermate skin, whereas similar numbers of total immune ($CD45^+$) cells and macrophages ($CD45^+/F4/80^+/CD11b^+/Ly6G^-$) were observed (Figure 2a-b; Figure S2a). These data demonstrate that loss of epidermal expression of *Ovol1* results in increased early influx of neutrophils in IMQ-treated skin.

We also examined the impact of *Ovol1* deletion on components of the adaptive immune response, which generally develops around 5-14 days after IMQ treatment (Miao et al., 2010). Specifically, we employed two-consecutive-IMQ applications to minimize indirect consequences from dramatic epidermal thickening and barrier disruption (Figure S1a-b), and, performed flow cytometry 6 days later. Compared to control counterparts, average numbers of both $CD45^+$ (immune) and $CD45^-$ cells were increased in *Ovol1* SSKO skin, but the differences were not statistically significant (Figure 2c; Figure S2b-c). Importantly, the percent of $CD3^+$ lymphocytes ($CD45^+CD3/Thy1^+$) out of total immune ($CD45^+$) cells was significantly lower in *Ovol1* SSKO skin than in control skin, whereas the percent of non-

lymphocytes was significantly elevated (Figure 2d-e). A significant reduction was observed for both the $CD4^+$ T cell and $CD8^-CD4^-$ T cell (which likely includes γδT cells; (Cai et al., 2011; Tigelaar et al., 1990)) subsets (Figure 2d,f), whereas the relative abundance of Tregs ($CD4^+Foxp3^+$) showed a trend of increase in the mutant mice (Figure 2g; Figure S2c-d). All these differences were normalized by 1-3 months after IMQ treatment (Figure S2e-h). Collectively, these data demonstrate that loss of epidermal *Ovol1* biases the skin's response to IMQ towards elevated neutrophil accumulation but reduced T cell abundance.

Ovol1 loss results in elevated *Il33* expression in inflamed skin, and inhibition of IL-33 signaling aggravates the IMQ-induced skin phenotypes of *Ovol1* SSKO mice

IL-33, a cytokine of the IL-1 family that is expressed in barrier tissues, has been identified as a risk factor and modulator of psoriatic inflammation (Balato et al., 2012; Duan et al., 2019; Griesenauer and Paczesny, 2017; Pichery et al., 2012). To seek potential targets of Ovol1 in the epidermis of inflamed skin, we first considered *Il33* as a candidate because recent reports show that *OVOL1* depletion in normal human epidermal keratinocytes (NHEKs) induces *IL33* expression (Tsuji et al., 2020). We found that both knockdown of *OVOL1* in NHEKs and adenovirus Cre-mediated acute knockout of *Ovol1* in primary mouse keratinocytes derived from $Ovol1^{f/f}$ mice resulted in elevated *IL33/Il33* expression (Figure 3a; Figure S3a). Thus, like OVOL1 in human, Ovol1 is capable of suppressing *Il33* expression in mouse epidermal cells.

Next, we asked if loss of *Ovol1* alters *Il33* expression in vivo. Interrogation of our previously published RNA-seq data on control and $Ovol1^{-/-}$ epidermis at 6 hours after IMQ treatment (Sun et al., 2021) revealed elevated *Il33* expression in the epidermis from $Ovol1^{-/-}$

mice (3.2x, $p<10^{-5}$). This said, RT-qPCR showed only a non-statistically significant increase for *Il33* expression in IMQ-treated *Ovol1*$^{-/-}$ epidermis, whereas the increased expression of *Il1a* was significant (Figure S3b). We also analyzed our published single-cell RNA-seq data on control and *Ovol1*$^{-/-}$ mice at 24 hours after IMQ treatment (Sun et al., 2021). In the interfollicular epidermis, *Il33* was found to be predominantly expressed by basal keratinocytes and the number of *Il33*-expressing basal cells increased in the mutant after IMQ treatment compared with the control (Figure 3b; Figure S3c-e). Moreover, control fibroblasts rarely showed detectable *Il33* expression, but fibroblasts from *Ovol1*$^{-/-}$ mice became *Il33*-positive after IMQ treatment (Figure 3c). Finally, RT-qPCR on RNAs isolated from whole skin of control and *Ovol1* SSKO mice revealed potential increases at 6 hours and 2-3 days, as well as a statistically significant increase at 6 days, after IMQ treatment for *Il33* expression (Kakkar and Lee, 2008) (Figure S3f). Taken together, these results suggest that epidermal loss of *Ovol1* results in mildly elevated expression of *Il33* in the epidermis, but remarkably increased expression in the dermis, of inflamed skin.

To investigate the effect of excessive *Il33* expression in the psoriasis-like microenvironment of IMQ-treated *Ovol1*-deficient mice, we intraperitoneally injected *Ovol1* SSKO mice with either IgG control or an IL-33 neutralizing antibody (Byrne et al., 2011; Liu et al., 2016; Ohno et al., 2011; Peng et al., 2017; Schmitz et al., 2005) prior to, and every day succeeding, two IMQ applications (Figure 3d). Interestingly, neutralization of IL-33 signaling led to more severe skin defects characterized by exacerbated erythema and scaling, enhanced epidermal barrier disruption, and apparent contraction of the IMQ-treated skin area (Figure 3e-h; Figure S3g-i). Consistent with enhanced epidermal hyperplasia at a histological level (Figure 3i-j), Ki67 immunostaining trended toward elevated proliferative

activity in the epidermal basal layer including cells lining the finger-like projections (Figure 3k-l). However, the expression of keratin 1 and loricrin appeared unchanged (Figure S3j-k), suggesting that the process of epidermal terminal differentiation is not affected by IL-33 neutralization. Despite previous reports of IL-33's effects on immune cell populations such as Tregs and neutrophils in other inflammatory models (Enoksson et al., 2013; Griesenauer and Paczesny, 2017; Lan et al., 2016; Matta et al., 2014), we did not detect any statistically significant change in non-lymphocytes and various T cell populations (including Tregs) after IL-33 neutralization in our model (Figure S3l-p). Collectively, these data suggest that the upregulated expression of *Il33* in *Ovol1* SSKO skin functions to suppress, rather than enhance, the IMQ-induced skin phenotypes and epidermal hyperplasia.

Identification of an *Ovol1*-*Cxcl1*-neutrophil regulatory axis that enhances IMQ-induced skin inflammation in *Ovol1* SSKO mice

To seek additional candidate targets that mediate the enhanced inflammation in *Ovol1*-deficient skin, we returned to the RNA-seq data on IMQ-treated *Ovol1*$^{-/-}$ and control epidermis (Sun et al., 2021), this time focusing on chemokines known to be involved in neutrophil recruitment. We found *Cxcl1* (2.1x), *Cxcl2* (3.0x), and *Cxcl3* (3.1x) to be significantly increased in IMQ-treated *Ovol1*$^{-/-}$ epidermis ($p<10^{-6}$). RT-qPCR analysis using independent samples confirmed the increased expression of *Cxcl1* in *Ovol1*$^{-/-}$ epidermis at both 6 and 24 hours after IMQ treatment, with the upregulation being more dramatic and statistically significant at 24 hours (Figure 4a-b). A possible increase in *Cxcl3* expression was also observed (Figure 4b).

Ovol1 encodes a transcriptional repressor (Nair et al., 2006, 2007). Thus, genes that

were upregulated in its absence might be direct Ovol1 targets. Indeed, the *Cxcl1* gene, but not *Cxcl2/3*, contains Ovol1-binding consensus motifs (CCGTTA) (Nair et al., 2007) at two different regions (R1, -3505 ~ -3411; R2, +1262 ~ +1355). To validate Ovol1 binding, we performed chromatin immunoprecipitation coupled with real-time quantitative PCR (ChIP-qPCR) on epidermal cells isolated from wild-type mice at 2-6 hours after IMQ treatment. ChIP-qPCR revealed strong Ovol1 binding to the promoter of a known Ovol1 target, *Id1* (Renaud et al., 2015), at -1073 ~ -997 (R1), but not at another site (R2, +1269 ~+1368) (Figure 4c). Binding to another known Ovol1 target, *c-Myc* (Nair et al., 2006), was also detected. Importantly, ChIP-qPCR revealed Ovol1 binding to the *Cxcl1* gene at both predicted sites (Figure 4c). Weak but statistically significant Ovol1 enrichment was also detected upstream of the *Il33* promoter at a region (-1986 ~ -1903) that contains an Ovol1-binding consensus motif. In contrast, no enrichment was seen for *Il1a* at three different regions (R1-R3). These results suggest that *Cxcl1* is a strong candidate as a direct Ovol1 target in skin epidermis, whereas *Il33* and *Il1a* are likely weakly or indirectly regulated by Ovol1.

The identification of *Cxcl1* as a potential Ovol1 target led us to look more closely at neutrophil dynamics in inflamed skin with *Ovol1* ablation. At 6 hours after the first IMQ application, sizable neutrophil clusters (Ly6G-positive) were already formed in *Ovol1* SSKO skin near the epidermis but were lacking in control littermates (Figure 5a). In *Ovol1*$^{-/-}$ mice, however, neutrophils were detected in the dermis at 6 hours post-IMQ, but visible large neutrophil aggregates were observed only at 12-72 hours post-IMQ in *Ovol1*$^{-/-}$ skin at locations near, across, and atop the epidermis (Figure 5b). At all timepoints examined, only scattered neutrophils were detected around the epidermis of control counterparts (Figure 5b). These data provide evidence that loss of *Ovol1* in epidermis results in increased

neutrophil accumulation, trafficking, and abscess formation near the epidermis of IMQ-treated skin.

To assess the functional contribution of neutrophils to IMQ-induced skin pathology of *Ovol1*-deficient mice, we depleted neutrophils using a neutralizing antibody against Ly6G (Daley et al., 2008) (Figure 5c). Both immunostaining and histological analysis revealed a reduced presence of neutrophils in IMQ-treated *Ovol1*$^{-/-}$ skin after Ly6G antibody injection relative to IgG injection (Figure 5d, Figure S4a). Epidermal thickness and number of Ki67-positive basal cells were not significantly different between IgG- and Ly6G antibody-injected skin at the end point of these experiments (day 3 after IMQ treatment) (Figure S4b-c). However, external symptoms such as erythema and scaling/plaque formation in *Ovol1*$^{-/-}$ mice were significantly improved by Ly6G antibody injection (Figure 5e-f; Figure S4d). These effects demonstrate that the accumulated neutrophils in *Ovol1*-deficient skin functionally contribute to IMQ-induced erythema and scaling/plaque formation.

DISCUSSION

Our work unravels novel mechanisms by which an epidermal keratinocyte-intrinsic transcription factor modulates innate and adaptive immune responses in skin in tandem with barrier maintenance. When the skin is chemically challenged or mechanically disrupted, Ovol1 helps maintain a functional barrier to protect from such perturbations. It likely does so by regulating the proliferation and differentiation of epidermal cells through repressing the expression of genes such as *Ovol1, c-Myc* (Nair et al., 2007), *Ovol2* (Teng et al., 2007), *Filaggrin* (Tsuji et al., 2017), and *Id1* (this work). Importantly, our work

identifies a role for epidermally expressed Ovol1 to directly and indirectly regulate the expression of cytokines and chemokines such as *Il1a, Il33*, and *Cxcl1*, thereby modulating the ensuing immune response.

Interestingly, the epidermal hyperplasia in IMQ-treated *Ovol1* SSKO mice appeared more severe than that in IMQ-treated *Ovol1*$^{-/-}$ mice (Sun et al., 2021). Moreover, neutrophil accumulation kinetics appears more rapid in *Ovol1* SSKO skin than *Ovol1*$^{-/-}$ skin. It is possible that this is due to differential IMQ responses of B6 vs. CD1 backgrounds (Swindell et al., 2011, 2017). Alternatively, non-epidermal cells in *Ovol1*$^{-/-}$ mice might play a modulatory role in the IMQ responses. In human psoriatic skin, neutrophils infiltrate into the dermis from blood vessels at the early inflammatory phase and migrate into the epidermis at the chronic phase of psoriasis (Albanesi et al., 2010). Neutrophil dynamics in inflamed tissues beyond neutrophil-vasculature interactions is an emerging area of research, and swarm-like migration patterns, termed neutrophil swarming, have been described in various tissue and disease contexts (Kienle and Lämmermann, 2016). The slower neutrophil kinetics in the *Ovol1*$^{-/-}$ model enabled our discovery that initial dermal infiltration of neutrophils does not depend on *Ovol1*, whereas *Ovol1* loss primarily affects the accumulation of neutrophils near or at the epidermis and the migration through the epidermis to form abscesses with keratinocytes. Our data suggest that *Ovol1* expression in epidermis constitutes a protective mechanism that prevents epidermal-proximal neutrophil accumulation and abscess formation in inflamed skin. Combined with our previous study (Sun et al., 2021), we propose that Ovol1 does so by direct transcriptional repression of *Cxcl1* expression in keratinocytes, and by maintaining a robust barrier, which in turn suppresses keratinocyte expression of *Il1a* (Rider et al., 2011; Sawant et al., 2015;

Sun et al., 2021). While a possibility for this type of regulation was suggested previously (Hwang et al., 2011), to our knowledge, this study presents the first example of an epidermally expressed transcription factor modulating neutrophil behaviors in skin inflammation through direct gene regulation.

Previous studies predominantly suggest a pro-inflammatory role of IL-33 in psoriasis (Balato et al., 2014; Duan et al., 2019; Miller et al., 2010; Sehat et al., 2018; Theoharides et al., 2010). However, it was recently reported that the introduction of recombinant IL-33 suppresses psoriatic inflammation and epidermal hyperplasia (Chen et al., 2020). Our results are consistent with this notion and suggest a protective role for IL-33 in the *Ovol1*-deficient mouse model against IMQ responses. It is possible that this protective function only manifests when the amount of IL-33 is excessive. IL-33 is an alarmin that can function both as a traditional cytokine (through receptor signaling) and as a nuclear transcriptional regulator (Haraldsen et al., 2009). Our antibody neutralization data implicate the signaling function of IL-33 in suppressing IMQ responses when *Ovol1* and barrier are deficient. In other tissues, IL-33 can recruit a particularly suppressive form of Tregs through the ST2 receptor (Halvorsen et al., 2019; Pastille et al., 2019; Siede et al., 2016). However, despite a trending increase of Tregs in *Ovol1* SSKO mice, after neutralizing IL-33, the total number of Tregs (including the $ST2^+$ subset) did not drastically vary. In this context, the IL-33/ST2 signaling axis may alter cytokine production by Tregs or other immune cells, rather than recruiting or inducing their proliferation (Hemmers et al., 2021). In Th2 allergic response, IL-33 can induce immune cells to release secreted proteins that induce proliferation of keratinocytes, potentially explaining the hyperplasia (Ryu et al., 2015). Alternatively, keratinocytes in *Ovol1*-deficient mice may respond directly to

excessive IL-33 signals and hyper-proliferate, since ST2L and pathways like ERK and c-Jun N-terminal kinase are activated by IL-33 (Du et al., 2016). While future work outside the scope of this study is needed to characterize the downstream cellular and molecular mediators of IL-33 function, our findings identify Ovol1 as an upstream regulator that directly suppresses *Il33* expression in mice.

Collectively, our study adds Ovol1 to a growing list of skin barrier-protective transcription factors (Cangkrama et al., 2013; Gordon et al., 2014; Hwang et al., 2011; Koegel et al., 2009; Li et al., 2017; Lin et al., 2013; Segre et al., 1999), but highlights its unique role in the adult epidermis to promote barrier robustness under external challenges in coordination with fine-tuning epidermal-immune cell cross-talk. In an *Ovol1*-deficient skin microenvironment, both anti- (*Il33*) and pro-inflammatory (*Cxcl1, Il1a,* neutrophils) components are upregulated and functionally contribute to skin pathology (Figure 6). These data underscore *Ovol1* function as part of a self-limiting, counter-balancing keratinocyte-intrinsic mechanism that maintains inflammation competence, but at the same time keep inflammation in check to restore tissue homeostasis. Dissecting the intricate and complex control of psoriasis-like inflammation by epidermal keratinocytes sheds new light onto our understanding of psoriasis pathogenesis in human patients.

Figure 3.1: Loss of *Ovol1* in epidermis aggravates IMQ-induced barrier disruption and epidermal hyperplasia.

A. TEWL measurements of *Ovol1*$^{-/-}$ with their control littermates after IMQ treatment. n=3 for control, n=5 for mkutant
B. TEWL measurements of *Ovol1*$^{-/-}$ after tape, starting at D0. n=3 pairs
C. TEWL measurements of *Ovol1* SSKO with their control littermates after IMQ treatment. n=3 pairs
D. External appearance at different days after the first IMQ application.
E. Skin histology at D0 and D5. Black and white arrows point to finger-like epidermal projections and neutrophil aggregates on the skin surface, respectively.

Data information: (Hom.) represents days before perturbation, or homeostasis. Scale bar: 100 μm in E. For statistical analysis in (A-C), we used an unpaired two-tailed Student's t-test. *** p<0.005; ** p<0.01; * p<0.05. Errors bars are represented as ± SD.

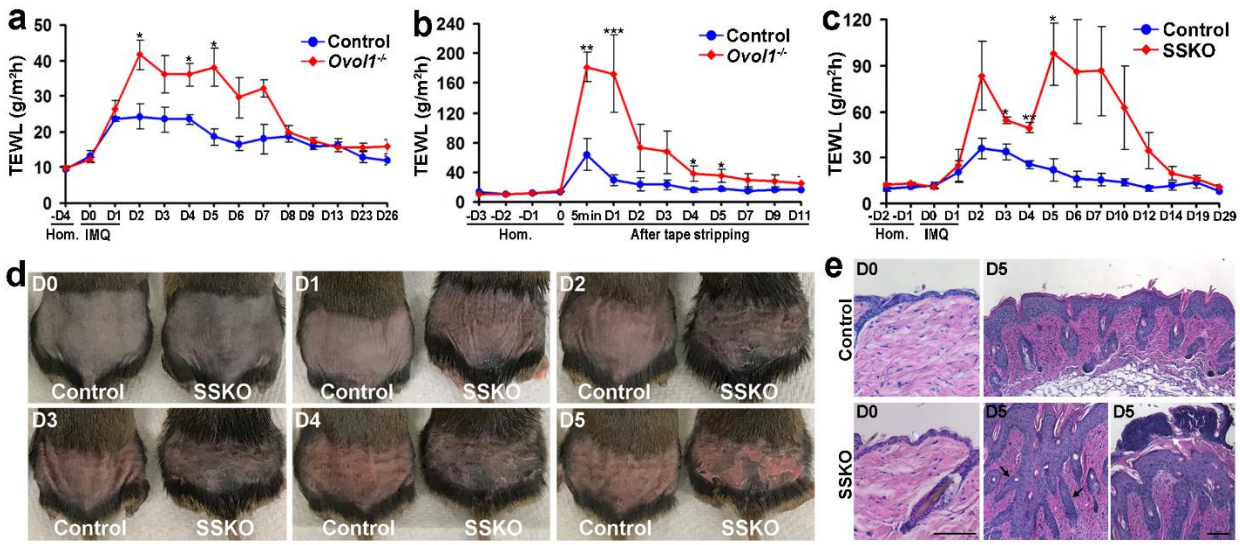

Supplemental Figure 3.1: *Ovol1* SSKO mice show exacerbated epidermal hyperplasia after only two IMQ applications.

A. Representative immunofluorescent staining of untreated *Ovol1* SSKO and littermate control back skin
B. Representative images of *Ovol1* SSKO mice and control littermates 6d after two IMQ applications.
C. External appearance and of the skin of *Ovol1*$^{-/-}$ (left) and *Ovol1* SSKO (right) mice and their respective control littermates at the indicated times after five IMQ treatments.
D. Histology of the skin of *Ovol1*$^{-/-}$ (left) and *Ovol1* SSKO (right) mice and their respective control littermates at the indicated times after five IMQ treatments. Bar = 100.

E. Data information: Scale bar: 15 μm in A and 100 μm. d, day; IMQ, imiquimod; K, keratin; LOR, loricrin; SSKO, skin epithelia–specific knockout for C-D.

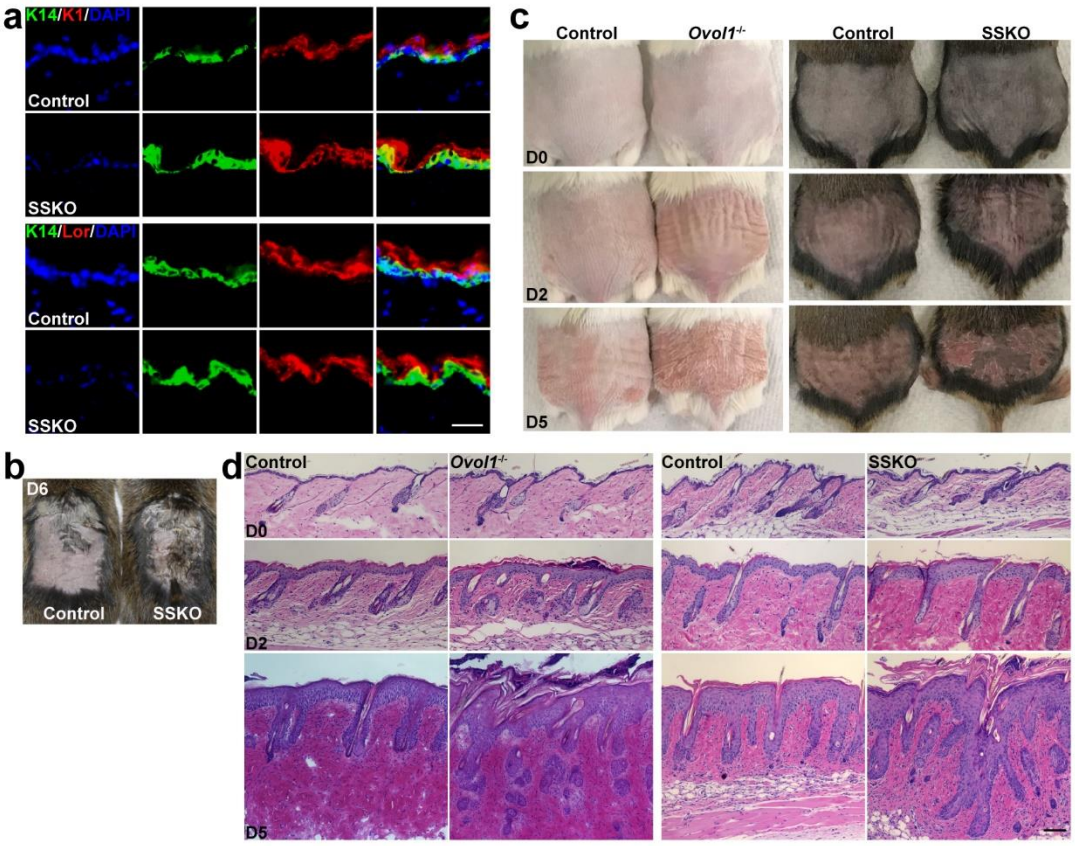

Figure 3.2: Immune cell profiles in IMQ-treated control and *Ovol1* SSKO skin.

A. Representative flow cytometry plots collected at 24 hours.
B. Summary of flow cytometry data collected at 24 hours. (n=3 pairs)
C. Summaries of flow cytometry data collected at 6 days after the second IMQ application. Representative flow plots are shown in Figure S2. n=7 control and n=6 mutants in C-G.
D. Representative flow cytometry plots collected at 6d after the second IMQ application for (E-F).
E. (E-G) Summaries of flow cytometry data collected at 6 days after the second IMQ application. Representative flow plots are shown in Figure S2. n=7 control and n=6 mutants in C-G.

Data information: For statistical analysis in (A-C), we used an unpaired two-tailed Student's t-test. *** $p<0.005$; ** $p<0.01$; * $p<0.05$. Errors bars are represented as ± SD.

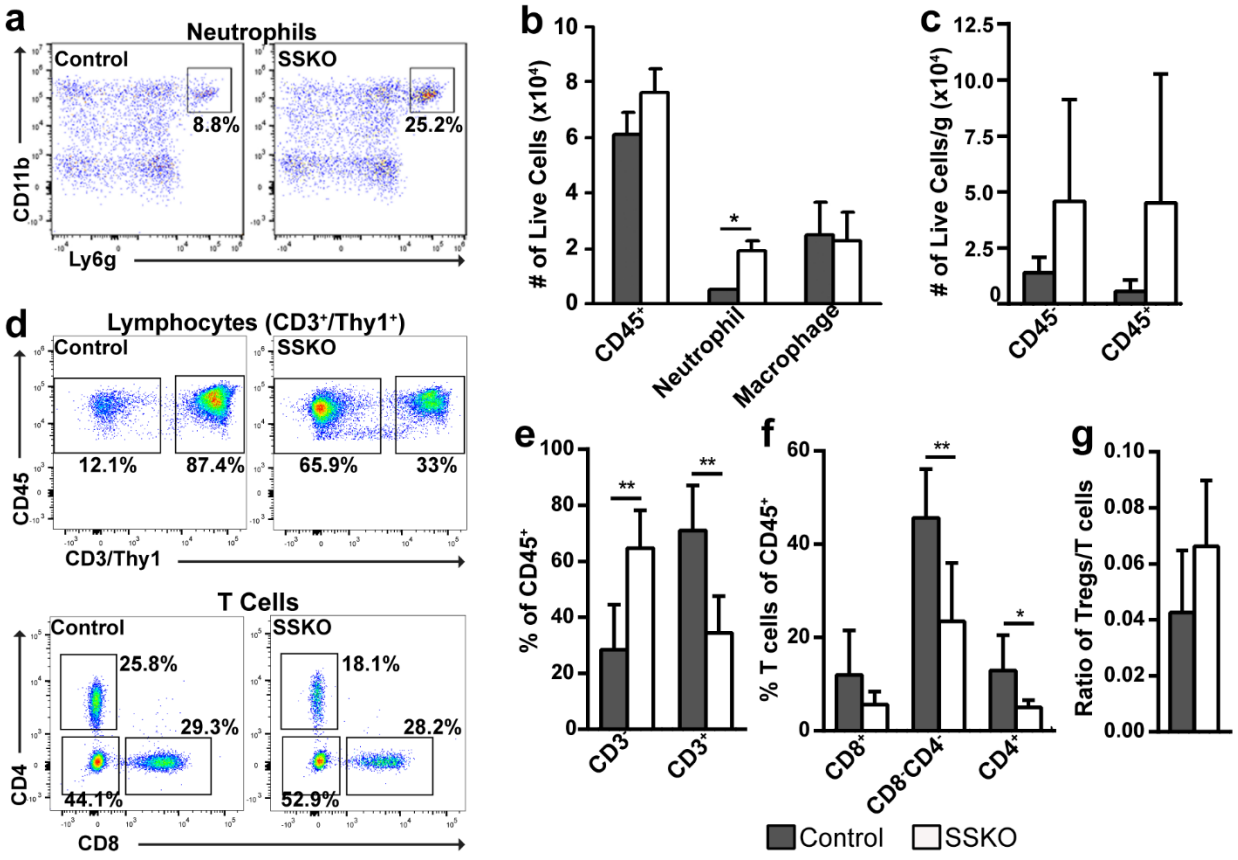

Supplemental Figure 3.2: Flow plots and immune cell profiles in control and *Ovol1* SSKO skin at 1-3 months after IMQ treatment.

- **A.** Representative flow cytometry plots for Figure 3.2 A.
- **B.** Gating strategy for Figure 3.2C-G.
- **C.** Representative flow cytometry plots for Figure 3.2 C,G.
- **D.** Representative immunofluorescent staining and quantification of $Foxp3^+$ Tregs in skin at 6 days after 2 IMQ applications. Arrows point to Tregs.
- **E.** (E-H) Summary of flow cytometry data for the respective immune cell populations 1-3 months after two IMQ applications. n=7 controls at 1 month and n=6 controls at 3 months. n=6 and =3 for *Ovol1* SSKO mice for 1 and 3 months, respectively.

Data information: Scale bar: 50 μm in D. For statistical analysis in (D-E), we used an unpaired two-tailed Student's t-test. *** $p<0.005$; ** $p<0.01$; * $p<0.05$. Errors bars are represented as ± SD.

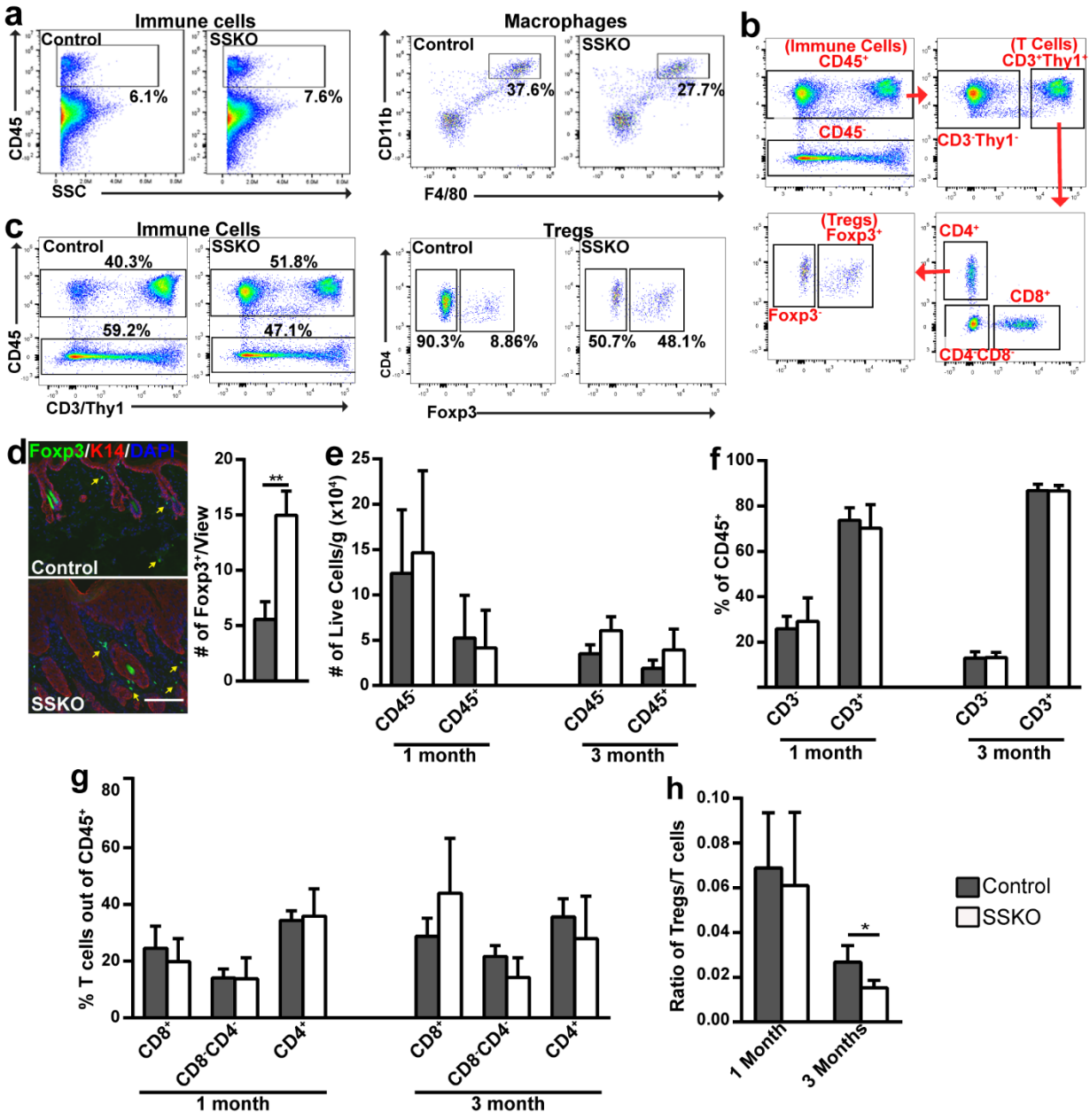
a
Immune cells
Control
SSKO
6.1%
7.6%
CD45
SSC
Macrophages
37.6%
27.7%
CD11b
F4/80
b
(Immune Cells) CD45+
CD45-
(T Cells) CD3+Thy1+
CD3-Thy1-
c
Immune Cells
40.3%
51.8%
59.2%
47.1%
CD3/Thy1
Tregs
90.3%
8.86%
50.7%
48.1%
CD4
Foxp3
(Tregs) Foxp3+
Foxp3-
CD4+
CD8+
CD4-CD8-
d
Foxp3/K14/DAPI
Control
SSKO
# of Foxp3+/View
e
# of Live Cells/g (x10⁴)
CD45-
CD45+
1 month
3 month
f
% of CD45+
CD3-
CD3+
g
% T cells out of CD45+
CD8+
CD8-CD4-
CD4+
h
Ratio of Tregs/T cells
1 Month
3 Months
Control
SSKO

Figure 3.3. Expression and function of *Il33* in *Ovol1*-deficient skin.

- **A.** RT-qPCR analysis on primary mouse keratinocytes derived from *Ovol1*$^{f/f}$ mice and infected with control (Adv-Ctr) or Cre-expressing (Adv-Cre) adenoviruses. Results from a single experiment are shown but are representative of 3 independent experiments.
- **B.** Violin plot showing the expression of *Il33* in interfollicular epidermal cells from scRNA-seq datasets (Sun et al. 2021).
- **C.** Violin plot showing the expression of *Il33* in fibroblasts from scRNA-seq datasets (Sun et al. 2021).
- **D.** Design of experiments for IL-33 neutralizing antibody (IL33n), or IgG control, on *Ovol1* SSKO mice E-L.
- **E.** External appearance of the skin at day (D)6.
- **F.** Time courses showing phenotype progression.
- **G.** Time courses showing TEWL measurements.
- **H.** Time courses showing treated back skin area (using images in Figure S3e).
- **I.** Skin histology at D6
- **J.** Quantification of epidermal thickness of (I) at D6.
- **K.** Representative immunofluorescence staining of proliferative basal (Ki67^{+}K14^{+}) cells at D6.
- **L.** Quantification of proliferative basal (Ki67^{+}K14^{+}) cells at D6 from epidermis in (K). n=3 pairs of IgG- and IL33n-treated *Ovol1* SSKO mice.

Data information: Scale bars: 50 μm in J. For statistical analysis in (A-K), we used an unpaired two-tailed Student's t-test. * p<0.05. Error bars represent mean +/- SD for (A, G, J, L) and SEM for (F,H).

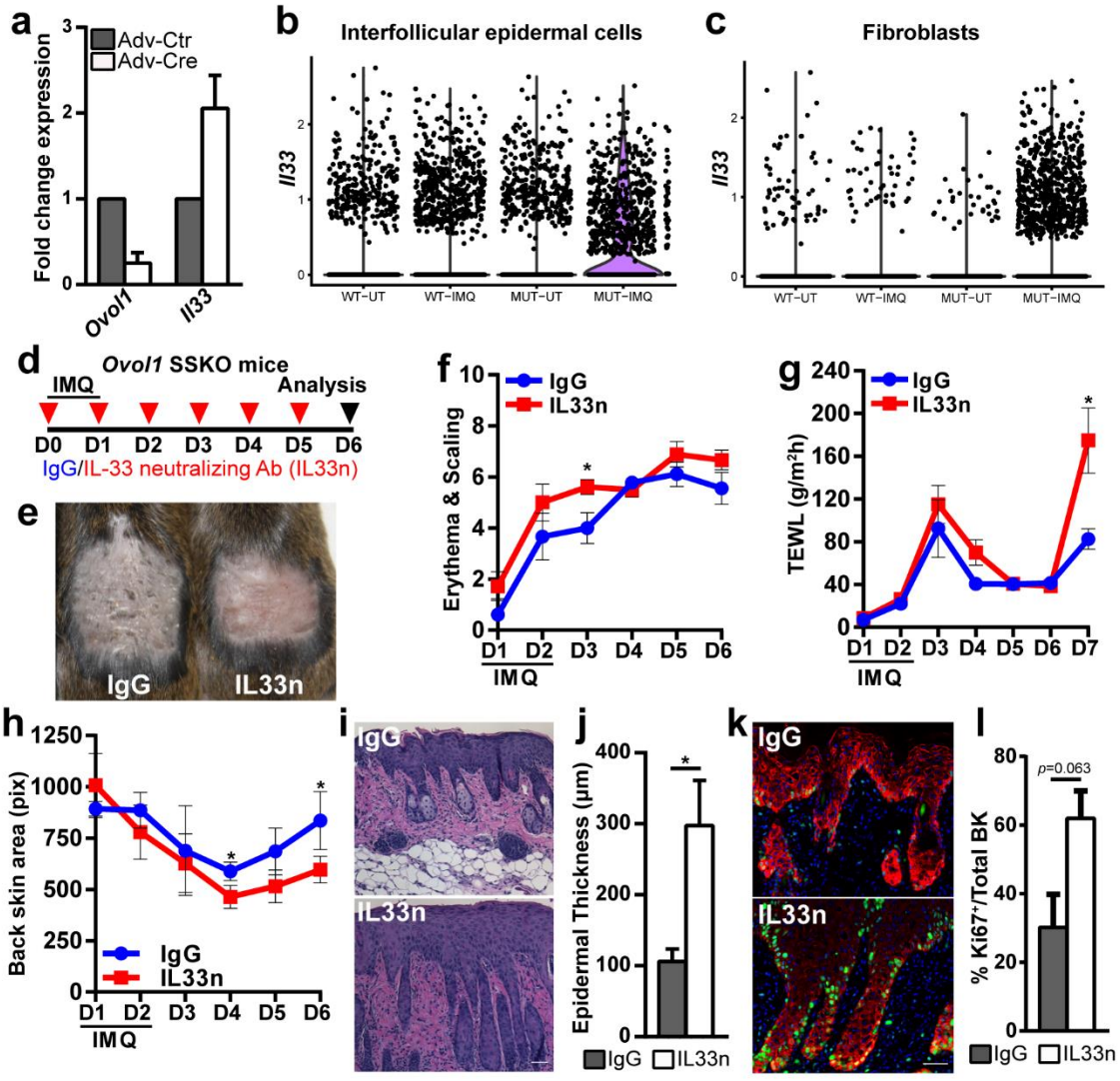
a
Fold change expression
Adv-Ctr
Adv-Cre
Ovol1
Il33
b
Interfollicular epidermal cells
Il33
WT-UT
WT-IMQ
MUT-UT
MUT-IMQ
c
Fibroblasts
Il33
WT-UT
WT-IMQ
MUT-UT
MUT-IMQ
d
Ovol1 SSKO mice
IMQ
Analysis
D0 D1 D2 D3 D4 D5 D6
IgG/IL-33 neutralizing Ab (IL33n)
e
IgG
IL33n
f
IgG
IL33n
Erythema & Scaling
D1 D2 D3 D4 D5 D6
IMQ
g
IgG
IL33n
TEWL (g/m²h)
D1 D2 D3 D4 D5 D6 D7
IMQ
h
Back skin area (pix)
IgG
IL33n
D1 D2 D3 D4 D5 D6
IMQ
i
IgG
IL33n
j
Epidermal Thickness (µm)
IgG
IL33n
k
IgG
IL33n
l
p=0.063
% Ki67+/Total BK
IgG
IL33n

Supplemental Figure 3.3: Supplementary data on the expression and function of *Il33* in *Ovol1*-deficient skin.

- **A.** RT-qPCR analysis on control (siCtr) and *Ovol1* siRNA-treated NHEK cells. Results from a single experiment are shown but are representative of 3 independent experiments.
- **B.** RT-qPCR analysis at 6 hours after IMQ treatment in *Ovol1*$^{-/-}$ mice. n=5 for *Ovol1*$^{-/-}$ and =4 for control littermates.
- **C.** Feature plot showing the expression of *Il33* in all cell types detected in single-cell analysis of mouse at 24 hours after IMQ treatment. tSNE plots from Sun et al. 2021 depicting the samples (center) and cell (right) types are included for comparison. Ctr-UT and Ctr-IMQ, untreated and IMQ-treated control littermate (*Ovol1*$^{+/-}$) skin, respectively. Null-UT and Null-IMQ, untreated and IMQ-treated *Ovol1*$^{-/-}$ skin, respectively.
- **D.** tSNE plots from single-cell data on interfollicular epidermal cells.
- **E.** Gene-specific feature plots from single-cell data on interfollicular epidermal cells.
- **F.** RT-qPCR analysis on whole skin of control and *Ovol1* SSKO mice at the respective times after two IMQ applications. n=2 pairs of *Ovol1* SSKO and controls for 6 hrs.; n=4 pairs of *Ovol1* SSKO and controls for 2-3 days; and n=3 pairs of *Ovol1* SSKO and controls for 6 days.
- **G.** External appearance of *Ovol1* SSKO mice treated with mIL-33 neutralizing antibody (IL33n), or IgG control.
- **H.** Erythema scoring at the indicated times of *Ovol1* SSKO mice treated with mIL-33 neutralizing antibody (IL33n), or IgG control.
- **I.** Scaling scoring at the indicated times of *Ovol1* SSKO mice treated with mIL-33 neutralizing antibody (IL33n), or IgG control.
- **J.** Representative immunofluorescent staining of the indicated markers at D6.
- **K.** The relative thickness of the K1- or Lor-positive layers relative to the total combined epidermal thickness was calculated and shown in (J).
- **L.** (L-P) Flow cytometry at D6 for the indicated cell populations. n=3 pairs of IgG- and IL33n-treated Ovol1 SSKO mice. * p<0.05. Error bars represent mean +/- SD for (a-b, e, g-h, j-o).

Data information: Scale bar: 50 μm in j. For statistical analysis in (A-C), we used an unpaired two-tailed Student's t-test. *** p<0.005; ** p<0.01; * p<0.05. * p<0.05. Error bars represent mean +/- SD for (A-B, E, G-H, J-O).

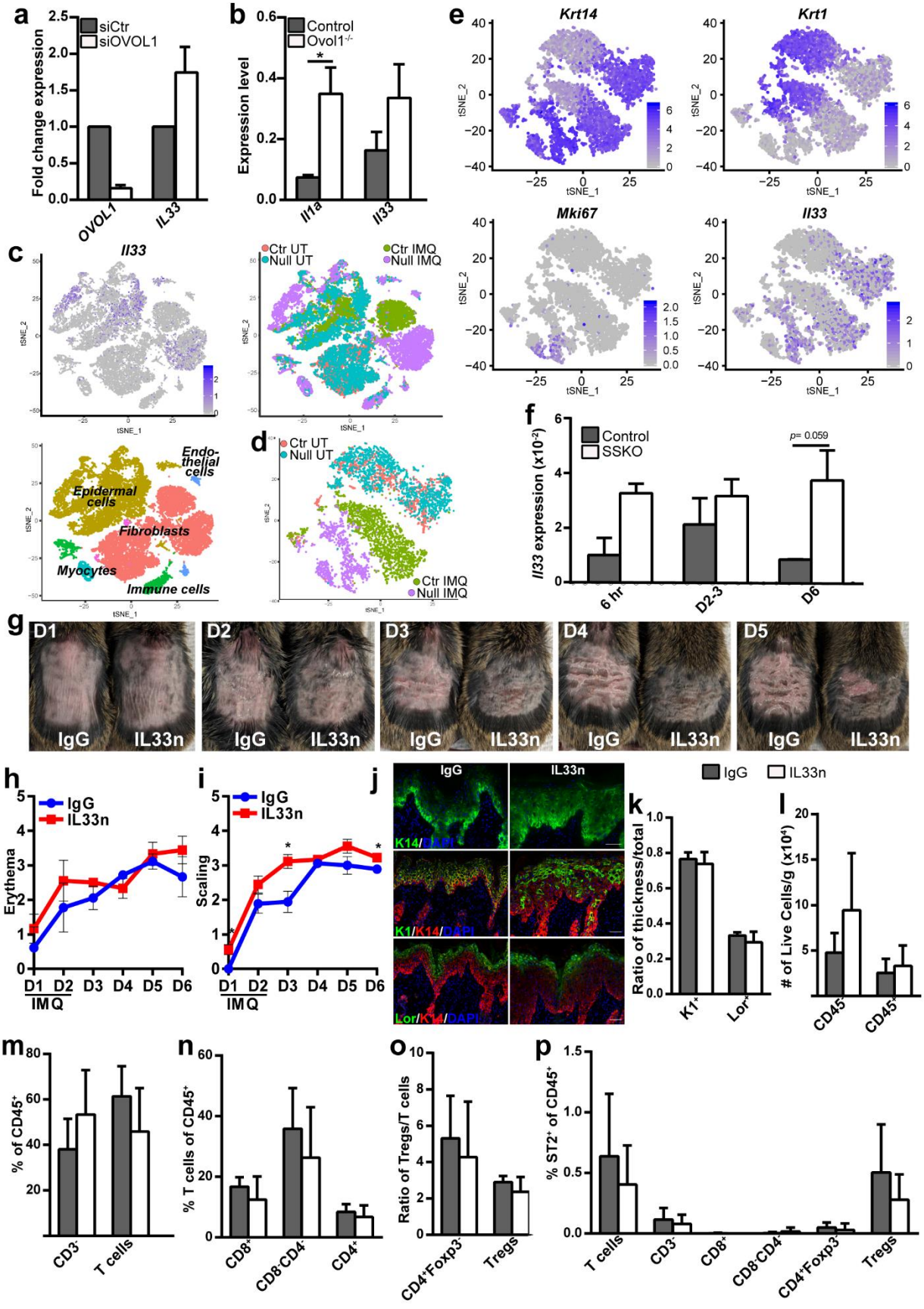
a
siCtr
siOVOL1
Fold change expression
OVOL1
IL33
b
Control
Ovol1-/-
Expression level
Il1a
Il33
c
Il33
Ctr UT
Null UT
Ctr IMQ
Null IMQ
Endo-thelial cells
Epidermal cells
Fibroblasts
Myocytes
Immune cells
d
e
Krt14
Krt1
Mki67
Il33
tSNE_1
tSNE_2
f
Control
SSKO
p= 0.059
Il33 expression (x10-2)
6 hr
D2-3
D6
g
D1
D2
D3
D4
D5
IgG
IL33n
h
IgG
IL33n
Erythema
D1 D2 D3 D4 D5 D6
IMQ
i
Scaling
j
K14/DAPI
K1/K14/DAPI
Lor/K14/DAPI
k
Ratio of thickness/total
K1+
Lor+
l
# of Live Cells/g (x10⁴)
CD45-
CD45+
m
% of CD45+
CD3-
T cells
n
% T cells of CD45+
CD8+
CD8-CD4-
CD4+
o
Ratio of Tregs/T cells
CD4+Foxp3-
Tregs
p
% ST2+ of CD45+
T cells
CD3-
CD8+
CD8-CD4-
CD4+Foxp3-
Tregs

Figure 3.4: Molecular analysis of Ovol1 targets in epidermis.

- **A.** RT-qPCR analysis at 6 hours after IMQ treatment. n=5 for *Ovol1*$^{-/-}$ and 4 for control littermates; note that 2 pairs of these mice were also used for RNA-seq analysis.
- **B.** RT-qPCR analysis at and 24 hours after IMQ treatment. n=5 pairs.
- **C.** ChIP-qPCR for the indicated genes in epidermal cells isolated from 2-6 hours post IMQ-treated adult skin. IgG control values were normalized to 1 for all. Results are summarized from 1-4 independent experiments.

Data information: For statistical analysis in (A-C), we used an unpaired two-tailed Student's t-test. *** p<0.005; ** p<0.01; * p<0.05. p values were calculated using two-tailed Student's paired *t*-test. Error bars represent mean +/- SEM.

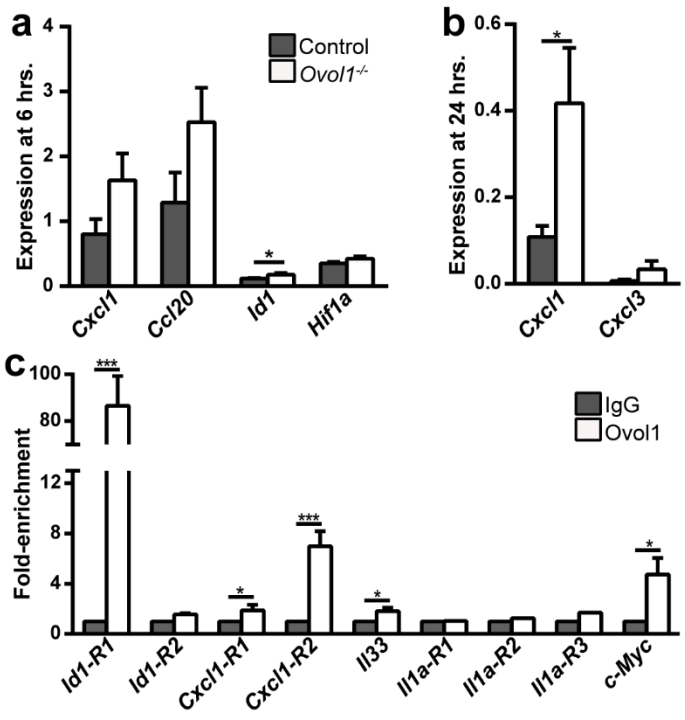

Figure 3.5: *Ovol1* loss alters neutrophil dynamics, and neutrophil depletion rescues psoriasis-like phenotypes in *Ovol1*$^{-/-}$ skin.

- **A.** Representative images of immunostaining in *Ovol1* SSKO mice
- **B.** Representative images of immunostaining *Ovol1*$^{-/-}$ mice.
- **C.** Design of neutrophil depletion experiments in (D-F). IgG was used as a control.
- **D.** Immunostaining at D3.
- **E.** External appearance of *Ovol1*$^{-/-}$ mice.
- **F.** Phenotypic score of *Ovol1*$^{-/-}$ mice at the respective times. n=3 pairs.

Data information: Arrows in (A), (B), and (D) point to neutrophils. Scale bar: 50 μm in A,B and 100 μm in D. For statistical analysis in (A-C), we used an unpaired two-tailed Student's t-test. * p<0.05. Errors bars are represented as mean ± SEM.

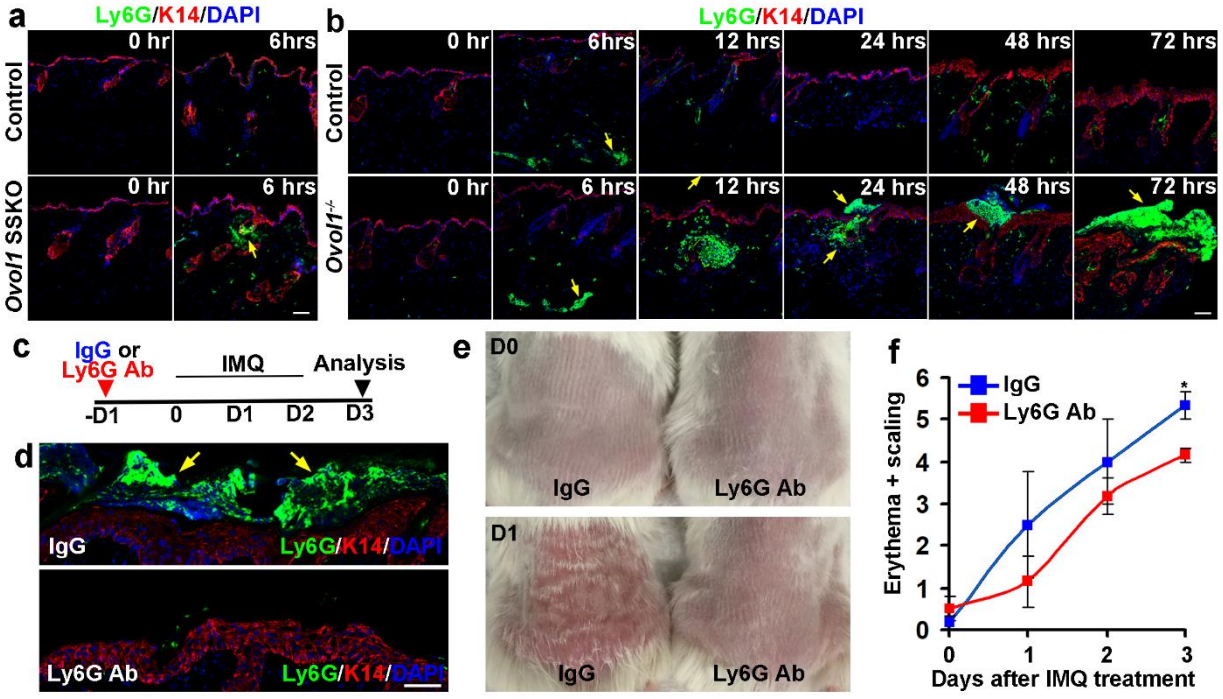

Supplemental Figure 3.4: Supplemental data on neutrophil depletion experiments.

- **A.** Skin histology of *Ovol1*$^{-/-}$ mice treated with IgG or Ly6G antibody at D3.
- **B.** Analysis of epidermal thickness in *Ovol1*$^{-/-}$ mice treated with IgG or Ly6G antibody at the experimental end point. n=3 for *Ovol1*$^{-/-}$, and n=1 for wild-type control littermate.
- **C.** Analysis of cell proliferation in *Ovol1*$^{-/-}$ mice treated with IgG or Ly6G antibody at the experimental end point. n=3 for *Ovol1*$^{-/-}$, and n=1 for wild-type control littermate.
- **D.** External appearance at different days before and after IMQ treatment. Note that these mice are distinct from those shown in Figure 5.

Data information: Scale bar: 100 μm in E. For statistical analysis in (A-C), we used an unpaired two-tailed Student's t-test. Error bars represent mean +/- SEM.

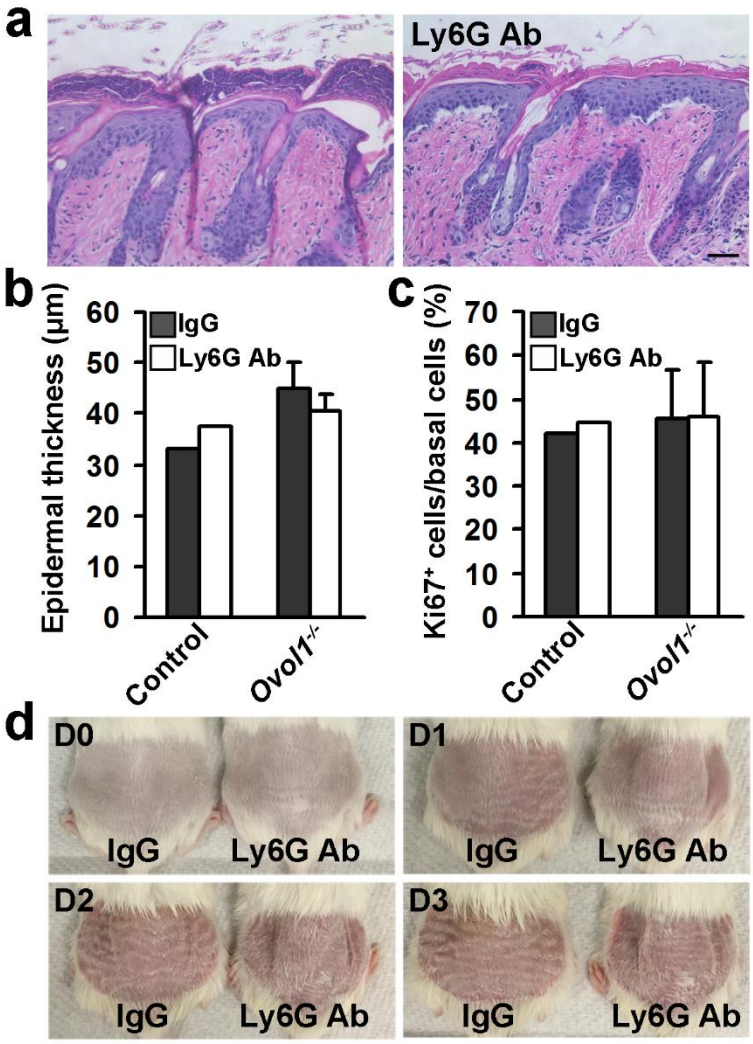

Figure 3.6: Working model of Ovol1 function in IMQ-induced skin inflammation

In normal skin treated with IMQ, epidermally expressed Ovol1 not only promotes barrier maintenance, thereby suppressing alarmin (IL-1α) production, but also directly represses the gene expression of *Cxcl1* chemokine and possibly *Il33* cytokine, to modulate the inflammatory and hyperproliferative responses. In *Ovol1*-deficient skin treated with IMQ, barrier is disrupted and *Il1a* and *Cxcl1* are upregulated, resulting in excessive and persistent neutrophil accumulation and exacerbated inflammation. On the other hand, *Il33* is upregulated likely as a protective mechanism to suppress excessive epidermal hyperplasia.

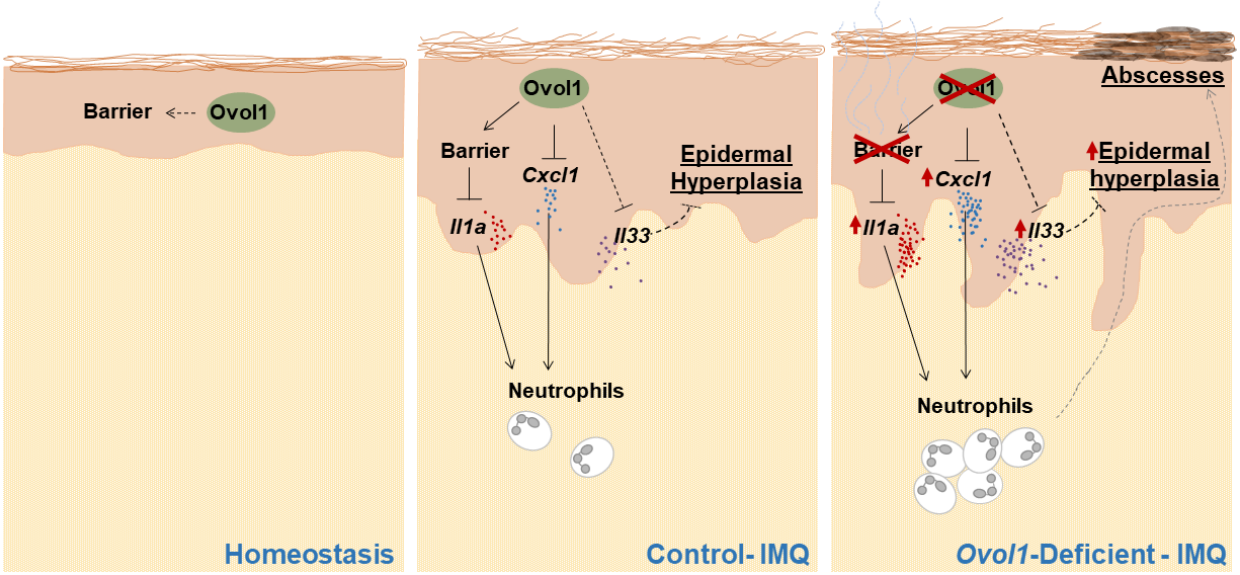

CHAPTER 4: Ovol loss-induced epidermal barrier dysregulation causes skin inflammation and metabolic adaptation

Morgan Dragan, Zeyu Chen, Yumei Li, Johnny Lee, Peng Sun, Daniel Haensel, Anh Pham, Amandine Verlande, Remy Vu, Guadalupe Gutierrez, We Li, Cholsoon Jang, Selma Masri, and Xing Dai

ABSTRACT

Skin epidermis constitutes the outer permeability barrier that protects the body from dehydration, heat loss, and myriad external assaults. Mechanisms that maintain barrier integrity in constantly challenged adult skin and how epidermal barrier dysregulation shapes the local immune microenvironment and whole-body metabolism remain poorly understood. Here we show that inducible and simultaneous ablation of transcription factor-encoding *Ovol1* and *Ovol2* in adult epidermis results in barrier dysregulation through impacting epithelial-mesenchymal plasticity, cell adhesion, cytoskeleton, and inflammatory gene expression of epidermal keratinocytes. We demonstrate that long-term aberrant immune composition then arises, characterized by precious epidermal Langerhans cell activation and aberrant T cell responses. Moreover, we identify failure to accumulate dermal and body fat as well as increase in carbohydrate-fueled energy expenditure as long-term consequences, and provide proof-of-principle evidence that skin inflammation partially contributes to these whole-body changes. Collectively, our study provides the first known adult epidermal-intrinsic mechanism that induces local skin inflammation and shapes whole-body metabolism.

INTRODUCTION

Skin is a vital permeability barrier that protects the body from dehydration and myriad environmental assaults. It is also the largest organ in the body, constituting ~10-15% of the body weight, and regulates important aspects of physiology including body temperature. How barrier dysregulation shapes the skin immune microenvironment is not fully understood, and little is known about how barrier-associated skin defects might instigate whole-body physiological and metabolic changes.

Within skin, terminal differentiation of the epidermal cells produces stratum corneum - a lipid-rich physical barrier, while innate and adaptive immune cells such as tissue resident Langerhans cells (LCs), dendritic cells, macrophages, and gamma delta T (γδT) lymphocytes collectively provide an immunological barrier to fend off pathogens and resolve insults (Chambers and Vukmanovic-Stejic, 2020; Elias, 2007; Niec et al., 2021). Barrier defects are associated with inflammatory skin diseases such as psoriasis and atopic dermatitis (Dainichi et al., 2018; Elias and Wakefield, 2014; Proksch et al., 2006). Furthermore, tantalizing links exist between skin inflammation and whole-body perturbation, evident through higher incidence of psoriasis and atopic dermatitis in patients with obesity (Brunner et al., 2017; Zheng, 2014), growth failure in patients with ichthyosis the clinical severity of which parallels the extent of barrier perturbation (Dereksson et al., 2012; Elias et al., 2012; Yamamoto et al., 2020), and weight loss in animals following acute inflammation (Gabay and Kushner, 1999; de Oliveira et al., 2022). However, the mechanistic connections and potential causality among skin barrier dysregulation, inflammation, and whole-body metabolism remain to be established.

A great deal has been learned about genetic mechanisms that regulate embryonic epidermal development and barrier acquisition (Hardman et al., 1998; Nair et al., 2006; Yu et al., 2006), but less is known about mechanisms that maintain barrier integrity in adult skin that is more heavily exposed to environmental aggressors (Natsuga, 2014; Proksch et al., 2006; Segre, 2006). This is a valid and important issue as adult skin differs from developing skin in barrier strength, overall structure, immune microenvironment, cellular heterogeneity, molecular makeup, as well as turnover rate and differentiation trajectory (Haensel et al., 2020; Henneke et al., 2021; Lin et al., 2020; Moretti et al., 2022; Moulin et al., 2001; Oranges et al., 2015; Rognoni et al., 2018).

Ovol1 and *Ovol2* encode two homologous transcription factors required for barrier development, and their constitutive and/or epidermal-specific deletion results in perinatal lethality (Lee et al., 2014; MacKay et al., 2006; Nair et al., 2006; Teng et al., 2007). By generating and analyzing mice in which both *Ovol1* and *Ovol2* are deleted specifically in epidermis and inducibly at adult stage, we identify a critical role for *Ovol1/2* in adult epidermal barrier maintenance and terminal differentiation through regulating overlapping target genes associated with epithelial-mesenchymal plasticity (EMP), actin cytoskeleton, cell adhesion, or inflammation. We show that *Ovol1/2* loss-induced epidermal dysregulation elicits altered skin immune cell changes that involves both innate and adaptive immune responses, reduction of dermal and body fats, and consequential metabolic adaptation featuring increased energy expenditure fueled by carbohydrates. We also provide evidence that anti-inflammatory agent dexamethasone (Dex) can partially restore fat and weight gain in *Ovol1/2*-deficient mice. Together, our findings not only identify key regulators of adult

barrier maintenance, but also suggest causal connections between skin barrier dysregulation, inflammation, and whole-body metabolism.

RESULTS

Inducible, simultaneous, and epidermal-specific deletion of *Ovol1* and *Ovol2* in adult skin results in defective barrier, disrupted cell-cell adhesion, and aberrant terminal differentiation

To ask if adult skin requires *Ovol* genes for barrier maintenance during homeostasis, we generated tamoxifen (TAM)-inducible double knockout or iDKO (*K14-CreER;Ovol1F/-;Ovol2f/-*) mice to enable the simultaneous deletion of *Ovol1* and *Ovol2* in adult epidermal cells. Successful deletion of both genes was evident through reduced expression of *Ovol1* and *Ovol2* mRNAs after TAM injection (Figure S1A-B).

Prior to TAM induction, adult iDKO mice showed no detectable difference from their control littermates in back skin trans-epidermal water loss (TEWL), suggesting normal barrier function before gene deletion (Figure 1A). Following TAM injections, both iDKO mice and their littermates with various control genotypes exhibited a trend of increased TEWL especially starting at ~15 days post-first injection (DPI), soon after one full epidermal turnover cycle (Koster, 2009) (Figure 1A). However, TEWL values were consistently and significantly higher in iDKO mice than in control littermates throughout the course of measurement (90 DPI) (Figure 1A). To understand the nature of the barrier defect, we performed morphological and metabolomics analyses to examine the structural and biochemical integrity of the iDKO epidermis. Both histology and transmission electron microscopy (TEM) revealed disrupted cell-cell adhesion and abnormal nuclear morphology

of epidermal cells, evident by 15 DPI, in the basal and suprabasal layers of iDKO mice but not control littermates (Figure 1B-C). Moreover, iDKO epidermal granular cells showed altered morphology of keratohyalin granules (Figure 1C), suggesting a dysregulation of the epidermal differentiation process (Hoober and Eggink, 2022). Metabolomics of trypsin-isolated epidermis for nonpolar metabolites revealed a significantly decreased production of urocanic acid and triacylglycerol (50:3), which are known to occur with skin barrier defect (Choi and Maibach, 2005; Fluhr et al., 2010), in iDKO epidermis at 52 DPI compared with control littermates (Figure 1D-E). Trending decreases in other metabolites associated with cellular stress and skin barrier, such as hypoxanthine and ceramide-dihydro (d18:0/26:0) (Coderch et al., 2003; Kim et al., 2017), were also observed (Figure S1C-D). Collectively, these findings demonstrate that *Ovol1* and *Ovol2* are required in adult skin for robust barrier maintenance, epidermal cell-cell adhesion, and optimal epidermal terminal differentiation.

Compared to back skin, mouse paw skin faces more physical abrasion and mechanical stress. Strikingly, as early as ~30 DPI (mice are 3-4 months of age), the iDKO mice started to show visibly elongated toenails which became exacerbated over time (Figures 1F-G, S1E-F). Underneath the iDKO nails we frequently observed blood clots, and their paw pads appeared more calloused and contained darker pigmentation (Figure 1F). The iDKO paws also appeared swollen, and the overall toe width was significantly increased compared with the control (Figure 1F-G). Sagittal sections through the toes revealed clearly longer nails, overall expanded epithelia and apparently thickened stratum corneum, especially in the ventral digit area (Figure 1H). While immunofluorescence using antibodies against Ki67, K14, K1, loricrin, and filaggrin proteins failed to reveal remarkable alterations in toe pad epidermal cell proliferation and early differentiation, the filaggrin-positive compartment in iDKO toe

pads was expanded and the size of their filaggrin-positive granules was significantly increased compared to the control counterparts (Figures 1I-J, S1G-K). As such, terminal differentiation of the paw epidermis is likely also perturbed by loss of *Ovol1* and *Ovol2*, reminiscent of the defect in back skin epidermis.

RNA sequencing (RNA-seq) analysis reveals unchecked EMP, dysregulated cell adhesion and cytoskeleton, aberrant inflammation, and reduction of growth-arrested basal transcriptional state in *Ovol1*/*Ovol2*-deficient adult epidermis

To dissect the molecular consequences of *Ovol1/Ovol2* deletion in adult epidermis, we performed RNA-seq analysis on trypsin-isolated epidermis (also contains LCs and dendritic epidermal T cells or DETCs; see below) from iDKO and control littermates at 25 DPI and 52 DPI. Only 31 differentially expressed genes (DEGs; ≥ 2-fold-change and $p < 0.05$) were detected at 25 DPI, of which 29 were upregulated and 2 downregulated in iDKO epidermis (Figure 2A-B; Table S1). By 52 DPI, 133 DEGs were detected, of which 89 were upregulated and 44 downregulated by≥ 2-fold ($p < 0.05$) in iDKO epidermis (Figure 2A-B; Table S1). Analysis of aggregated data from 25 DPI and 52 DPI revealed a similar number of DEGs, among which 12 genes were upregulated at both time points (Figure 2B). These include 1) *Zeb1,* a known direct target of Ovol2 transcriptional repression that encodes a transcription factor capable of inducing epithelial-mesenchymal transition (EMT), an extreme form of EMP (Lee et al., 2014; Watanabe et al., 2014; Yang et al., 2020); 2) those associated with membrane/cytoskeletal processes: *Lix1l, Flot2, Dennd5a, Ccdc88a, Cep170, Sacs,* and *Fez1* (Bärenz et al., 2018; Gentil et al., 2019; Moore et al., 2022; Suzuki et al., 2005; Völlner et al., 2016; Wang et al., 2018; Yoshimura et al., 2010); 3) other genes with apprarently diverse or

unknown functions: *Fkbp14*, (Ishikawa and Bächinger, 2014), *Zcchc24* (Cieply et al., 2016), *Klk10* (Hu et al., 2015), and *Gm4265*. *Vim*, another Ovol2 direct target and well-known EMT/mesenchymal cell marker (Haensel and Dai, 2018; Lee et al., 2014; Watanabe et al., 2014), was not among the DEGs at 25 DPI but was significantly upregulated in iDKO epidermis at 52 DPI. RT-qPCR analysis of epidermal RNAs from additional pairs of control and iDKO mice confirmed the significantly elevated expression of several of these genes including *Zeb1*, *Vim, Flot2, Dennd5a*, and *Ccdc88a*, in iDKO epidermis at both 25 and 52 DPI (Figure 2C).

To further elucidate the impacted cellular and molecular processes in iDKO epidermis, we performed gene ontology (GO) analysis on the DEGs at 52 DPI using Enrichr (Chen et al., 2013; Kuleshov et al., 2016; Xie et al., 2021). The top two GO molecular terms enriched for the 89 genes that were upregulated in iDKO epidermis are actin binding (*Ccdc88a, Fscn1, Lcp1, Fxyd5, Iqgap2*, and *Coro1A*) and sialyltransferase activity (*St3gal4* and *St6galnac6*) (Figure 2D), both important for cellular migration (Guo et al., 2021; Qi et al., 2020; Wu et al., 2018). Of note, GO analysis also identified the upregulated expression of serine-type peptidase activity, specifically *Klk5/6/8* - members of the kallikrein (KLK) family of secreted serine proteases involved in regulating desquamation and inflammation (Kishibe, 2014; Nauroy and Nyström, 2020). The top two GO terms enriched for the 44 genes that were downregulated in iDKO epidermis included receptor ligand activity (e.g., *Bmp2/3, Epgn,* and *Wnt16*) and neurotrophin binding (e.g., *Ngfr* and *Ntrk2*) (Figure 2E), some of which are known to be involved in epidermal fate control and keratinocyte proliferation/survival (Adly et al., 2017; Cai et al., 2019; Kandyba et al., 2013; Mendoza-Reinoso and Beverdam, 2018; Richardson et al., 2009).

We also performed gene set enrichment analysis (GSEA) on genes expressed in iDKO vs. control epidermis using Hallmark gene signatures, which identified EMT and apical junction as being significantly enriched in iDKO epidermis (Figure 2F; Table S2). Interestingly, GSEA also identified a significant enrichment of inflammatory gene signatures (e.g., inflammatory response, interferon gamma response, IL2-STAT signaling, and complement) in iDKO epidermis (Figure 2F). A closer look into the immune-associated genes revealed the increased expression of different cytokines, chemokines and chemokine receptors (Table S2). Of particular interest, several genes known to be enriched in LCs, which include T cell chemokine gene *Ccl22* and major histocompatibility complex (MHC) class II genes *H2-Aa, H2-Ab1,* and *H2-Eb1* (Cumberbatch et al., 1991; Esaki et al., 2015), were also upregulated in iDKO epidermis (Figure 2A-B; Tables S1-2). RT-qPCR analysis of epidermal RNAs confirmed the significantly elevated expression of *Ccl22* in iDKO epidermis at both 25 and 52 DPI (Figure 2G). Collectively, our data so far underscore the altered expression of genes associated with EMP, cell adhesion, actin cytoskeleton, and inflammatory response as molecular consequences of *Ovol1/2* deletion in adult epidermis.

In previously published single-cell RNA-seq studies, we identified molecular signatures of epidermal basal and spinous cells and dermal fibroblasts in adult homeostatic skin (Haensel et al., 2020; Vu et al., 2022). To better define how *Ovol1/2* loss impacts the process of epidermal differentiation, we performed GSEA on genes expressed in iDKO vs. control epidermis using these signatures. Our analysis revealed significantly enriched expression of fibroblast markers and a trending enrichment of spinous markers in iDKO epidermis, whereas the expression of basal markers was significantly de-enriched (Vu et al., 2022) (Figure 2H; Table S2). As basal cells in adult skin exist in four major transcriptional

states, namely *Col17a1H*^{igh}, early response (ER), proliferative, and growth arrested (GA) (Haensel et al., 2020), we also performed GSEA using top markers of these basal cell states. Interestingly, a significant de-enrichment was seen for ER and GA state markers, but not for *Col17a1H*^{igh} or proliferative state markers (Figure 2I; Table S2). Taking these molecular alterations together with aberrant EMP gene expression detected by analyses from above, we extrapolate that *Ovol1/2*-deficient adult epidermal cells gain fibroblast-like molecular characteristics at the specific expense of basal ER/GA transcriptional states, whereas the basal stem-like (*Col17a1H*^{igh}) and spinous states are apparently spared (Figure 2J).

Chromatin immunoprecipitation (ChIP)-seq and integrative analyses reveal both cytoskeleton-associated and immune-modulatory genes as common, direct downstream targets of Ovol1 and Ovol2

To further elucidate the molecular mechanisms of Ovol1/2 function, we performed ChIP-seq analysis on adult skin epidermis to identify potential direct Ovol1 targets genome-wide. Using MACS2 narrow peak calling, a total of 1177 Ovol1-bound peaks were identified that passed a significance threshold (q value < $^{0.05}$) (Table S3). A large fraction (59.3%) of the peaks were found to reside in gene promoter regions within 1 kb of the transcription start site (TSS) (Figure 3A), suggesting preferential binding of Ovol1 to proximal gene promoters. Substantial binding to promotor regions at 1-3 kb upstream of TSS (6.4%) and to distal intergenic sequences (16.8 %) was also seen (Figure 3A). Homer analysis revealed that 49.95% of the Ovol1-bound loci contain at least one consensus binding motif (CCGTTA) (Figure 3B), which is identical to the consensus sequence previously identified for recombinant Ovol1 binding using an in vitro site selection assay (Nair et al., 2007).

Mediascape analysis of the Ovol1-bound genes revealed cell cycle process, regulation of cytoskeleton organization, and cell part morphogenesis as top terms (Figure 3C; Table S4), suggesting a direct role of Ovol1 in regulating these processes.

Ovol2 binds to a similar DNA sequence motif as Ovol1 both in vitro and in cultured mammary epithelial cells (MECs) (Nair et al., 2007; Watanabe et al., 2014; Wells et al., 2009). To compare Ovol1-bound and Ovol2-bound loci, we reanalyzed our previously published Ovol2 ChIP-seq data (Watanabe et al., 2014) using the same parameters used for Ovol1 ChIP-seq. As reported (Watanabe et al., 2014), Ovol2 also preferentially binds to gene promoter regions (59.6%) and distal intergenic sequences (16.5%) (Figure 3A). Interesting, the exact spatial patterns of promoter occupancy differ for Ovol1 and Ovol2 (Figure 3D), possibly reflecting differences in cell types (epidermis vs. MECs) and/or precise protein-DNA interfaces. This said, and despite each having its own unique binding loci (697 for Ovol1 and 849 for Ovol2), 361 genes bound by Ovol1 in epidermis are also bound by Ovol2 in MECs (Figure 3E). Comparing Ovol1 and Ovol2 ChIP-seq tracks at select target loci against tracks for histone modifications (H3K27Ac, H3K4me1, and H3K4me3, marks for active chromatin, enhancer, and promoter, respectively) in mouse epidermis (Bae and Lesch, 2020; Rada-Iglesias et al., 2011; Sethi et al., 2017; Spicuglia and Vanhille, 2012) revealed the co-localization of Ovol1- and/or Ovol2-binding peaks with one or more of these histone marks (Figures 3F, S2A). The emerging picture is that Ovol1 and Ovol2 can bind to both weakly and strongly active promoters or enhancers.

GOCompare analysis (https://github.com/ccsosa/GOCompare) of all Ovol1-bound versus Ovol2-bound genes revealed common terms such as phospholipid binding, transcription coregulator activity, actin binding, tubulin binding, and microtubule binding

(Figure 3G). Furthermore, Metascape analysis of genes bound by both Ovol1 and Ovol2 identified cell cycle process, positive regulation of organelle organization, and regulation of microtubule-based process as top functional terms (Figure S2A; Table S4). These findings underscore the potential of Ovol1 and Ovol2 to regulate common downstream target genes and cellular/molecular processes, which include cytoskeleton-associated functions. This said, results of the GOCompare and Metascape analyses also suggested some functional specialization, with Ovol1 primarily being involved in epidermal cell homeostasis/differentiation and Ovol2 in cell adhesion and migration (Figures 3G, S2B; Table S4).

We also compared Ovol1-bound and Ovol2-bound genes to the Genotype-Tissue Expression (GTEx) datasets. Ovol1/2-bound genes that are expressed in skin (sun-exposed and non-exposed) were found to most closely correlate with genes expressed in epithelial tissues such as vagina, esophagus, salivary gland, kidney, prostate, and intestine (Table S5). This finding supports the possibility that Ovol1 and Ovol2 may play a general regulatory role in maintaining epithelial tissue functions.

To identify functional and direct targets of Ovol1 and Ovol2 (i.e., bound by Ovol1 and/or Ovol2 and differentially expressed between iDKO and control epidermis), we compared Ovol1 and Ovol2 ChIP-seq datasets with the RNA-seq data from above. GSEA of 52 DPI RNA-seq data against ChIP-seq targets showed that genes with elevated expression in iDKO compared with control epidermis, but not genes with reduced expression, trended toward being enriched for both Ovol1- and Ovol2- bound peaks (Figure 3H; Table S4). This data is consistent with the reported finding that Ovol1/2 proteins act predominantly as transcriptional repressors (Nair et al., 2006, 2007; Watanabe et al., 2014). Comparison of

Ovol1/2-bound gene lists with >2-fold DEG lists at 25 and 52 DPI revealed a small number of top Ovol1 and/or Ovol2 target genes, most of which were upregulated upon *Ovol1/2* loss (Figure 3I; Table S4). Importantly, the core set of genes upregulated in iDKO epidermis at both 25 and 52 DPI, which include *Zeb1*, *Vim, Lix1l, Flot2, Dennd5a*, and *Ccdc88a,* are among the top targets bound by both Ovol1 and Ovol2 (Figure 3F).

Considering that Ovol1/2-bound loci may exert long-range gene regulatory activities, we used BEDTools closest function (Quinlan and Hall, 2010) to find which gene's TSS is closest to a given peak and compared the resulting expanded list with DEGs >2-fold upregulated in iDKO epidermis at 25 and 52 DPI. This yielded a greater number of potential Ovol1/2 target genes, and a majority of them (e.g., 29 for Ovol1, 37 for Ovol2, and 22 for Ovol1/2 at 52 DPI) were upregulated upon *Ovol1/2* loss (Figures 3J, S2C-D; Table S4). Metascape analysis of the Ovol-bound and upregulated-at-52DPI genes showed Ovol1 targets to be associated with terms including MHC II protein complex assembly (e.g., *H2-Aa, H2-Ab1*, and *H2-Eb1*), skin development, and cell-substrate adhesion; Ovol2 targets to be associated with terms including lymphocyte activation, response to wounding, and actin filament organization; and Ovol1/2 common targets to be associated with terms including negative regulation of neuron projection development and positive regulation of leukocyte cell-cell adhesion (Figure S2C; Table S4). *Ccl22* was identified as a d gene bound by both Ovol1 and Ovol2 in the list of the "expanded" peaks that overlap with DEGs upregulated in iDKO at 52 DPI (Tables S1, S4). Peaks for Ovol1, Ovol2, and H3K27Ac were identified in the downstream intergenic region (~21.8 kb from the *Ccl22* promoter) that contains an Ovol consensus motif, suggesting this site might be a potential enhancer (Figure 3J). Although not significantly upregulated in iDKO epidermis at the time points examined, additional

inflammation-associated genes, such as *Il12b*, *Il6*, *Nfkb2*, *Cx3cl1*, *Ccl27a* and *Ccl17* were found to be adjacent to Ovol1-bound or Ovol2-bound enhancers/promoters (Table S3), suggesting that they are also potential Ovol1/2 targets.

Taken together, our results show that Ovol1 and Ovol2 regulate both overlapping and distinct target genes that are involved in diverse biological processes, of which two main categories are EMP/cytoskeleton and inflammation/immunity.

Ovol1/*Ovol2* iDKO skin exhibits precocious LC activation and heightened γδT/CD4$^+$ T cell responses and abnormal immune composition changes

The identification of inflammatory genes as Ovol1/2 targets prompted us to examine whether loss of *Ovol1* and *Ovol2* from the epidermis induces local changes in skin immune cells. The mouse epidermis contains two resident immune cell types: 1) LCs, epidermal-resident, dendritic-like antigen-presenting cells that maintain tolerance in homeostasis but instigate an inflammatory response after perturbation (Doebel et al., 2017; Merad et al., 2008; Vulcano et al., 2001); 2) DETCs, which normally contribute to epidermal homeostasis but release cytokine/chemokines to recruit inflammatory cells and facilitate keratinocyte-immune cell cross-talk in response to perturbation (MacLeod and Havran, 2011). Interestingly, the abundance and morphology of LCs have been shown to depend on neighboring epidermal cells (Park et al., 2021). Flow cytometry on trypsin-isolated epidermis from iDKO and control mice revealed that although there may be a trending decrease in percent of LCs of CD45$^+$ (all immune) cells in iDKO, the total numbers of immune cells, LCs and DETCs per gram of tissue were not significantly affected (Figures 4A, S3A-B). Interestingly however, the mean fluorescent intensity of MHCII staining was significantly

higher in LCs from iDKO epidermis compared with control counterparts (Figure 4B). As MHC II upregulation is a feature of activated LCs that are known to exhibit a more rounded morphology(Van den Bossche and Van Ginderachter, 2013; Yan et al., 2020), we performed whole-mount immunostaining on back skin epidermal sheets to visualize the langerin$^+$ (CD207) LCs in their natural environment. We also co-stained the epidermal sheets for adherence junction component β-catenin, which revealed somewhat reduced membrane signals in iDKO samples (Figure 4C), consistent with reduced epidermal cell adhesion observed in preceding sections. Compared to LCs in control epidermis that extended multiple dendrites (Yang et al., 2021), LCs in iDKO epidermis showed a more rounded morphology and lack extensive dendritic projections (Figure 4C-D). Collectively, these data show that LCs in iDKO epidermis are in a preciously "activated" state (Kubo et al., 2009; Nishibu et al., 2006; Redd et al., 2016).

We also surveyed the immune cell populations in control and iDKO dermis. There was a trending increase in the number of immune cells (CD45$^+$) and of T cells (CD3$^+$) per gram of tissue in iDKO dermis compared to control dermis, but the differences were not statistically significant (Figure S3C-D). γδT cells are dermal resident, innate-like T cells important for cutaneous immunosurveillance (Castillo-González et al., 2021; O'Brien and Born, 2015; Sumaria et al., 2011). Their relative abundance out of immune cells was significantly increased, and their quantity per gram of tissue was trending toward being increased, in iDKO dermis compared to control dermis (Figures 4E, S3E). Contrastingly, the abundance of FoxP3$^+$ regulatory T cells (Tregs), shown to be immune-suppressive and with a role in hair follicle cycling (Ali and Rosenblum, 2017; Ali et al., 2017), was not significantly altered (Figures 4E, S3E). CD4$^+$ T cells were a relatively minor immune cell population in control

skin and their percent out of immune cells was significantly increased in iDKO dermis (Figure 4F, S3F). Of the innate, myeloid-derived immune cells, $CD11B^+$ $F4/80^-$ cells and macrophages were the most abundant populations (>30% each out of total immune cells), whereas neutrophils were barely detectable (Figures 4G, S3G). The relative abundance of these populations was unchanged between control and iDKO dermis (Figures 4G, S3G). Importantly, we also observed significantly increased abundance of T cells, specifically □□T and $CD4^+$ T cells, out of immune cells but unchanged as cells per gram of tissue in the iDKO paw skin relative to the control paw skin (Figures 4H, S3H). Concurrent reductions in dermal γδT and $CD4^+$ T cells have been previously observed (Sumaria et al., 2011). Taken together, our data suggest heightened γδT and $CD4^+$ T cell responses in both back and paw skin of iDKO mice.

$CD4^+$ T cells are known to be activated in regional skin-draining lymph nodes (LNs) and then migrate to skin (García Nores et al., 2018). We found that compared to littermate controls, skin-draining LNs in iDKO mice were significantly larger (Figure 4I-J) and contained an increased number of immune cells (Figure 4K). While we did not observe skewing towards any specific T cell subset (Figure S3I), the total numbers of all T cell populations examined (e.g., γδT, $CD4^+$) per LN were increased in iDKO mice (Figure 4L-M). Moreover, the total numbers of LCs and $MHCII^+$ cells were higher in the skin-draining LNs of iDKO mice compared to the controls (Figure 4N-O). These data, together with the precocious activation of LCs and increased abundance of dermal γδT /$CD4^+$ T cells in iDKO skin support the notion that iDKO mice suffer from local long term immune cell changes that features aberrant innate and adaptive T cell responses.

***Ovol1/2* iDKO mice fail to accumulate fats, increase carbohydrate-fueled energy expenditure, and their whole-body defects are partially rescued by Dex treatment**

Immune cell dysfunction and chronic inflammation can affect both metabolism and body weight (Bindels and Thissen, 2016; Chen et al., 2019; Freigang et al., 2013; Pfitzenmaier et al., 2003). Thus, the iDKO mice offered a useful model for us to examine potential long-term consequences of *Ovol1/Ovol2* deletion at the whole-body level. Interestingly, around 85 DPI (~4 months of age), iDKO mice started to exhibit a visibly smaller body size than their control littermates, a phenotype that further exacerbated over time (Figures 5A-C, S4A). By ~200 DPI (8 months of age), these mice also showed signs of premature aging (e.g., hunched stature and puffy eyes) (Figure S4A). Consistently, GSEA of the 52 DPI RNA-seq data revealed enriched expression of genes upregulated in skin basal cells of aged mice compared to young counterparts in two published datasets (Ge et al., 2020; Keyes et al., 2016) (Figure S4B). Older iDKO mice also exhibited ruffled and greasier fur than their littermate controls (Figures 5A, S4C-D). While the percent of various hair types, average hair lengths, and hair cycle progression were not obviously different between iDKO and control mice (Figures 5D, S4C-D), the iDKO skin showed a significant reduction of adiposity in their dermal fats (dWAT) by 3 MPI, and by 9 MPI the dWAT near-completely disappeared in some cases (Figure 5D-E). Furthermore, RT-qPCR analysis revealed significant (*Tnfa*) and trending (e.g., *Il1B, Cxcl10*) expression increases of several inflammatory cytokine/chemokines in dWAT of iDKO mice (Figure S4E), consistent with an overall inflammatory skin microenvironment.

Tracking body weight over time revealed that compared with control littermates, iDKO mice failed to gain weight (rather than losing weight) and this became particularly evident starting at ~3 MPI (4 months of age) (Figure 5A,C). As a control, iDKO mice that were

not treated by TAM gained weight properly (Figure S4F). Using EchoMRI to analyze body mass composition, we found that iDKO mice show reduced fat mass (but no change in lean mass) compared to their littermate controls detectable at ~4 MPI (5 months of age) but not at ~2-3 MPI (3-4 months of age) (Figures 5F, S4G; also see below). Reduced body fat can be caused by activation of thermogenesis in brown adipose tissue (BAT) (Cannon and Nedergaard, 2004; Matsushita et al., 2021), but our RT-qPCR analysis did not detect any statistically significant difference in the expression of thermogenesis-associated genes in iDKO BAT (Figure S4H). We also did not observe any detectable difference in the body temperature between iDKO and control mice (Figure S4I). Interestingly, analysis of inguinal white adipose tissue (iWAT) revealed statistically significant decrease in the expression of *Lipe* and *Mgll,* as well as trending decrease in *Atgl*, all encoding enzymes involved in lipolysis, in iDKO mice compared with their littermate controls (Figure S4J). In contrast, the expression of *Fasn*, encoding fatty acid synthase, was not different between control and iDKO iWAT (Figure S4J). Moreover, inflammatory genes previously implicated in cachexia-associated weight loss, *Ifng, Il1a*, and *Tnf* (Baazim et al., 2019, 2021) showed trending or significant increases in expression in iDKO iWAT (Figure S4K). These findings reveal overall body fat loss accompanied by decreased lipolysis as a long-term consequence that associate with adult-onset *Ovol1/2* deletion in epidermis.

To further understand the global metabolic changes occurring in iDKO mice, we performed metabolic cage analysis. At all ages examined, food intake of the iDKO mice were not significantly different from the control littermates, and movement was slightly decreased at 4-5 MPI (~5-6 months of age) (Figures 5G-H, S4L-M). At 2-3 MPI (~3-4 months of age) when weight phenotype was not yet pronounced, there was no statistically significant

difference between iDKO and control mice in respiratory exchange ratio (RER) (Figure S4N-O). By 4-5 MPI when body weight difference was evident, RER was significantly higher at night in iDKO mice than control littermates and the difference was exacerbated by exposure to cold temperature (Figure 5I-J), suggesting that epidermal *Ovol1/2* loss led to a switch in fuel utilization from fats to carbohydrates (Ramos-Jiménez et al., 2008; Škop et al., 2020; Speakman, 2013). Importantly, iDKO mice compared to the controls showed trending and significant increases in energy expenditure/kg body weight at 2-3 MPI and 4-5 MPI, respectively, that persisted upon cold exposure (Figure 5K, S4P). These whole-body metabolic changes are not accompanied by detectable metabolic reprogramming of epidermal cells per se, as mitochondrial respiration and glycolysis - measured as oxygen consumption rate (OCR) and extracellular acidification rate (ECAR), respectively - in iDKO epidermis were comparable to the control counterparts (Figure S4Q). Together, our results demonstrate that the barrier-deficient iDKO mice fail to accumulate fat and they undergo whole-body metabolic adaptation to increase carbohydrate usage and energy expenditure but not at the expense of lean mass.

To begin probing whether aberrant immune response and inflammation in iDKO mice contribute to their whole-body phenotype, we first performed experiments to block γδTcell function through i.p. injection of a neutralizing antibody against γδTCR (Figure S5A). While γδT cells exhibited reduced γδTCR detection in flow cytometry suggesting effectiveness of the treatment, the γδTCR antibody-treated iDKO mice still showed detectable barrier dysfunction, displaying higher TEWL than that of antibody- or IgG-treated control littermates and similar to that of the IgG-treated iDKO littermates at 4 MPI (Figure S5B-D). Intriguingly, γδTCR blockage seemed to increase the body weight of both iDKO and control

mice, but the weight and fat percentage differences between respective iDKO and control mice persisted (Figure S5E-H). Furthermore, the difference between control and iDKO mice in the size of skin-draining LNs remained despite γδTCR antibody treatment, whereas the size of spleens was the same across genotypes/conditions (Figure S5I-J). These data argue against a role for γδT cells in causing the weight/fat reduction of iDKO mice.

We next turned to administering Dex, a widely used inflammatory suppressant in mice and human (Barshes et al., 2004; Giles et al., 2018; Lay et al., 2018), to the skin of iDKO and control mice (Figure 6A-B). Dex treatment drastically reduced the size of both spleen and skin-draining LNs (Figure 6C-D). Interestingly, it reduced the MFI of MHC II on LCs in the epidermis and reduced the total number of immune cells such as LCs, MHC II expressing cells, and various T cell populations within the LNs, of both control and iDKO mice (Figure 6E-J), consistent with its known immune-suppressive effect. While the differences between control and iDKO mice in LN size and antigen-presenting cells (MHC II^+, including LCs) content persisted despite Dex treatment (Figure 6D, G-H), Dex was able to normalize the numbers of T cell populations in iDKO LNs to the same levels as that in Dex-treated control littermates (Figure 6D-J). Importantly, Dex-treated iDKO mice no longer differed significantly in TEWL and body weight from their Dex-treated control littermates monitored through 4-5 MPI (Figure 6B, K-L). Furthermore, in contrast to non-DEX-treated iDKO mice showing significant deviations in fat and lean mass from control littermates at 4 MPI (Figures 5F, and 6M-N), Dex-treated iDKO mice at this stage showed largely similar body fat content as their Dex-treated control littermates (Figure 6M-N). These findings show that Dex administration partially rescues the T cell responses as well as the barrier, weight and fat

phenotypes in iDKO mice, providing tantalizing evidence that immune cell changes in the skin of iDKO mice contributes to their whole-body changes.

DISCUSSION

Our study has unraveled previously unknown transcriptional regulators of adult barrier maintenance. Similar to their roles in embryonic barrier development (Lee et al., 2014), *Ovol1* and *Ovol2* suppress the aberrant expression of EMT-associated genes such as *Zeb1* and *Vim*, highlighting a shared function in controlling the extent of EMP in embryonic and adult epidermis. Importantly, our work identifies other common direct and functional targets of Ovol1/2 that include genes associated with cytoskeletal structure and cellular adhesion (e.g., *Lix1l, Flot2, Ccdc88a,* and *Dennd5a*). These overlapping molecular functions provide a mechanistic explanation for the redundant/compensatory roles of Ovol1 and Ovol2 in skin barrier development and maintenance, and they broaden the initial view that Ovol1 and Ovol2 are simply EMT regulators. The *Ovo* prototype, *Drosophila Ovo/Svb* is known to be a master regulator of actin cytoskeletal reorganization (Stern and Franke, 2013), and our data now show that this function is evolutionarily conserved in mammalian skin. Based on our finding that Ovol1/2 downstream targets align with genes expressed in various other epithelial tissues throughout the body, particularly the stratified epithelia such as vagina and esophagus (Xiao et al., 2020), we speculate that *Ovol1/2* play a general role in regulating epithelial cytoskeleton and adhesion especially in barrier tissues.

The specific and significant reduction of ER/GA basal transcriptional states but not *Col17a1H*^{igh} basal, proliferative basal, and spinous transcriptional/cell states, together with the upregulation of fibroblast-like gene expression in iDKO epidermis raises interesting points regarding epidermal homeostasis and mechanism of *Ovol1/2* action. 1) The GA basal

state is likely a point of divergence where *Ovol1/2*-deficient epidermal cells lose proper control of EMP and gain aberrant mesenchymal features. This is interesting in light of our previous finding that GA basal transcriptional state scores the highest for EMT-like gene signature and is enriched predominantly at the migrating front during wound healing (Haensel et al., 2020). It is probable that GA represents a transient plastic state to enable the migration and subsequent differentiation of epidermal basal stem/progenitor cells, but this plasticity needs to be strictly controlled to ensure proper homeostasis and repair ((Haensel et al., 2020); this work). By directly regulating cytoskeletal organization and keeping EMP in check, *Ovol* genes likely occupy a central position in promoting the plasticity of GA cells but at the same time preventing them from going "overboard" to gain excessive mesenchymal traits. 2) Although our previous computational work predicts a sequential progression of basal cells through GA to become spinous cells (Haensel et al., 2020), it seems that a GA state and spinous gene expression can be uncoupled at least under some conditions such as in iDKO epidermis. In the absence of functional *Ovol1/2*, basal cells occupying the GA transcriptional state may even precociously but aberrantly undergo spinous differentiation leading to their own depletion.

Epidermal barrier dysfunction has been linked to skin inflammation such as in psoriasis and AD, but its causal and mechanistic roles remain elusive. Importantly, we find evidence that epidermis-originated *Ovol1/2* loss is sufficient to trigger local, low-grade immune composition changes in skin. iDKO mice exhibit precocious LC mobilization, an apparent shift in immune cell populations favoring γδT and $CD4^+$ T cells evident in both back and paw skin, as well as enlarged skin-draining LNs with increased abundance of LCs and T cells. It has been speculated that loss of contact with epidermal cells drives transcriptional

changes in LCs to promote tolerogenic T cell response and immune homeostasis (Sirvent et al., 2020). Evidence also suggests that LC dendrite structure and morphology adapt to epidermal cell junctional spaces (Park et al., 2021). Finally, keratinocytes and LCs are known to share transcripts through intercellular connections (De La Cruz Diaz and Kaplan, 2019; Su and Igyártó, 2019). Indeed, *Ovol1* and *K14* transcripts are detected in LCs (http://rstats.immgen.org/Skyline_microarray/skyline.html) (and our data not shown). Along these lines, the reduced adhesive properties of *Ovol1/2*-deficient epidermal cells likely drive aberrant activation of LCs. We also cannot formally exclude the possibilities that Ovol1/2 act cell-autonomously within LCs, or that *Ovol1/2*-deficient epidermal cells alter their expression of inflammatory cytokines that normally signal to LCs. Among the immune-modulating genes upregulated in iDKO epidermis and/or bound by Ovol1/2, *Ccl22* is of particular interest because it can recruit either Tregs or effector T cells depending on the local immune microenvironment (D'Ambrosio et al., 1998; Iellem et al., 2001). In addition to enrichment in LCs, *Ccl22* is known to be upregulated in keratinocytes of lesional atopic dermatitis skin (Guttman-Yassky et al., 2009). Therefore, dysregulation of *Ccl22* potentially ties together epidermal perturbation, precious LC activation, and T cell accumulation in iDKO skin. Future experiments are needed to test these intriguing possibilities.

Skin-specific deletion of several genes in mice have led to changes in body weight (Binczek et al., 2007; Chen et al., 2019; Egawa et al., 2016; Oji et al., 2010; Sampath et al., 2009; Sano, 2015; Schmuth et al., 2015). For example, overexpression of Tslp, a cytokine involved in T helper cell 2 immune response associated with atopic dermatitis-like inflammation, protects against weight gain and fat accumulation, and mutation in *Gasdermin-A3* triggers thermogenesis in BAT through epidermal secretion of IL-6 cytokine (Chen et al.,

2019; Choa et al., 2021). Similarly, *K14-Cre*-driven deletion of *Scd1* causes reductions in fats and body weight due to lack of insulation and increased thermogenesis (Sampath et al., 2009). Our study now adds *Ovol1/2* iDKO to the growing list of genetic perturbations in mouse skin epidermis that result in adipocyte and whole-body defects. Importantly, our proof-of-principle finding that Dex treatment partially rescues the LC activation in the epidermis, LN, T cell, body weight and adiposity changes in iDKO mice underscores immune cells as a critical missing link between epidermal dysregulation and whole-body metabolism.

A defective epidermal barrier would result in excessive heat and water loss. In order to sustain all metabolic functions including maintaining a stable body temperature, animals must counter heat loss through behavioral changes (e.g., huddling), mechanical insulation (e.g., increasing fur density), or increasing the active generation of heat through metabolic reprogramming (Forni et al., 2017). Energy expenditure can occur in many forms: through internal metabolism, heat production, and physical activity (Wilson et al., 2019). Since iDKO mice move less and muscle mass is the same, and not increased (Periasamy et al., 2017; Weiss et al., 2017) between iDKO mice and control, one conclusion is that iDKO mice are releasing more energy as heat. This is curious as I did not detect any consistent changes in thermogenesis gene expression from BAT (one of the main thermogenic tissues in mice) (Speakman, 2013; Zhao et al., 2022). Another possibility is that iDKO mice expend more energy as shivering which can also utilize carbohydrate stores as shown by cold exposure studies (Research et al., 1996; Vallerand and Jacobs, 1989). However, more metabolic studies would need to be done to isolate the exact metabolic tissues responsible for increase energy demand in iDKO mice. Tracking isotype labeled glucose molecules is one such experiment that could reveal the tissues with a higher energy demand in iDKO mice

(Haman et al., 2004; Jung et al., 2021). Due to their proximity to the epidermis, it has been postulated that the dermal fats can shuttle fatty acids to keratinocytes to help facilitate barrier maintenance (Rivera-Gonzalez et al., 2014). It would be interesting to test whether increasing the availability of fat or carbohydrates would be sufficient to rescue the body weight, alter the energy metabolism, and help rescue barrier. Understanding the metabolic landscape could provide insights into how barrier defects and inflammation can affect metabolism.

Given the literature showing connections between inflammation and metabolism we speculated that barrier defects might be causing low-grade, chronic inflammation that was affecting weight gain. While γδT cells were among one of the few immune cells in skin to be altered in the mutant, blocking antibody against γδT cells did not affect barrier defects nor body weight changes in mice. This suggests that alteration in γδT cells populations is likely a consequence of damaged barrier than a trigger for localized inflammation. However, γδT cells are found in and may affect metabolic processes in many other tissues, including iWAT, so we cannot rule out the possibility that inhibition of γδT cells was not causing a direct effect on fat pads (Hu et al., 2020). Importantly, I found that inhibiting inflammation using the steroid dexamethasone was able to partially rescue the weight/fat phenotype and notably reducing lymph node size and T cell populations. This suggests that inflammation is at least to some extent responsible for the metabolic changes. However, since dexamethasone has known functions in activating adipogenesis, further work would need to be done to understand the direct contribution of dexamethasone to fat accumulation in iDKO mice (Zubiría et al., 2020). Interesting to note, is that dexamethasone brought baseline levels of immune cells down in the lymph nodes, but differences still existed between iDKO and

control. This suggests that the triggers for differences in immune composition within the iDKO mice are not rescued, just reduced down to levels that are no longer as detrimental to the mice. One speculation is that LCs and MHC II^+ cells are still slightly more activated in the iDKO mice compared with control and this is responsible for the subtle changes in T cell composition. Similar to universal medicines used in the clinic, this work shows that even though specific differences between control and iDKO could not be rescued, there are threshold levels of inflammation that permit rescue despite resilient triggers.

Our findings suggest that increased energy production from carbohydrates is a way by which barrier-deficient iDKO mice meet the increased metabolic demands. In contrast, iDKO mice show decreased expression of lipolysis genes in iWAT, suggesting that they do not efficiently use lipolysis as a means to mobilize triglyceride stores for energy production (Ahmadian et al., 2007; Grabner et al., 2021). Adipocyte tissue lipids are mobilized for energy through lipolysis during acute inflammation and sepsis (Feingold et al., 1992; Jha et al., 2014; Sherwood et al., 1970), whereas catecholamine-induced lipolysis is reduced in chronic metabolic inflammation (Mowers et al., 2013). Moreover, chemical inhibition of lipolytic enzyme Atgl inhibits adipose tissue lipolysis while protecting mice from high fat diet-induced obesity (Schweiger et al., 2017). Thus, it is possible that epidermal barrier dysregulation and its associated aberrant immune cell responses instigate whole-body metabolic reprogramming in a manner that differs from what occurs during acute inflammation.

Figure 4.1: Induced deletion of *Ovol1* and *Ovol2* in adulthood leads to skin epidermal defects.

- **A.** Time course of TEWL measurements in control and iDKO mice prior to (-2 DPI – 0 DPI) and following TAM injections. n=4 pairs.
- **B.** H/E images of mouse epidermis from control and iDKO mice at 15 DPI.
- **C.** TEM images of control and iDKO mice at 15 DPI. Red arrows point to gaps in cellular adhesion and yellow arrows point to abnormal keratohyalin granules. SC is stratum corneum.
- **D.** Volcano plot of differential lipid contents between control and iDKO epidermis.
- **E.** Ion counts of the indicated lipid species. Control: n=7; iDKO: n=4.
- **F.** Images of the paws of control and DKO mice at 7 months post-first injection (MPI) (~9 months old).
- **G.** Quantification of toe thickness in control and DKO mice (n=6 pairs).
- **H.** H/E images of toes at 7 MPI.
- **I.** Representative immunofluorescent images of the toe pad for filaggrin (FLG). K14 marks basal keratinocytes and DAPI marks nuclei.
- **J.** Quantification of the average size of filaggrin$^+$ deposits at 52 DPI as shown in (I). n=3 pairs.

Data information: Scale bar: 20 μm in (B), 1 μm in (C), 250 μm in (H), and 25 μm in (J). For statistical analysis in (A, G, J), we used an unpaired two-tailed Student's t-test. *** $p<0.005$; ** $p<0.01$; * $p<0.05$. Errors bars are represented as ± SD.

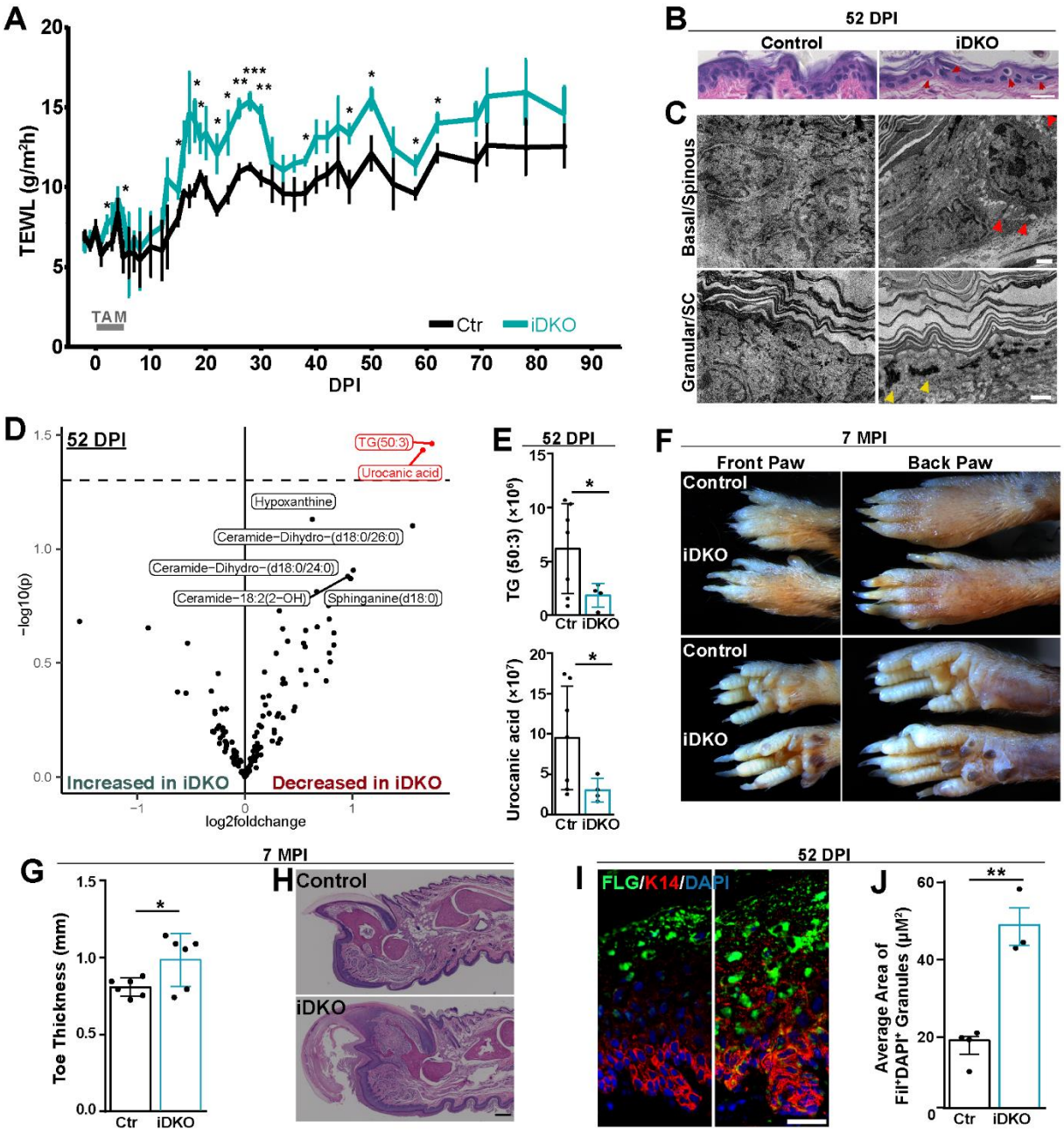
A
TEWL (g/m²h)
DPI
TAM
Ctr
iDKO
B
52 DPI
Control
iDKO
C
Basal/Spinous
Granular/SC
D
52 DPI
TG(50:3)
Urocanic acid
Hypoxanthine
Ceramide−Dihydro−(d18:0/26:0)
Ceramide−Dihydro−(d18:0/24:0)
Ceramide−18:2(2−OH)
Sphinganine(d18:0)
−log10(p)
log2foldchange
Increased in iDKO
Decreased in iDKO
E
52 DPI
TG (50:3) (×10⁶)
Urocanic acid (×10⁷)
Ctr iDKO
F
7 MPI
Front Paw
Back Paw
Control
iDKO
G
7 MPI
Toe Thickness (mm)
Ctr iDKO
H
Control
iDKO
I
52 DPI
FLG/K14/DAPI
J
Average Area of Fil⁺DAPI⁺ Granules (μM²)
Ctr iDKO

Supplemental Figure 4.1: Additional data on back and paw skin defects in iDKO mice.

- **A.** RT-qPCR of the indicated genes in epidermis at 25 DPI. n=4 pairs.
- **B.** RT-qPCR of the indicated genes in epidermis at 52 DPI. Control: n=10; iDKO: n=6.
- **C.** Ion counts of the indicated lipid species: hypoxanthine.
- **D.** Ion counts of the indicated lipid species: ceramide-dihydro(d18:0/26:0).
- **E.** Images of front (left) and back (right) paws of control and DKO mice at the indicated times.
- **F.** Quantification of toe thickness in control and iDKO mice at 52 DPI. Control: n=5; iDKO: n=3.
- **G.** Representative immunofluorescent staining of the indicated proteins in toe pads at 52 DPI.
- **H.** Quantification of immunofluorescent staining of the indicated markers. n=3 pairs for K1/Lor.
- **I.** Quantification of immunofluorescent staining of the indicated markers. n=4, 2 pairs for Fil.
- **J.** Representative immunofluorescent staining of the indicated proteins in toe pads at 52 DPI.
- **K.** Quantification of immunofluorescent staining of the indicated markers. n=2 pairs for Ki67.

Data information: Scale bar: 100 μm in E. For statistical analysis in (A-K), we used an unpaired two-tailed Student's t-test. *** $p<0.005$; ** $p<0.01$; * $p<0.05$. Errors bars are represented as ± SD.

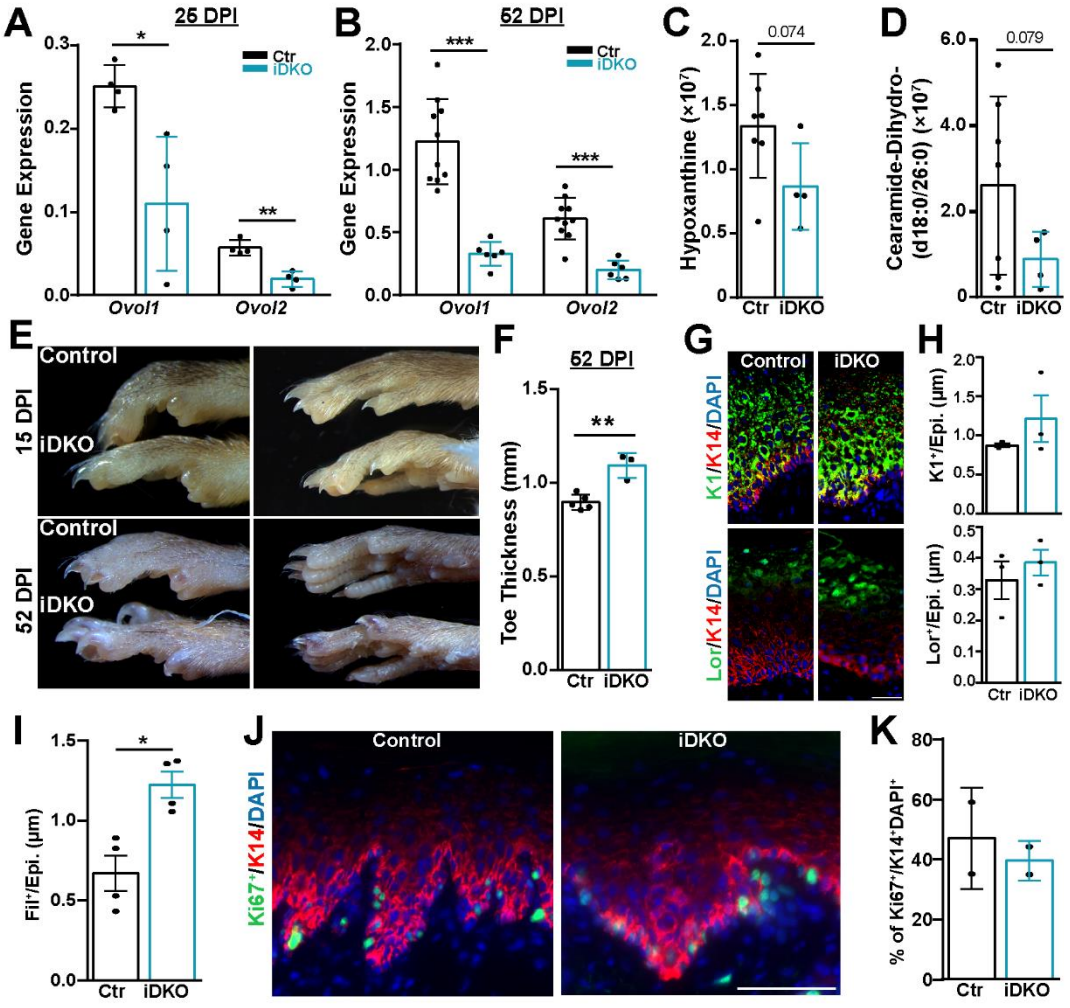
A
25 DPI
Gene Expression
Ctr
iDKO
Ovol1
Ovol2
B
52 DPI
C
Hypoxanthine (×10⁷)
0.074
D
Cearamide-Dihydro-(d18:0/26:0) (×10⁷)
0.079
E
Control
iDKO
15 DPI
52 DPI
F
Toe Thickness (mm)
G
K1/K14/DAPI
Lor/K14/DAPI
H
K1⁺/Epi. (μm)
Lor⁺/Epi. (μm)
I
Fil⁺/Epi. (μm)
J
Ki67⁺/K14/DAPI
K
% of Ki67⁺/K14⁺DAPI⁺

Figure 4.2: Transcriptional and cell state changes in adult epidermis as a consequence of *Ovol1/2* deficiency.

- **A.** (A-B, D-F, H-I) RNA-seq of control and iDKO mouse epidermis at 25 and 52 DPI. n=2 pairs per time point. (A) Volcano plots.
- **B.** Venn diagrams of DEGs from separate Ovol1 vs. Ovol2 data (top) and aggregated data (bottom) analyses. The 12 DEGs shared between 25 and 52 DPI is shown in the orange box.
- **C.** RT-qPCR of the indicated genes in epidermis at the indicated times. For 25 DPI, n=4 pairs. For 52 DPI, Control: n=10; iDKO: n=6.
- **D.** Enricher Go molecular function analysis of genes up-regulated in iDKO epidermis compared with control.
- **E.** Enricher Go molecular function analysis of genes down-regulated in iDKO epidermis compared with control.
- **F.** GSEA using the indicated Hallmark gene pathway signatures.
- **G.** RT-qPCR of the indicated genes in epidermis at the indicated times. For 25 DPI, n=4 pairs. For 52 DPI, Control: n=10; iDKO: n=6.
- **H.** GSEA using top 100 marker genes of skin cell types (Vu et al., 2022).
- **I.** GSEA using top 100 marker genes of epidermal basal cell states (Haensel et al. 2019).
- **J.** Working model of epidermal differentiation trajectories in control and iDKO mice.

Data information: For statistical analysis in (C,G), we used an unpaired two-tailed Student's t-test. *** $p<0.005$; ** $p<0.01$; * $p<0.05$. Errors bars are represented as ± SD.

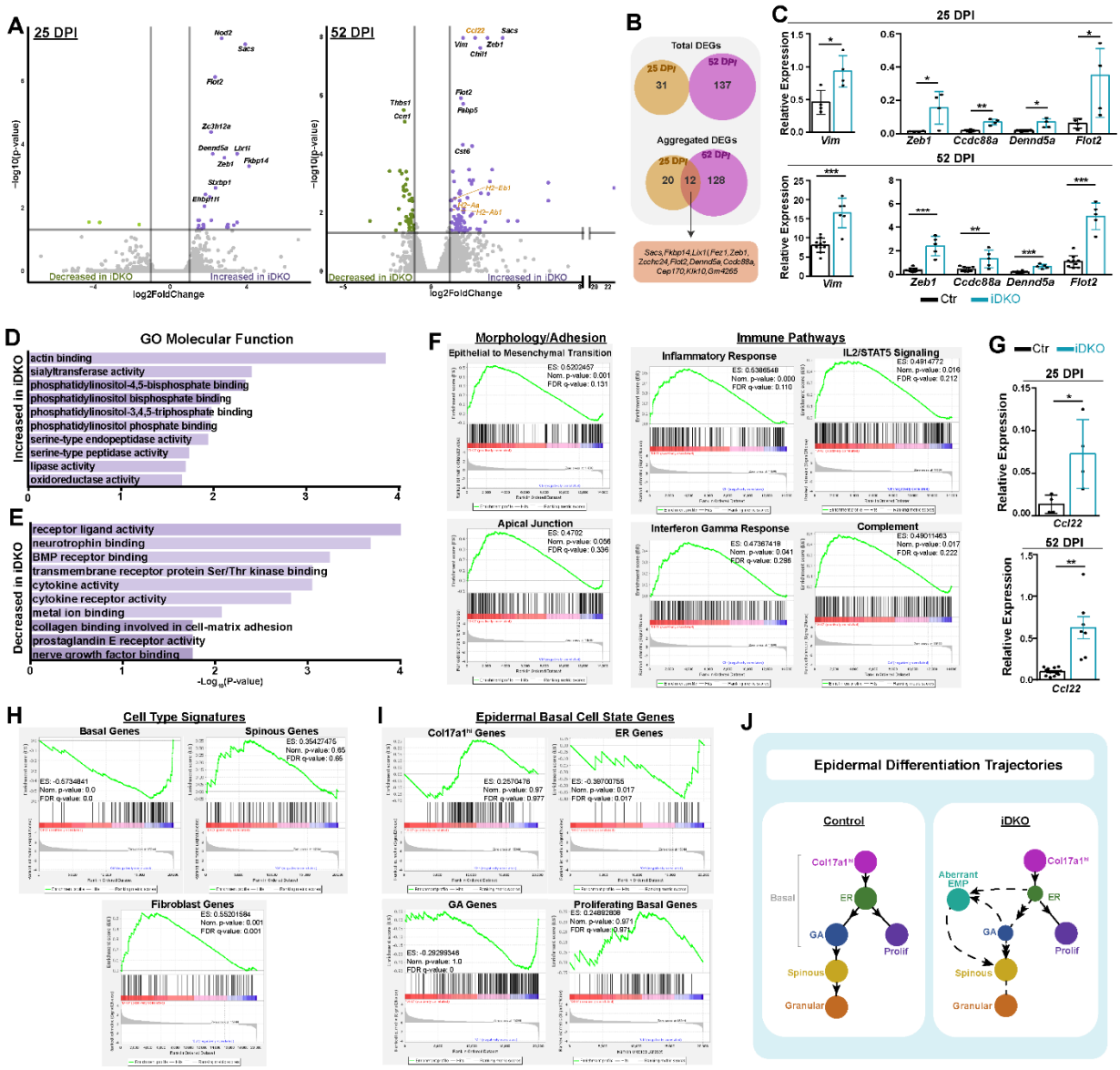
A
25 DPI
52 DPI
Decreased in iDKO
Increased in iDKO
log2FoldChange
B
Total DEGs
25 DPI
52 DPI
31
137
Aggregated DEGs
20
12
128
Sacs,Fkbp14,Lix1l,Fez1,Zeb1,
Zcchc24,Flot2,Dennd5a,Ccdc88a,
Cep170,Klk10,Gm4265
C
25 DPI
52 DPI
Relative Expression
Vim
Zeb1
Ccdc88a
Dennd5a
Flot2
Ctr
iDKO
D
GO Molecular Function
Increased in iDKO
actin binding
sialyltransferase activity
phosphatidylinositol-4,5-bisphosphate binding
phosphatidylinositol bisphosphate binding
phosphatidylinositol-3,4,5-triphosphate binding
phosphatidylinositol phosphate binding
serine-type endopeptidase activity
serine-type peptidase activity
lipase activity
oxidoreductase activity
E
Decreased in iDKO
receptor ligand activity
neurotrophin binding
BMP receptor binding
transmembrane receptor protein Ser/Thr kinase binding
cytokine activity
cytokine receptor activity
metal ion binding
collagen binding involved in cell-matrix adhesion
prostaglandin E receptor activity
nerve growth factor binding
-Log10(P-value)
F
Morphology/Adhesion
Epithelial to Mesenchymal Transition
Apical Junction
Immune Pathways
Inflammatory Response
IL2/STAT5 Signaling
Interferon Gamma Response
Complement
G
Ctr
iDKO
25 DPI
52 DPI
Relative Expression
Ccl22
H
Cell Type Signatures
Basal Genes
Spinous Genes
Fibroblast Genes
I
Epidermal Basal Cell State Genes
Col17a1hi Genes
ER Genes
GA Genes
Proliferating Basal Genes
J
Epidermal Differentiation Trajectories
Control
iDKO
Col17a1hi
Basal
ER
GA
Prolif
Spinous
Granular
Aberrant EMP

Figure 4.3: Identification of Ovol1/2 direct targets.

- **A.** (A-G) ChIP-seq analysis of Ovol1 and Ovol2. (A) Pie charts depicting annotated genomic features of called ChIP-seq peaks.
- **B.** Homer motif analysis for Ovol1, showing the predominance of the Ovol consensus motif.
- **C.** GO Enrichment analysis for all the genes associated with peaks for Ovol1 or Ovol2. Individual genes associated with the top two terms are shown in the box below.
- **D.** Spatial distribution of Ovol1- or Ovol2-bound peaks in relationship to the transcriptional start site (TSS).
- **E.** Venn diagram depicting the numbers of Ovol1- or Ovol2-specific and overlapping peaks.
- **F.** ChIP-seq tracks of Ovol1, Ovol2, and histone marks of the select loci.
- **G.** Dot plot of GO Enrichment analysis for genes that contain peaks for Ovol1 or Ovol2.
- **H.** GSEA comparing Ovol1 or Ovol2 ChIP-seq peaks with 52-DPI RNA-seq data pre-ranked by highest fold change enrichment in iDKO compared with control.
- **I.** Venn diagram comparing the overlap between DEGs and Ovol1- and/or Ovol2-bound genes identified using a narrow range for distance to ChIP peaks.
- **J.** Venn diagram comparing the overlap between DEGs and Ovol1- and/or Ovol2-bound genes identified using an expanded range for distance to ChIP peaks.
- **K.** Metascape analysis on narrowly defined Ovol1-bound and/or Ovol2-bound genes that overlap with all 52-DPI DEGs. Genes associated with relevant select top terms are shown in the boxes below.
- **L.** Metascape analysis on expanded Ovol1-bound and/or Ovol2-bound genes that overlap with only upregulated DEGs. Genes associated with relevant select top terms are shown in the boxes below.

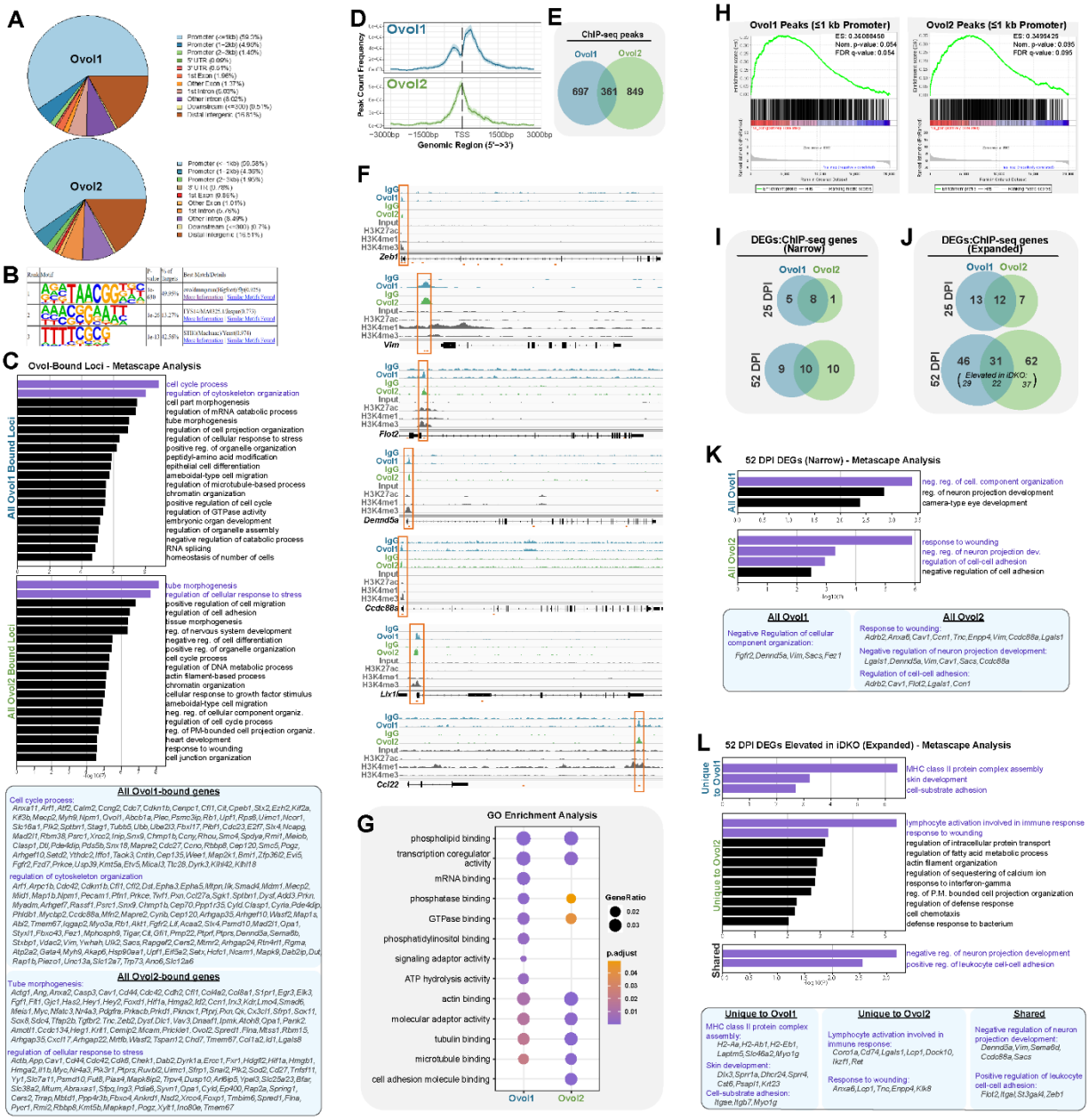
A
Ovol1
Ovol2
B
C
Ovol-Bound Loci - Metascape Analysis
All Ovol1 Bound Loci
All Ovol2 Bound Loci
All Ovol1-bound genes
All Ovol2-bound genes
D
Ovol1
Ovol2
Peak Count Frequency
Genomic Region (5'-->3')
E
ChIP-seq peaks
Ovol1
Ovol2
697
361
849
F
Zeb1
Vim
Flot2
Dennd5a
Cccdc88a
Lix1
Ccl22
G
GO Enrichment Analysis
phospholipid binding
transcription coregulator activity
mRNA binding
phosphatase binding
GTPase binding
phosphatidylinositol binding
signaling adaptor activity
ATP hydrolysis activity
actin binding
molecular adaptor activity
tubulin binding
microtubule binding
cell adhesion molecule binding
GeneRatio
p.adjust
H
Ovol1 Peaks (≤1 kb Promoter)
Ovol2 Peaks (≤1 kb Promoter)
I
DEGs:ChIP-seq genes (Narrow)
25 DPI
52 DPI
5
8
1
9
10
10
J
DEGs:ChIP-seq genes (Expanded)
13
12
7
46
31
62
Elevated in iDKO
29
22
37
K
52 DPI DEGs (Narrow) - Metascape Analysis
All Ovol1
All Ovol2
neg. reg. of cell. component organization
reg. of neuron projection development
camera-type eye development
response to wounding
neg. reg. of neuron projection dev.
regulation of cell-cell adhesion
negative regulation of cell adhesion
All Ovol1
Negative Regulation of cellular component organization:
Fgfr2,Dennd5a,Vim,Sacs,Fez1
All Ovol2
Response to wounding:
Adrb2,Anxa6,Cav1,Ccn1,Tnc,Enpp4,Vim,Cccdc88a,Lgals1
Negative regulation of neuron projection development:
Lgals1,Dennd5a,Vim,Cav1,Sacs,Ccdc88a
Regulation of cell-cell adhesion:
Adrb2,Cav1,Flot2,Lgals1,Ccn1
L
52 DPI DEGs Elevated in iDKO (Expanded) - Metascape Analysis
Unique to Ovol1
Unique to Ovol2
Shared
MHC class II protein complex assembly
skin development
cell-substrate adhesion
lymphocyte activation involved in immune response
response to wounding
regulation of intracellular protein transport
regulation of fatty acid metabolic process
actin filament organization
regulation of sequestering of calcium ion
response to interferon-gamma
reg. of P.M. bounded cell projection organization
regulation of defense response
cell chemotaxis
defense response to bacterium
negative reg. of neuron projection development
positive reg. of leukocyte cell-cell adhesion
Unique to Ovol1
MHC class II protein complex assembly:
H2-Aa,H2-Ab1,H2-Eb1,Laptm5,Slc46a2,Myo1g
Skin development:
Dlx3,Sprr1a,Dhcr24,Sprr4,Cst6,Psap1,Krt23
Cell-substrate adhesion:
Itgae,Itgb7,Myo1g
Unique to Ovol2
Lymphocyte activation involved in immune response:
Coro1a,Cd74,Lgals1,Lcp1,Dock10,Ikzf1,Ret
Response to wounding:
Anxa6,Lcp1,Tnc,Enpp4,Klk8
Shared
Negative regulation of neuron projection development:
Dennd5a,Vim,Sema6d,Ccdc88a,Sacs
Positive regulation of leukocyte cell-cell adhesion:
Flot2,Itgal,St3gal4,Zeb1

Supplemental Figure 4.2: Ovol1/2 directly regulate genes involved in cellular structure and adhesion. Related to Figure 3.

- **A.** Metascape analysis on narrowly defined Ovol1- and/or Ovol2-bound genes.
- **B.** ChIP-seq tracks of Ovol1, Ovol2, and histone marks of the select loci.
- **C.** Metascape analysis on the expanded list of Ovol1- and/or Ovol2-bound genes that overlap with DEGs from 52 DPI
- **D.** Metascape analysis on the expanded list of Ovol1- and/or Ovol2-bound genes that overlap with DEGs from 25 DPI (D) RNA-seq. For

Data Information: Genes associated with select top terms are shown in the boxes below for (A, C-D).

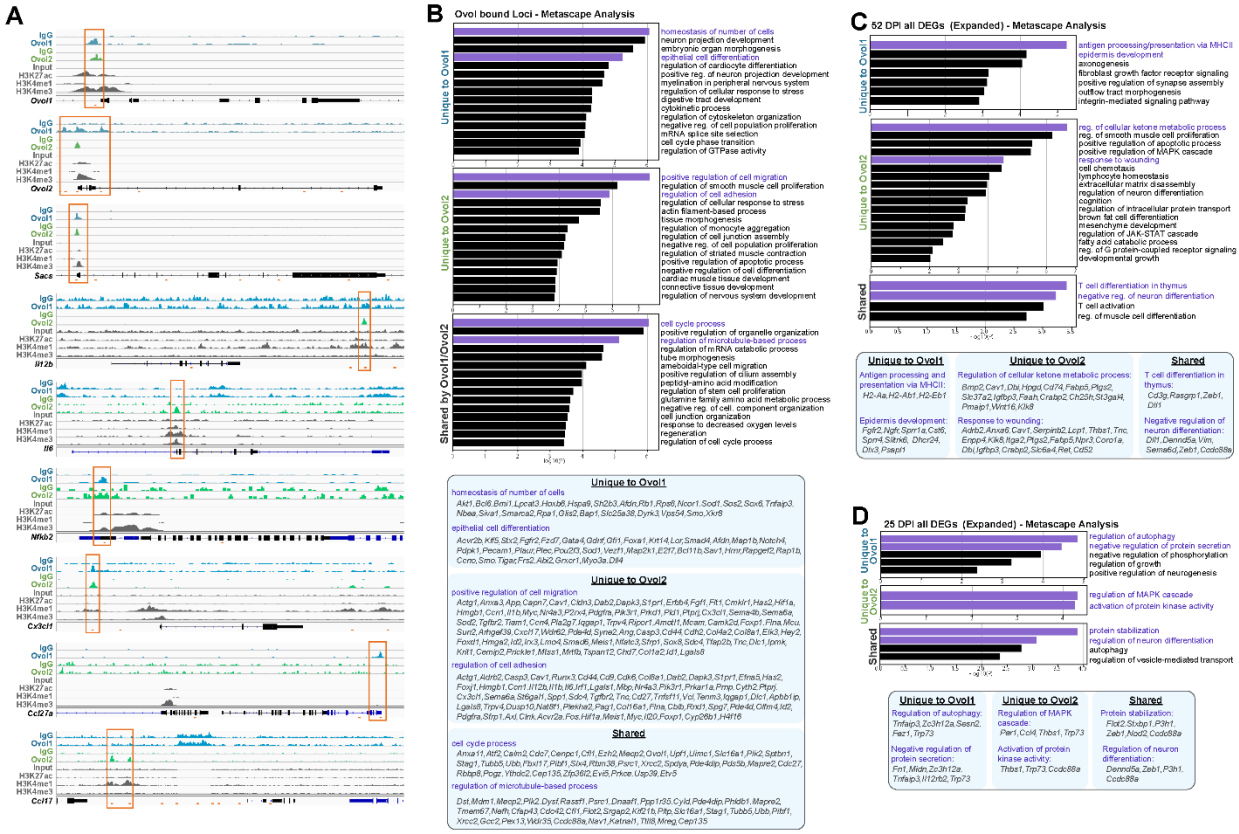

Figure 4.4: iDKO mice exhibit altered immune composition in the skin and skin-draining LN.

- **A.** Flow cytometry analysis of isolated epidermis at 52 DPI. Control: n=8; iDKO: n=7.
- **B.** Flow cytometry analysis of isolated epidermis at 52 DPI. Control: n=8; iDKO: n=7. MFI, mean fluorescence intensity.
- **C.** Representative whole-mount immunofluorescent staining of LCs in mouse back skin at 52 DPI.
- **D.** Quantification of primary dendrites in LCs as shown in (C). Control: n=5; iDKO: n=4.
- **E.** Flow cytometry analysis of isolated dermis at 52 DPI. Control: n=10; iDKO: n=5.
- **F.** Flow cytometry analysis of isolated dermis at 52 DPI. Control: n=4; iDKO: n=3.
- **G.** Flow cytometry analysis of isolated dermis at 52 DPI. Control: n=4; iDKO: n=3.
- **H.** Flow cytometry analysis of paw at 52 DPI. Control: n=6; iDKO: n=5.
- **I.** Representative images of skin draining LNs.
- **J.** Quantification of LN weight. Control: n=12; iDKO: n=7.
- **K.** (K-O) Flow cytometry analysis of LNs at 52 DPI. Control: n=10, iDKO: n=5 for (K-M). n=4 pairs for (N-O).

Data information: Scale bars: 50 μm (left) and 20 μm (two right images) for C. statistical analysis in (A-O), we used an unpaired two-tailed Student's t-test. *** $p<0.005$; ** $p<0.01$; * $p<0.05$. Errors bars are represented as ± SD.

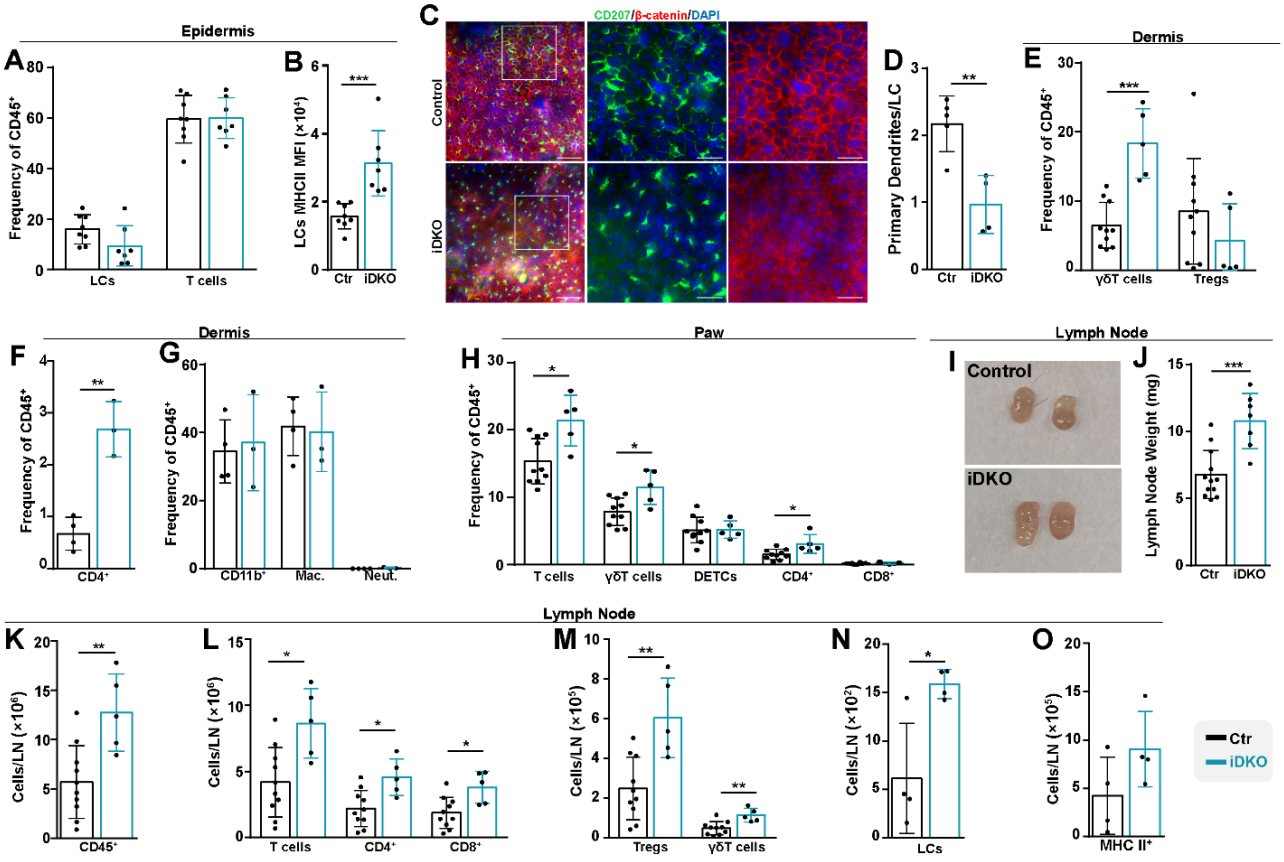
Epidermis
A
Frequency of CD45+
LCs
T cells
B
LCs MHCII MFI (×10³)
Ctr
iDKO
C
CD207/β-catenin/DAPI
Control
iDKO
D
Primary Dendrites/LC
Ctr
iDKO
Dermis
E
Frequency of CD45+
γδT cells
Tregs
Dermis
F
Frequency of CD45+
CD4+
G
Frequency of CD45+
CD11b+
Mac.
Neut.
Paw
H
Frequency of CD45+
T cells
γδT cells
DETCs
CD4+
CD8+
Lymph Node
I
Control
iDKO
J
Lymph Node Weight (mg)
Ctr
iDKO
Lymph Node
K
Cells/LN (×10⁶)
CD45+
L
Cells/LN (×10⁶)
T cells
CD4+
CD8+
M
Cells/LN (×10⁵)
Tregs
γδT cells
N
Cells/LN (×10²)
LCs
O
Cells/LN (×10⁵)
MHC II+
Ctr
iDKO

Supplemental Figure 4.3: Flow cytometry data on back skin epidermis and dermis, paw skin, and lymph nodes from control and iDKO mice.

A. Shown are matching data for Figure 4A-B, E, F-H, and K-O now represented as cell number per gram of tissue (A-H) or frequency of all live cells (I).

Data information: For statistical analysis in (A-I), we used an unpaired two-tailed Student's t-test. *** $p<0.005$; ** $p<0.01$; * $p<0.05$. Errors bars are represented as ± SD.

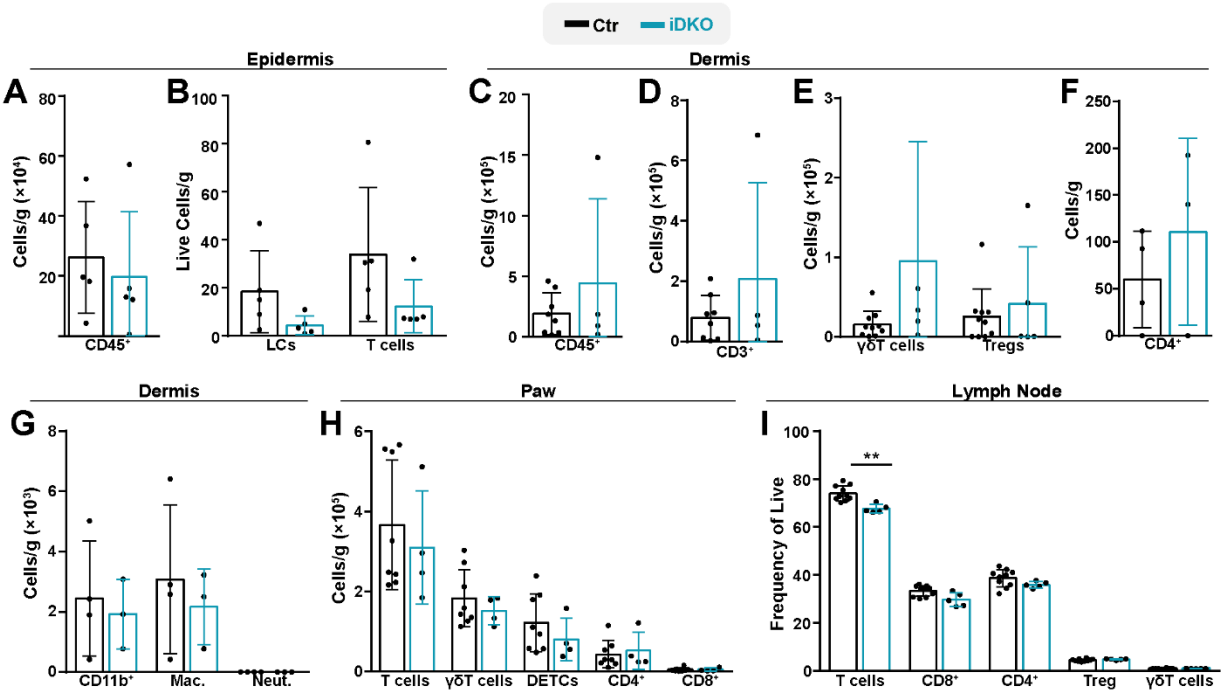

Figure 4.5: Whole-body defects and metabolic adaptation in iDKO mice

- **A.** Timeline of *Ovol1/2* DKO phenotypes.
- **B.** Representative images of control and iDKO mice at 3 MPI.
- **C.** Body weight measurements of paired control and DKO mice over time. n=9 pairs.
- **D.** H/E images of control and iDKO mice at the indicated times showing changes in dWAT. Scale bar: 100 µm.
- **E.** Quantification of fat cell area in (D). n=4 pairs.
- **F.** EchoMRI measurements of body composition at 4 MPI. n=5 pairs.
- **G.** (G-K) Results from metabolic cage analysis of 4-5-MPI control and iDKO mice at room temperature (RT; white band) or after cold exposure (CE; blue band). Gray bands designate night. (G) Quantification of average food intake/day. n=5 pairs.
- **H.** Quantification of average movement/day. n=5 pairs.
- **I.** Quantification of body weight. n=5 pairs.
- **J.** Quantification of average RER/day. n=5 pairs.
- **K.** Quantification of average energy expenditure/day. n=5 pairs.

Data information: For statistical analysis in (A-K), we used an unpaired two-tailed Student's t-test. *** p<0.005; ** p<0.01; * p<0.05. Errors bars are represented as ± SD.

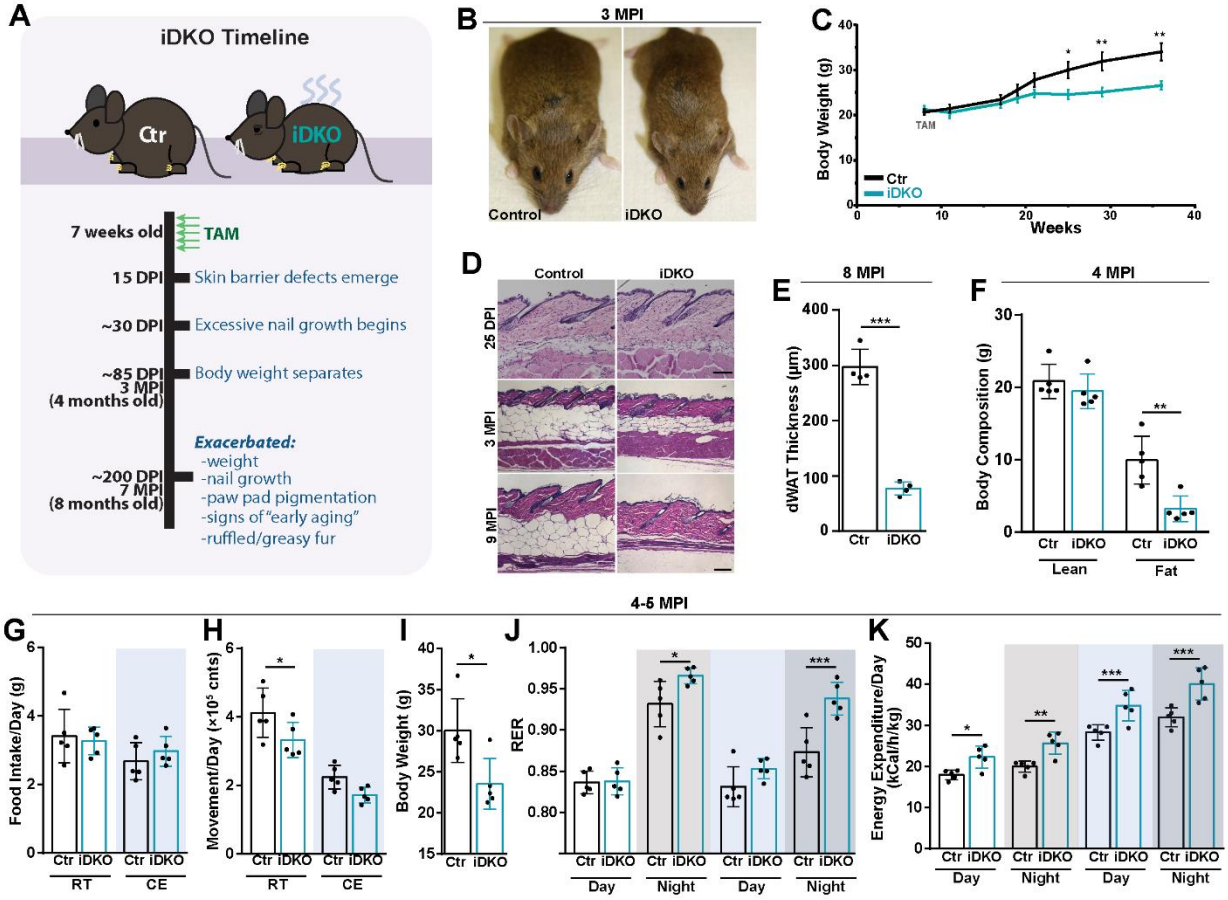

Supplemental Figure 4.4: Characterization of the aging, hair, and whole-body metabolic defects in iDKO mice. Related to Figure 5

- **A.** Images of control and iDKO mice at 9 months of age (~7 MPI).
- **B.** GSEA using genes known to be upregulated in aged skin over young (Ge et al., 2020; Keyes et al., 2016).
- **C.** Quantitative analysis of the type (top) and length (bottom) of hairs plucked from control and iDKO mice at 9 months of age.
- **D.** Images of shaved back skin from control and iDKO males at the indicated times. "p" = postnatal day.
- **E.** RT-qPCR of the indicated immune-related genes in dWAT of control and iDKO mice at 4-5 MPI. n=4.
- **F.** Body weight measurements of non-TAM-injected control and iDKO mice over time. n=9 pairs.
- **G.** EchoMRI measurements of body composition at 2-3 MPI (3–4-month-old). Control: n=6; iDKO: n=5.
- **H.** RT-qPCR of the indicated genes in BAT of control and iDKO mice at 4-5MPI (5-6-month-old). n=6 pairs.
- **I.** Representative FLIR thermogun images and quantification of body temperature at 5 MPI (6-month-old). n=4 pairs.
- **J.** RT-qPCR of genes involved in lipolysis or "fatty acid synthesis" (FAS) in iWAT of control and iDKO mice at 4-5 MPI. Control: n=4; iDKO: n=3.
- **K.** RT-qPCR of genes involved in immune-related genes in iWAT of control and iDKO mice at 4-5 MPI. Control: n=4; iDKO: n=3.
- **L.** (L-P) Results from metabolic cage analysis of control and iDKO mice at 2-3 MPI (3-4-month-old). Quantification of average food intake/day. Control: n=5; iDKO: n=4.
- **M.** Quantification of average movement/day. Control: n=5; iDKO: n=4.
- **N.** Quantification of body weight. Control: n=5; iDKO: n=4.
- **O.** Quantification of average RER/day. Control: n=5; iDKO: n=4.
- **P.** Quantification of average energy expenditure/day. Control: n=5; iDKO: n=4.
- **Q.** Seahorse analysis for OCR and ECAR on epidermis from control and iDKO mice at 2 MPI (3-month-old). n=3 pairs.

Data information: statistical analysis in (A-Q), we used an unpaired two-tailed Student's t-test. *** $p<0.005$; ** $p<0.01$; * $p<0.05$. Errors bars are represented as ± SD.

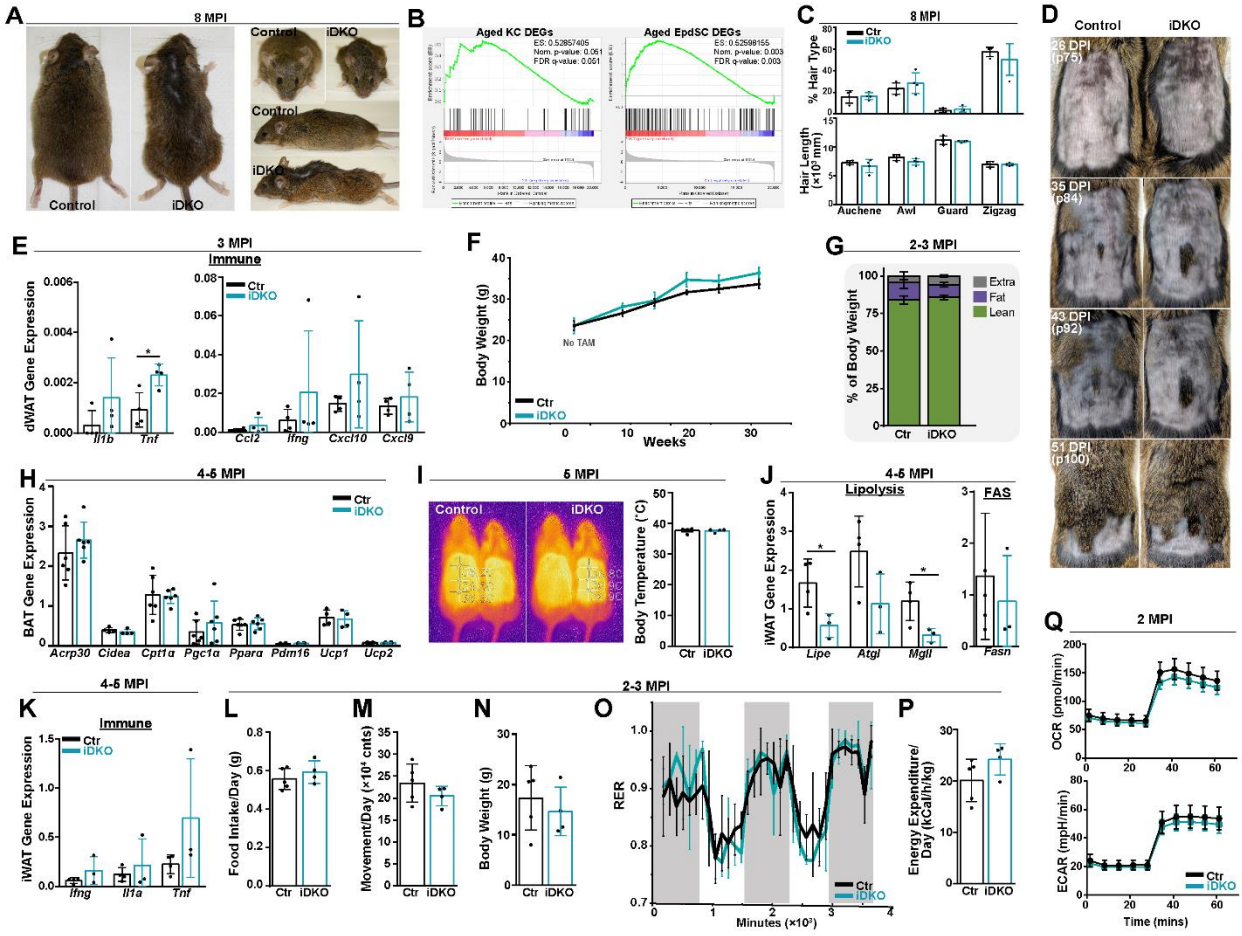
A
8 MPI
Control
iDKO
B
Aged KC DEGs
Aged EpdSC DEGs
C
8 MPI
Ctr
iDKO
% Hair Type
Hair Length (×10 mm)
Auchene
Awl
Guard
Zigzag
D
Control
iDKO
26 DPI (p75)
35 DPI (p84)
43 DPI (p92)
51 DPI (p100)
E
3 MPI
Immune
dWAT Gene Expression
Il1b
Tnf
Ccl2
Ifng
Cxcl10
Cxcl9
F
Body Weight (g)
No TAM
Weeks
G
2-3 MPI
% of Body Weight
Extra
Fat
Lean
H
4-5 MPI
BAT Gene Expression
Acrp30
Cidea
Cpt1α
Pgc1α
Ppara
Pdm16
Ucp1
Ucp2
I
5 MPI
Body Temperature (°C)
J
4-5 MPI
Lipolysis
FAS
iWAT Gene Expression
Lipe
Atgl
Mgll
Fasn
Q
2 MPI
OCR (pmol/min)
ECAR (mpH/min)
Time (mins)
K
4-5 MPI
Immune
iWAT Gene Expression
Ifng
Il1a
Tnf
L
2-3 MPI
Food Intake/Day (g)
M
Movement/Day (×10⁴ cnts)
N
Body Weight (g)
O
RER
Minutes (×10³)
P
Energy Expenditure/ Day (kcal/h/kg)

Figure 4.6: Dex partially rescues epidermal LC activation, immune composition in the LN and the body weight phenotype of iDKO mice.

A. Schematic depicting treatment strategy for dexamethasone (Dex) experiments in (B-G).
B. Images of mice with the indicated treatment at 4 MPI.
C. Quantification of spleen weight. Control-PBS: n=13; iDKO-PBS: n=4; Control-Dex: n=8; iDKO-Dex: n=7.
D. Quantification of LN weight. Control-PBS: n=10; iDKO-PBS: n=4; Control-Dex: n=9; iDKO-Dex: n=7.
E. Flow cytometry analysis of MFI of MHC II on LCs in epidermis at 52 DPI. Control-PBS: n=9; iDKO-PBS: n=4; Control-Dex: n=7; iDKO-Dex: n=5.
F. Flow cytometry analysis of LNs at 52 DPI. Control-PBS: n=8; iDKO-PBS: n=4; Control-Dex: n=5; iDKO-Dex: n=4.
G. Flow cytometry analysis of LNs at 52 DPI. Control-PBS: n=7; iDKO-PBS: n=4; Control-Dex: n=5; iDKO-Dex: n=5.
H. Flow cytometry analysis of LNs at 52 DPI. Control-PBS: n=7; iDKO-PBS: n=4; Control-Dex: n=5; iDKO-Dex: n=5.
I. Flow cytometry analysis of LNs at 52 DPI. Control-PBS: n=8; iDKO-PBS: n=4; Control-Dex: n=5; iDKO-Dex: n=4.
J. Flow cytometry analysis of LNs at 52 DPI. Control-PBS: n=8; iDKO-PBS: n=4; Control-Dex: n=5; iDKO-Dex: n=4.
K. TEWL measurements after the indicated treatments. Control-PBS: n=9; iDKO-PBS: n=4; Control-Dex: n=8; iDKO-Dex: n=6.
L. Body weight over time represented as a percentage of the starting weight. Control-PBS: n=13; iDKO-PBS: n=4; Control-Dex: n=9; iDKO-Dex: n=5.
M. EchoMRI measurements of body composition at the indicated times. For 30 DPI Control-PBS: n=10; iDKO-PBS: n=3; Control-Dex: n=7; iDKO-Dex: n=6. For 4 MPI Control-PBS: n=12; iDKO-PBS: n=4; Control-Dex: n=9; iDKO-Dex: n=6.
N. Bar graphs showing iDKO/Ctr fold change in fat content at 4 MPI for PBS control and Dex treated mice, calculated from (M).

Data information: For statistical analysis in (C-I), we used one-way Anova. For (J-K, M) we used 2-way Anova. *** $p<0.005$; ** $p<0.01$; * $p<0.05$. Errors bars are represented as ± SD.

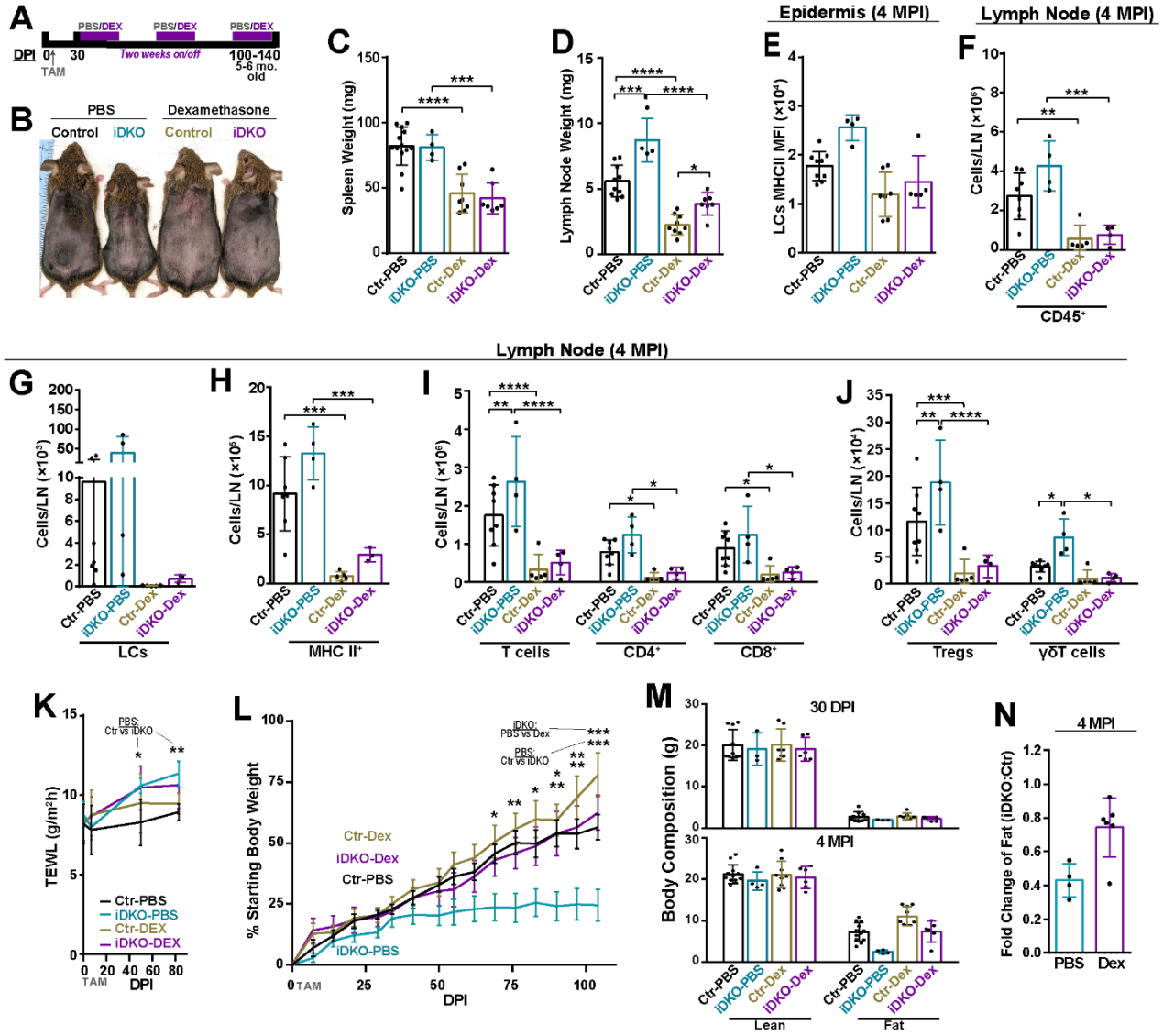
A
PBS/DEX
PBS/DEX
PBS/DEX
DPI
0
TAM
30
Two weeks on/off
100-140
5-6 mo. old
B
PBS
Dexamethasone
Control
iDKO
Control
iDKO
C
Spleen Weight (mg)
D
Lymph Node Weight (mg)
Epidermis (4 MPI)
E
LCs MHCII MFI (×10⁴)
Lymph Node (4 MPI)
F
Cells/LN (×10⁶)
CD45⁺
Ctr-PBS
iDKO-PBS
Ctr-Dex
iDKO-Dex
Lymph Node (4 MPI)
G
Cells/LN (×10³)
LCs
H
Cells/LN (×10⁶)
MHC II⁺
I
Cells/LN (×10⁶)
T cells
CD4⁺
CD8⁺
J
Cells/LN (×10⁴)
Tregs
γδT cells
K
TEWL (g/m²h)
PBS: Ctr vs iDKO
Ctr-PBS
iDKO-PBS
Ctr-DEX
iDKO-DEX
TAM
DPI
L
% Starting Body Weight
iDKO: PBS vs Dex
PBS: Ctr vs iDKO
Ctr-Dex
iDKO-Dex
Ctr-PBS
iDKO-PBS
TAM
DPI
M
30 DPI
4 MPI
Body Composition (g)
Lean
Fat
N
4 MPI
Fold Change of Fat (iDKO:Ctr)
PBS
Dex

Supplemental Figure 4.5: γδTCR blocking antibody fails to normalize body weight deviation of iDKO mice. Related to Figure 6.

A. Schematic depicting treatment strategy for IgG/γδTCR blocking antibody experiments in (B-H). Tissues were harvested at 4 MPI. n=3.
B. Representative flow cytometry plots of γδTCR staining from the indicated tissues.
C. Quantification of $\gamma\delta TCR^+$ cells in the lymph node.
D. TEWL measurements after the indicated treatments.
E. Body weight over time represented as a percentage of the starting weight.
F. EchoMRI measurements of body composition at the indicated times.
G. Bar graphs showing relative lean, fat, and other (extra) masses in control and iDKO mice with the indicated treatments.
H. iDKO/Ctr fold change in fat content at 4 MPI, calculated from (G).
I. Lymph node weight of the indicated genotypes.
J. Spleen weight of the indicated genotypes.

Data information: For statistical analysis in (C, H-J), we used one-way Anova. For (D-E, G) we used 2-way Anova. *** $p<0.005$; ** $p<0.01$; * $p<0.05$. Errors bars are represented as ± SD.

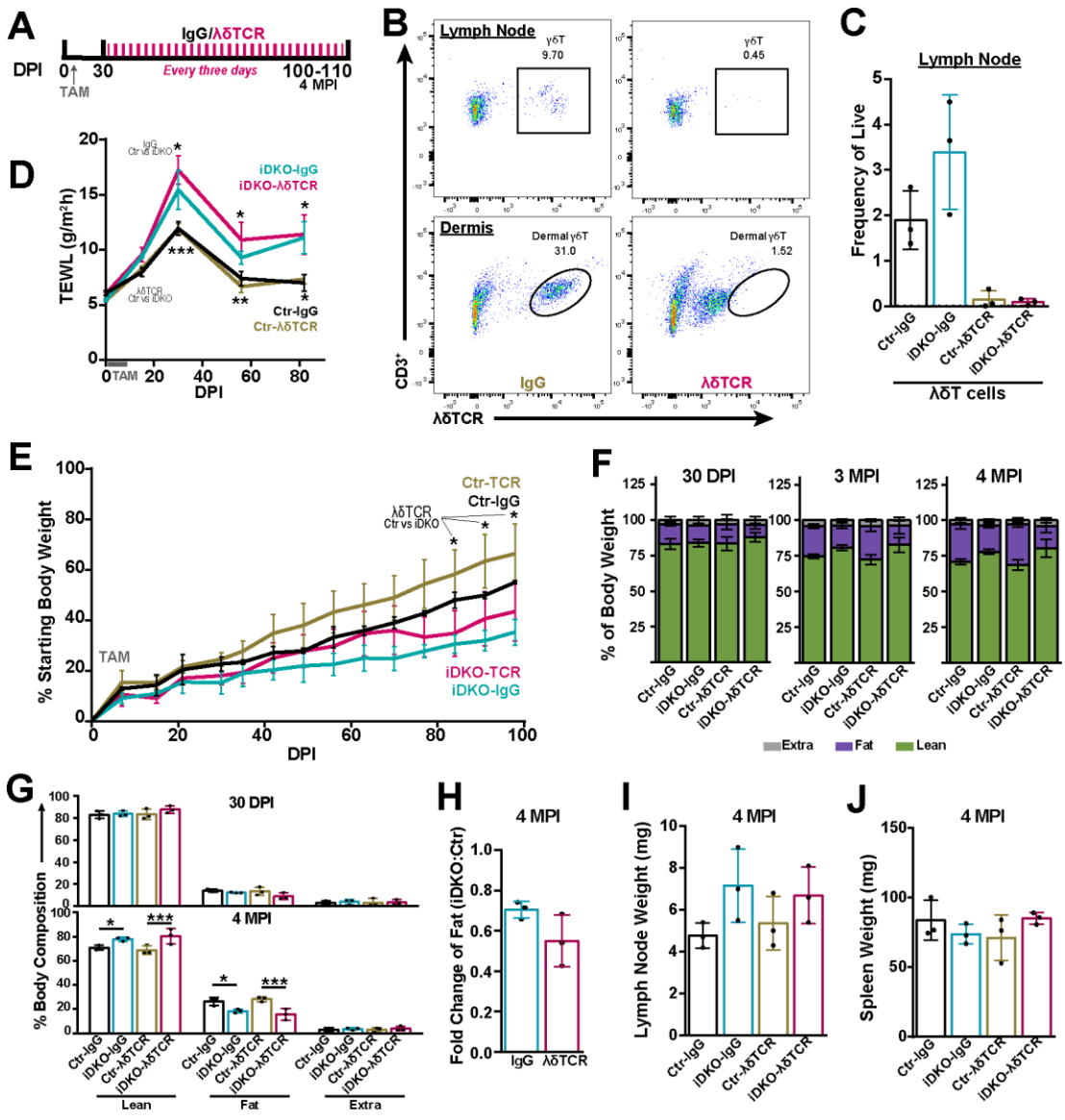
A
IgG/λδTCR
DPI
0
30
Every three days
100-110
4 MPI
TAM
B
Lymph Node
γδT
9.70
γδT
0.45
Dermis
Dermal γδT
31.0
Dermal γδT
1.52
CD3+
IgG
λδTCR
λδTCR
C
Lymph Node
Frequency of Live
Ctr-IgG
iDKO-IgG
Ctr-λδTCR
iDKO-λδTCR
λδT cells
D
TEWL (g/m²h)
IgG
Ctr vs iDKO
iDKO-IgG
iDKO-λδTCR
λδTCR
Ctr vs iDKO
Ctr-IgG
Ctr-λδTCR
TAM
DPI
E
% Starting Body Weight
Ctr-TCR
Ctr-IgG
λδTCR
Ctr vs iDKO
TAM
iDKO-TCR
iDKO-IgG
DPI
F
30 DPI
3 MPI
4 MPI
% of Body Weight
Ctr-IgG
iDKO-IgG
Ctr-λδTCR
iDKO-λδTCR
Extra
Fat
Lean
G
% Body Composition
30 DPI
4 MPI
Ctr-IgG
iDKO-IgG
Ctr-λδTCR
iDKO-λδTCR
Lean
Fat
Extra
H
4 MPI
Fold Change of Fat (iDKO:Ctr)
IgG
λδTCR
I
4 MPI
Lymph Node Weight (mg)
Ctr-IgG
iDKO-IgG
Ctr-λδTCR
iDKO-λδTCR
J
4 MPI
Spleen Weight (mg)
Ctr-IgG
iDKO-IgG
Ctr-λδTCR
iDKO-λδTCR

CHAPTER 5: Conclusions and Perspectives

Overview

Much work has been done to show that a functional skin barrier is integral for maintaining skin homeostasis, and that defects in barrier are associated with inflammation or can be detrimental. For my thesis I used epithelial-specific genetic mouse models that are either susceptible to, or have, epidermal barrier defects to address questions about epidermally-driven inflammatory responses and how barrier defects can activate systemic responses. While the context of these projects is different – induced inflammation vs homeostasis, both centers around transcriptional regulation of epidermis and barrier. Here I (1) identified a function for Ovol1 to modulate barrier and hyperplasia of epidermis and facilitate recruitment of neutrophils in an inflammatory disease model, and (2) utilized a global approach to show that Ovol1 and Ovol2 maintain barrier through regulating genes involved in cytoskeletal structure and adhesion, and barrier defects instigate metabolic defects partially triggered by localized aberrant immune response that seems distinct from typical inflammation. Collectively my work focuses on the function of keratinocyte-intrinsic transcription factors to epidermal barrier and inflammation, and how epidermal barrier defects affect inflammation and physiology.

Chapter 3

Chapter 3 of the dissertation includes published work that highlights the role of *Ovol1* in psoriatic-like inflammation and the role it pays in neutrophil recruitment and barrier integrity (Dragan et al., 2022). Using various *in vivo* and cell-biological assays I

report that Ovol1 provides a protective function in epidermis by modulating the epithelial and immunological response to inflammation (Dragan et al., 2022). Strikingly, Ovol1 modulates this response using multiple regulatory branches including (1) through protecting barrier, (2) through promoting hyperplasia, (3) through repression of *Cxcl1*-neutrophil recruitment (Dragan et al., 2022).

Ovol1 has been extensively studied in the context of cancer and morphogenesis, but the function of Ovol1 in inflammation is less known (Renaud et al., 2015; Saxena et al., 2022). Moreover, the function of chemoattractant in recruiting immune cells has been well-studied in a plethora of contexts and models, but less is known about the molecular regulators of these molecules beyond the canonical inflammatory signaling pathways (e.g., TNF and IFN signaling). My work provides evidence of another epidermally-derived transcription factor that can both directly and indirectly modulate recruitment of neutrophils to skin. Interestingly, time course imaging of neutrophils in *Ovol1*$^{-/-}$ mice shows more accumulation and migration from the dermis through the epidermis forming plaque-like abscesses on the surface. However, it is still unclear the exact dynamics of and the molecular mediators that instigating extravasation from the dermis through the epidermis especially at particular locations. Based on our previous finding that IL-1α inhibition reduced neutrophil accumulation, we can speculate that it is one of the molecules that recruit neutrophils to the epidermal surface. However, we cannot rule out Cxcl1, a combination of both Cxcl1/IL-1α, or a novel molecule as triggers for neutrophil extravasation through the skin. Studies on neutrophil extravasation through endothelium show that neutrophils migrate though using a combination of chemoattractant signals and integrin “crawling” (McDonald et al., 2010). Live imaging of neutrophil extravasation may

provide lights to the physical and temporal dynamics of neutrophil migration though the epidermis/HF and whether well-timed blocking Cxcl1 or IL-1α or additional candidate molecules can prevent neutrophil migration after swarming.

From a clinical standpoint, the neutrophil-induced abscesses observed in the *Ovol1* SSKO mice closely resemble pustular psoriatic plaques, suggesting the *Ovol1*$^{-/-}$/SSKO mice might provide a great model for understanding and finding more targeted treatments for this disease. Currently, this study broadens our understanding of the potential epidermal and neutrophil landscape of pustular psoriasis and may offer a new marker to test for severity of disease. While much work needs to be done, this study takes the first steps to explain the dynamics of neutrophil infiltration and migration and shows keratinocyte-intrinsic mechanism that can regulate it.

While most groups report a pro-inflammatory role of IL-33 in psoriasis, we find that our experiment is consistent with a study where overexpression of IL-33 suppress psoriatic inflammation and epidermal hyperplasia (Balato et al., 2014; Chen et al., 2020; Duan et al., 2019; Miller et al., 2010). It is important to note that this protective function might only occur when IL-33 is in excess. One likely possibility is that IL-33 activates other immune cells to secrete proteins that induce proliferation of KCs, like in the case of T helper type 2 allergic responses, which would explain the hyperplasia (Ryu et al., 2015). Another possibility is that IL-33 itself induces hyperproliferation of KCs through ST2L and signaling pathways such as extracellular signal-regulated kinase and c-Jun N-terminal kinase (Du et al., 2016). However, more work needs to be done to test both the regulation of *Il33*—to provide exacting evidence that Ovol1 is direct regulator—and how IL-33 molecularly regulates keratinocyte proliferation.

Chapter 4

In chapter 4 of the dissertation, I provide novel insights into the function of Ovol1 and Ovol2 in maintaining epidermal barrier and investigate a new context for how barrier defects are physiologically detrimental. Using a combination of morphological, metabolomics and high throughput sequencing assays, I show new functions for Ovol1 and Ovol2 to regulate adult skin barrier through regulating EMT-like genes, cytoskeletal structure and adhesion and effective terminal differentiation. I then show, using metabolic, immunological, and *in vivo* techniques, that iDKO mice have an altered immune response followed by reduced fat and weight gain which can be, in part, rescued by inhibiting inflammation.

While Ovol genes are master regulators of EMT-associated genes, most studies conducted on Ovol1 and Ovol2 have been under the context of epithelial development and cancers and the molecular basis for Ovol1/Ovol2 functional redundancy lacked clarity (Renaud et al., 2015; Saxena et al., 2022). In this work I use an unbiased approach to classify the unique and redundant functions of Ovol1 in Ovol2 that are preserved in adulthood where Ovol1 and Ovol2 both control the extent of EMP (e.g., *Zeb1* and *Vim*) and cellular adhesion (e.g., *Lix1l* and *Dennd5a*), but also add to that list a novel and conserved function in regulating cytoskeletal structure (e.g., *Flot2* and *Ccdc88a*). Moreover, my work expands upon previous data that defines basal transcriptional states and shows that the ER and GA cell states are likely the most plastic among all basal cell states and are subjected to intricate regulation. Additionally I show differentiation progression is intact provided the key drivers are still functional even if gene expression of many cellular processes is disturbed. Likely, GA cells need this flexibility to allow for both migration and

differentiation of epidermal cells during upward stratification or during wound healing. Future work can focus on the plasticity of basal cells through these states to understand the key regulatory drivers of epidermal differentiation.

Most current research show a relation between barrier and metabolism caused by increased thermogenesis while others show an association of barrier defects with inflammation, but few studies show a relation between all three processes (Brunner et al., 2017; Dereksson et al., 2012; Elias et al., 2012; Gabay and Kushner, 1999; Yamamoto et al., 2020; Zheng, 2014). Skin barrier-associated inflammation is generally dependent on the disease where psoriasis is characterized by a Th17 response and atopic dermatitis is driven more by a Th2 response (B. Brandt, 2011; Benhadou et al., 2019). In this work I aimed to bridge this gap and I show that aberrant immune response is in part responsible for weight loss in mice with barrier defects.

While this connection is interesting, much work needs to be done to understand the mechanisms of these phenomenon and probe deeper into the specifics of the immune response that does not seem to involve activation of classical inflammatory molecules such as IL-6 and TNF-α. First, we hypothesize that LC activation in skin activates T cells in the skin-draining lymph node; however, future studies need to provide evidence that LCs are activating the T cells. Furthermore, more work must be done to determine how LCs are activated and whether *Ccl22,* a cytokine most commonly released by LCs, is a direct target of Ovol1/2 (Vulcano et al., 2001). Currently, there are two main hypothesis to explain this: 1) loss of adhesion/contact with epidermal cells may drive changes, possibly transcriptional, in LCs that activate them (Sirvent et al., 2020); and 2) since keratinocytes share transcripts with LCs (Su and Igyártó, 2019), which express transcripts of *K14* and

Ovol1 (http://rstats.immgen.org/Skyline_microarray/skyline.html), then Ovol1 and Ovol2 may have cell autonomous functions in LCs.

Preliminary RT-qPCR data on sorted LCs from control and iDKO mice showed decreased expression of *Ovol1, Ovol2 K14,* and *Ccl22* in LCs, however, expression of other Ovol1/2 target genes involved in cytoskeletal structure and adhesion and found to be highly expressed in normal LCs from the Immgen database, were unchanged in iDKO LCs (Appendix B). *Ccl22* is a chemokine that can facilitate recruitment of T cells (Vulcano et al., 2001). Interesting to note is that *Ccl22* expression seemed to mostly come from LCs, and Ovol1/2 binds to an enhancer region of *Ccl22* which makes it tempting to speculate that Ovol1/2 may have a LC-specific function to partially regulate *Ccl22* expression. Much work including luciferase reporter assay of this *Ccl22* peak and *in vitro* knock down of *Ovol1/2* from sorted LCs would be needed to prove this point. Moreover, to understand if loss of contacts with LCs are enough to drive activation, in vivo studies can be done at an early timepoint after tamoxifen-deletion of Ovol1/2 to characterize keratinocyte-LC adhesion and determine whether it is enough to activate LCs. Furthermore in vitro analysis of LC-keratinocyte adhesions would also provide enlightening insights.

Second, iDKO mice exhibit altered metabolism. Energy expenditure can occur in many forms: through internal metabolism, heat production, and physical activity (Wilson et al., 2019). While my work focused on the connection between skin, immune cells, and weight gain, more metabolic studies would need to be done to isolate the exact metabolic tissues responsible for increase energy demand in iDKO mice. Tracking isotype labeled glucose molecules is one such experiment that could reveal the tissues with a higher energy demand in iDKO mice (Haman et al., 2004; Jung et al., 2021). Due to their proximity to the

epidermis, it has been postulated that the dermal fats can shuttle fatty acids to keratinocytes to help facilitate barrier maintenance (Rivera-Gonzalez et al., 2014). It would be interesting to test whether increasing the availability of fat or carbohydrates would be sufficient to rescue the body weight, alter the energy metabolism, and help rescue barrier. Understanding the metabolic landscape could provide insights into how barrier defects and inflammation can affect metabolism.

Lastly, my data suggest that inflammation was partially responsible for lack of weight gain in iDKO mice. However, since dexamethasone has known functions in activating adipogenesis, further work would need to be done to understand the direct contribution of dexamethasone to fat accumulation in iDKO mice (Zubiría et al., 2020). Moreover, the molecular regulators driving metabolic changes within the iDKO mice are still unknown and leaves for an interesting area to investigate from both immune and epidermal cells. Clinically, this research is important for patients with inherent barrier defects or with skin inflammatory diseases and, along with other studies, shows that skin diseases can have systemic effects and could be more detrimental that anticipated. Understanding how these processes are regulated and how barrier defects affect other tissues is important for alleviating secondary symptoms and providing insights into future therapeutics.

Overall, my work contributes new understanding of epidermally-originated regulation of skin barrier maintenance, inflammation, and physiological adaptation to barrier defects. I first show the protective function of Ovol1 in epidermis upon psoriasis-like inflammation and describe a key function for Ovol1 in mediating barrier and neutrophil response through both directly and indirectly mediating neutrophil attracting

factors *Il1α* and *Cxcl1* and though promoting hyperplasia though causing repression of *Il33*. I then show that Ovol1 and Ovol2 maintain barrier by regulating genes involved in cytoskeletal structure and adhesion. Finally, I show that dysfunctional barrier leads to altered metabolism and that some of these changes can be partially rescued through inhibiting inflammation.

REFERENCES

Albanesi, C., Scarponi, C., Bosisio, D., Sozzani, S., and Girolomoni, G. (2010). Immune functions and recruitment of plasmacytoid dendritic cells in psoriasis. Autoimmunity *43*, 215–219.

Alexander, H., Brown, S., Danby, S., and Flohr, C. (2018). Research Techniques Made Simple: Transepidermal Water Loss Measurement as a Research Tool. J Invest Dermatol *138*, 2295-2300 e1.

Ali, N., and Rosenblum, M.D. (2017a). Regulatory T cells in skin. Immunology *152*, 372.

Ali, N., and Rosenblum, M.D. (2017b). Regulatory T cells in Skin. Immunology.

Ali, N., Zirak, B., Rodriguez, R.S., Pauli, M.L., Truong, H.A., Lai, K., Ahn, R., Corbin, K., Lowe, M.M., Scharschmidt, T.C., et al. (2017). Regulatory T Cells in Skin Facilitate Epithelial Stem Cell Differentiation. Cell *169*, 1119-1129 e11.

Aoki, M., and Murase, T. (2019). Obesity-associated insulin resistance adversely affects skin function. PLoS One *14*.

Aragona, M., Dekoninck, S., Rulands, S., Lenglez, S., Mascré, G., Simons, B.D., and Blanpain, C. (2017). Defining stem cell dynamics and migration during wound healing in mouse skin epidermis. Nat. Commun. *8*, 1–14.

Arnoux V., Come C., Kusewitt D., S.P. (2005). Cutaneous Wound Reepithelialization: A Partial and Reversible EMT. In Rise and Fall of Epithelial Phenotype: Concepts OfEpithelial-Mesenchymal T, S. P., ed. pp. 111–134.

Arwert, E.N., Hoste, E., and Watt, F.M. (2012). Epithelial stem cells, wound healing and cancer. Nat. Rev. Cancer *12*, 170–180.

B. Brandt, E. (2011). Th2 Cytokines and Atopic Dermatitis. J. Clin. Cell. Immunol. *02*.

Baazim, H., Schweiger, M., Moschinger, M., Xu, H., Scherer, T., Popa, A., Gallage, S., Ali, A., Khamina, K., Kosack, L., et al. (2019). CD8 + T cells induce cachexia during chronic viral infection. Nat. Immunol. *20*, 701–710.

Balato, A., Lembo, S., Mattii, M., Schiattarella, M., Marino, R., De Paulis, A., Balato, N., and Ayala, F. (2012). IL-33 is secreted by psoriatic keratinocytes and induces pro-inflammatory cytokines via keratinocyte and mast cell activation. Exp. Dermatol. *21*, 892–894.

Balato, A., Di Caprio, R., Canta, L., Mattii, M., Lembo, S., Raimondo, A., Schiattarella, M., Balato, N., and Ayala, F. (2014). IL-33 is regulated by TNF-α in normal and psoriatic skin. Arch. Dermatol. Res. *306*, 299–304.

Barland, C.O., Zettersten, E., Brown, B.S., Ye, J., Elias, P.M., and Ghadially, R. (2004). Imiquimod-induced interleukin-1 alpha stimulation improves barrier homeostasis in aged murine epidermis. J Invest Dermatol *122*, 330–336.

Beaudry, V.G., Ihrie, R.A., Jacobs, S.B.R.R., Nguyen, B., Pathak, N., Park, E., and Attardi, L.D. (2010). Loss of the desmosomal component Perp impairs wound healing in vivo. Dermatol. Res. Pract. *2010*.

Belokhvostova, D., Berzanskyte, I., Cujba, A.M., Jowett, G., Marshall, L., Prueller, J., and Watt, F.M. (2018). Homeostasis, regeneration and tumour formation in the mammalian epidermis. Int. J. Dev. Biol. *62*, 571–582.

Benhadou, F., Mintoff, Di., and Del Marmol, V. (2019). Psoriasis: Keratinocytes or Immune Cells - Which Is the Trigger? Dermatology *235*, 91–100.

Binczek, E., Jenke, B., Holz, B., Günter, R.H., Thevis, M., and Stoffel, W. (2007). Obesity resistance of the stearoyl-CoA desaturase-deficient (scd1 -/-) mouse results from

disruption of the epidermal lipid barrier and adaptive thermoregulation. Biol. Chem. *388*, 405–418.

Bonnet, M.C., Preukschat, D., Welz, P.S., Van Loo, G., Ermolaeva, M.A., Bloch, W., Haase, I., and Pasparakis, M. (2011). The adaptor protein FADD protects epidermal keratinocytes from necroptosis in vivo and prevents skin inflammation. Immunity *35*, 572–582.

Van den Bossche, J., and Van Ginderachter, J.A. (2013). E-cadherin: from epithelial glue to immunological regulator. Eur. J. Immunol. *43*, 34–37.

Briso, E.M., Guinea-Viniegra, J., Bakiri, L., Rogon, Z., Petzelbauer, P., Eils, R., Wolf, R., Rincón, M., Angel, P., and Wagner, E.F. (2013). Inflammation-mediated skin tumorigenesis induced by epidermal c-Fos. Genes Dev. *27*, 1959.

Bruhs, A., Proksch, E., Schwarz, T., and Schwarz, A. (2018). Disruption of the Epidermal Barrier Induces Regulatory T Cells via IL-33 in Mice. J Invest Dermatol *138*, 570–579.

Brunner, P.M., Guttman-Yassky, E., M Leung, D.Y., and York, N. (2017). The immunology of atopic dermatitis and its reversibility with broad-spectrum and targeted therapies. J. Allergy Clin. Immunol. *139*, S65–S76.

Byrne, S.N., Beaugie, C., O'Sullivan, C., Leighton, S., and Halliday, G.M. (2011). The Immune-Modulating Cytokine and Endogenous Alarmin Interleukin-33 Is Upregulated in Skin Exposed to Inflammatory UVB Radiation. Am. J. Pathol. *179*.

Cai, Y., Shen, X., Ding, C., Qi, C., Li, K., Li, X., Jala, V.R., Zhang, H. ge, Wang, T., Zheng, J., et al. (2011). Pivotal Role of Dermal IL-17-Producing γδ T Cells in Skin Inflammation. Immunity *35*, 596–610.

Cangkrama, M., Ting, S.B., and Darido, C. (2013). Stem cells behind the barrier. Int J Mol Sci *14*, 13670–13686.

Castellana, D., Paus, R., and Perez-Moreno, M. (2014). Macrophages contribute to the cyclic activation of adult hair follicle stem cells. PLoS Biol *12*, e1002002.

Castillo-González, R., Cibrian, D., and Sánchez-Madrid, F. (2021). Dissecting the complexity of γδ T-cell subsets in skin homeostasis, inflammation, and malignancy. J. Allergy Clin. Immunol. *147*, 2030–2042.

Chen, Q., Shi, P., Wang, D., Liu, Q., Li, X., Wang, Y., Zou, D., Huang, Z., Gao, X., and Lin, Z. (2019). Epidermis-Activated Gasdermin-A3 Enhances Thermogenesis of Brown Adipose Tissue through IL-6/Stat3 Signaling. Am. J. Pathol. *189*, 1041–1052.

Chen, Z., Hu, Y., Gong, Y., Zhang, X., Cui, L., Chen, R., Yu, Y., Yu, Q., Chen, Y., Diao, H., et al. (2020). Interleukin-33 alleviates psoriatic inflammation by suppressing the T helper type 17 immune response. Immunology *160*, 382–392.

Chiang, C.C., Cheng, W.J., Korinek, M., Lin, C.Y., and Hwang, T.L. (2019). Neutrophils in Psoriasis. Front Immunol *10*, 2376.

Chiang, M.F., Yang, S.Y., Lin, I.Y., Hong, J.B., Lin, S.J., Ying, H.Y., Chen, C.M., Wu, S.Y., Liu, F.T., and Lin, K.I. (2013). Inducible deletion of the Blimp-1 gene in adult epidermis causes granulocyte-dominated chronic skin inflammation in mice. Proc. Natl. Acad. Sci. U. S. A. *110*, 6476–6481.

Cho, J.S., Pietras, E.M., Garcia, N.C., Ramos, R.I., Farzam, D.M., Monroe, H.R., Magorien, J.E., Blauvelt, A., Kolls, J.K., Cheung, A.L., et al. (2010). IL-17 is essential for host defense against cutaneous Staphylococcus aureus infection in mice. J. Clin. Invest. *120*, 1762–1773.

Cho, Y.S., Challa, S., Moquin, D., Genga, R., Ray, T.D., Guildford, M., and Chan, F.K.M. (2009). Phosphorylation-driven assembly of the RIP1-RIP3 complex regulates programmed necrosis and virus-induced inflammation. Cell *137*, 1112–1123.

Choa, R., Tohyama, J., Wada, S., Meng, H., Hu, J., Okumura, M., May, R.M., Robertson, T.F., Langan Pai, R.A., Nace, A., et al. (2021). Thymic stromal lymphopoietin induces adipose loss through sebum hypersecretion. Science (80-.). *373*.

Coderch, L., López, O., De La Maza, A., and Parra, J.L. (2003). Ceramides and skin function. Am. J. Clin. Dermatol. *4*, 107–129.

Coulombe, P.A. (1997). Towards a molecular definition of keratinocyte activation after acute injury to stratified epithelia. Biochem. Biophys. Res. Commun. *236*, 231–238.

Coulombe, P.A. (2003). Wound Epithelialization: Accelerationg the Pace of Discovery. J. Invest. Dermatol. *121*, 219–230.

Cumberbatch, M., Singh, M., Dearman, R.J., Young, H.S., Kimber, I., and Griffiths, C.E.M. (2006). Impaired Langerhans cell migration in psoriasis. J. Exp. Med. *203*, 953–960.

Dai, X., and Segre, J.A. (2004). Transcriptional control of epidermal specification and differentiation. Curr. Opin. Genet. Dev. *14*, 485.

Dai, X., Schonbaum, C., Degenstein, L., Bai, W., Mahowald, A., and Fuchs, E. (1998). The ovo gene required for cuticle formation and oogenesis in flies is involved in hair formation and spermatogenesis in mice. Genes Dev *12*, 3452–3463.

Daley, J.M., Thomay, A.A., Connolly, M.D., Reichner, J.S., and Albina, J.E. (2008). Use of Ly6G-specific monoclonal antibody to deplete neutrophils in mice. J Leukoc Biol *83*, 64–70.

Danecek, P., Bonfield, J.K., Liddle, J., Marshall, J., Ohan, V., Pollard, M.O., Whitwham, A., Keane, T., McCarthy, S.A., Davies, R.M., et al. (2021). Twelve years of SAMtools and BCFtools. Gigascience *10*, 1–4.

Deckers, J., Hammad, H., and Hoste, E. (2018). Langerhans cells: Sensing the environment in health and disease. Front. Immunol. *9*.

Dekoninck, S., and Blanpain, C. (2019). Stem cell dynamics, migration and plasticity during wound healing. Nat. Cell Biol. *21*, 18–24.

Dereksson, K., Kjartansson, S., Hjartardóttir, H., and Arngrimsson, R. (2012). Rare disease: Ichthyosis prematurity syndrome with separation of fetal membranes and neonatal asphyxia. BMJ Case Rep. *2012*.

Doebel, T., Voisin, B., and Nagao, K. (2017). Langerhans Cells – The Macrophage in Dendritic Cell Clothing. Trends Immunol. *38*, 817–828.

Dragan, M., Sun, P., Chen, Z., Ma, X., Vu, R., Shi, Y., Villalta, S.A., and Dai, X. (2022). Epidermis-Intrinsic Transcription Factor Ovol1 Coordinately Regulates Barrier Maintenance and Neutrophil Accumulation in Psoriasis-Like Inflammation. J. Invest. Dermatol. *142*, 583-593.e5.

Du, H.Y., Fu, H.Y., Li, D.N., Qiao, Y., Wang, Q.W., and Liu, W. (2016). The Expression and Regulation of Interleukin-33 in Human Epidermal Keratinocytes: A New Mediator of Atopic Dermatitis and Its Possible Signaling Pathway. J. Interf. Cytokine Res. *36*, 552–562.

Duan, Y., Dong, Y., Hu, H., Wang, Q., Guo, S., Fu, D., Song, X., Kalvakolanu, D. V., and Tian, Z. (2019). IL-33 contributes to disease severity in Psoriasis-like models of mouse. Cytokine *119*, 159–167.

Duff, M., Demidova, O., Blackburn, S., and Shubrook, J. (2015). Cutaneous manifestations of diabetes mellitus. Clin. Diabetes *33*, 40–48.

Egawa, G., Kabashima, K., Saitama, K., and Japan, S. (2016). Multifactorial skin barrier deficiency and atopic dermatitis: Essential topics to prevent the atopic march. J. Allergy Clin. Immunol. *138*, 350-358.e1.

Eidsmo, L., and Martini, E. (2018). Human Langerhans cells with pro-inflammatory features

relocate within psoriasis lesions. Front. Immunol. *9*.

Elias, P.M., Williams, M.L., and Feingold, K.R. (2012). Abnormal barrier function in the pathogenesis of ichthyosis: Therapeutic implications for lipid metabolic disorders. Clin. Dermatol. *30*, 311.

Eming, S.A., Martin, P., and Tomic-canic, M. (2014). Wound repair and regeneration : Mechanisms , signaling , and translation. Sci. Transl. Med. *6*.

Enoksson, M., Möller-Westerberg, C., Wicher, G., Fallon, P.G., Forsberg-Nilsson, K., Lunderius-Andersson, C., and Nilsson, G. (2013). Intraperitoneal influx of neutrophils in response to IL-33 is mast cell-dependent. Blood *121*, 530–536.

Feingold, K.R. (2007). Thematic review series: skin lipids. The role of epidermal lipids in cutaneous permeability barrier homeostasis. J Lipid Res *48*, 2531–2546.

van der Fits, L., Mourits, S., Voerman, J.S.A., Kant, M., Boon, L., Laman, J.D., Cornelissen, F., Mus, A.-M.M., Florencia, E., Prens, E.P., et al. (2009). Imiquimod-induced psoriasis-like skin inflammation in mice is mediated via the IL-23/IL-17 axis. J Immunol *182*, 5836–5845.

Fluhr, J.W., Elias, P.M., Man, M.Q., Hupe, M., Selden, C., Sundberg, J.P., Tschachler, E., Eckhart, L., Mauro, T.M., and Feingold, K.R. (2010). Is the Filaggrin–Histidine–Urocanic Acid Pathway Essential for Stratum Corneum Acidification? J. Invest. Dermatol. *130*, 2141.

Freeman, S.C., and Sonthalia, S. (2022). Histology, Keratohyalin Granules. StatPearls.

Fuchs, E., and Raghavan, S. (2002). Getting under the skin of epidermal morphogenesis. Nat. Rev. Genet. *3*, 199–209.

Fuchs, E., Dowling, J., Segre, J., Lo, S.H., and Yu, Q.C. (1997). Integrators of epidermal growth and differentiation: distinct functions for β1 and β4 integrins. Curr. Opin. Genet. Dev. *7*, 672–682.

Furue, K., Ito, T., Tsuji, G., Ulzii, D., Vu, Y.H., Kido-Nakahara, M., Nakahara, T., and Furue, M. (2019). The <scp>IL</scp> -13– <scp>OVOL</scp> 1– <scp>FLG</scp> axis in atopic dermatitis. Immunology *158*, 281–286.

Gabay, C., and Kushner, I. (1999). Acute-phase proteins and other systemic responses to inflammation. N. Engl. J. Med. *340*, 448–454.

Garrod, D.R., Berika, M.Y., Bardsley, W.F., Holmes, D., and Tabernero, L. (2005). Hyper-adhesion in desmosomes: its regulation in wound healing and possible relationship to cadherin crystal structure. J. Cell Sci. *118*, 5743–5754.

Gay, D., Kwon, O., Zhang, Z., Spata, M., Plikus, M. V., Holler, P.D., Ito, M., Yang, Z., Treffeisen, E., Kim, C.D., et al. (2013). Fgf9 from dermal γδ T cells induces hair follicle neogenesis after wounding. Nat. Med. 2013 197 *19*, 916–923.

Gonzales, K.A.U., and Fuchs, E. (2017). Skin and Its Regenerative Powers: An Alliance between Stem Cells and Their Niche. Dev. Cell *43*, 387–401.

Gordon, W.M., Zeller, M.D., Klein, R.H., Swindell, W.R., Ho, H., Espetia, F., Gudjonsson, J.E., Baldi, P.F., and Andersen, B. (2014). A GRHL3-regulated repair pathway suppresses immune-mediated epidermal hyperplasia. J Clin Invest *124*, 5205–5218.

Gould, L., Abadir, P., Brem, H., Carter, M., Conner-Kerr, T., Davidson, J., Dipietro, L., Falanga, V., Fife, C., Gardner, S., et al. (2015). Chronic Wound Repair and Healing in Older Adults: Current Status and Future Research. J. Am. Geriatr. Soc. *63*, 427.

Griesenauer, B., and Paczesny, S. (2017). The ST2/IL-33 axis in immune cells during inflammatory diseases. Front. Immunol. *8*, 475.

Griffiths, C.E.M. (2003). The immunological basis of psoriasis. J. Eur. Acad. Dermatology Venereol. *17*, 1–5.

Grinnell, F. (1992). COMMENTARY Wound repair, keratinocyte activation and integrin modulation. J. Cell Sci. *101*, 1–5.

Guerrero-Juarez, C.F., and Plikus, M. V. (2018). Emerging non-metabolic functions of skin fat. Nat. Rev. Endocrinol. *14*, 163.

Guinea-Viniegra, J., Zenz, R., Scheuch, H., Hnisz, D., Holcmann, M., Bakiri, L., Schonthaler, H.B., Sibilia, M., and Wagner, E.F. (2009). TNFα shedding and epidermal inflammation are controlled by Jun proteins. Genes Dev. *23*, 2663.

Haensel, D., and Dai, X. (2018). Epithelial-to-mesenchymal transition in cutaneous wound healing: Where we are and where we are heading. Dev. Dyn. *247*, 473–480.

Haensel, D., Sun, P., MacLean, A.L., Ma, X., Zhou, Y., Stemmler, M.P., Brabletz, S., Berx, G., Plikus, M. V, Nie, Q., et al. (2019). An Ovol2-Zeb1 transcriptional circuit regulates epithelial directional migration and proliferation. EMBO Rep. *20*.

Haensel, D., Jin, S., Sun, P., Cinco, R., Dragan, M., Nguyen, Q., Cang, Z., Gong, Y., Vu, R., MacLean, A.L., et al. (2020). Defining Epidermal Basal Cell States during Skin Homeostasis and Wound Healing Using Single-Cell Transcriptomics. Cell Rep. *30*, 3932-3947.e6.

Haftek, M., Oji, V., Feldmeyer, L., Hohl, D., Hadj-rabia, S., and Abdayem, R. (2022). The Fate of Epidermal Tight Junctions in the stratum corneum: Their Involvement in the Regulation of Desquamation and Phenotypic Expression of Certain Skin Conditions. Int. J. Mol. Sci. *23*, 7486.

Halvorsen, E.C., Franks, S.E., Wadsworth, B.J., Harbourne, B.T., Cederberg, R.A., Steer, C.A., Martinez-Gonzalez, I., Calder, J., Lockwood, W.W., and Bennewith, K.L. (2019). IL-33 increases ST2 + Tregs and promotes metastatic tumour growth in the lungs in an amphiregulin-dependent manner. Oncoimmunology *8*, e1527497.

Haman, F., Péronnet, F., Kenny, G.P., Doucet, É., Massicotte, D., Lavoie, C., and Weber, J.M. (2004). Effects of carbohydrate availability on sustained shivering I. Oxidation of plasma glucose, muscle glycogen, and proteins. J. Appl. Physiol. *96*, 32–40.

Hänel, K.H., Cornelissen, C., Lüscher, B., and Baron, J.M. (2013). Cytokines and the Skin Barrier. Int. J. Mol. Sci. 2013, Vol. 14, Pages 6720-6745 *14*, 6720–6745.

Haraldsen, G., Balogh, J., Pollheimer, J., Sponheim, J., and Küchler, A.M. (2009). Interleukin-33 - cytokine of dual function or novel alarmin? Trends Immunol. *30*, 227–233.

Harden, J.L., Krueger, J.G., and Bowcock, A.M. (2015). The immunogenetics of Psoriasis: A comprehensive review. J Autoimmun *64*, 66–73.

He, S., Wang, L., Miao, L., Wang, T., Du, F., Zhao, L., and Wang, X. (2009). Receptor interacting protein kinase-3 determines cellular necrotic response to TNF-alpha. Cell *137*, 1100–1111.

Hemmers, S., Schizas, M., and Rudensky, A.Y. (2021). T reg cell-intrinsic requirements for ST2 signaling in health and neuroinflammation. J. Exp. Med. *218*.

Hirota, T., Takahashi, A., Kubo, M., Tsunoda, T., Tomita, K., Sakashita, M., Yamada, T., Fujieda, S., Tanaka, S., Doi, S., et al. (2012). Genome-wide association study identifies eight new susceptibility loci for atopic dermatitis in the Japanese population. Nat. Genet. *44*, 1222–1226.

Hirt, P.A., Castillo, D.E., Yosipovitch, G., and Keri, J.E. (2019). Skin changes in the obese patient. J. Am. Acad. Dermatol. *81*, 1037–1057.

Ho, A.W., and Kupper, T.S. (2019). T cells and the skin: from protective immunity to inflammatory skin disorders. Nat. Rev. Immunol. 2019 198 *19*, 490–502.

Hsu, Y.C., and Fuchs, E. (2022). Building and Maintaining the Skin. Cold Spring Harb. Perspect. Biol. *14*, a040840.

Hsu, Y.C., Li, L., and Fuchs, E. (2014). Emerging interactions between skin stem cells and their niches. Nat. Med. *20*, 847.

Hwang, J., Kita, R., Kwon, H.S., Choi, E.H., Lee, S.H., Udey, M.C., and Morasso, M.I. (2011). Epidermal ablation of Dlx3 is linked to IL-17-associated skin inflammation. Proc. Natl. Acad. Sci. U. S. A. *108*, 11566–11571.

Ikeda, F., Deribe, Y.L., Skånland, S.S., Stieglitz, B., Grabbe, C., Franz-Wachtel, M., Van Wijk, S.J.L., Goswami, P., Nagy, V., Terzic, J., et al. (2011). SHARPIN forms a linear ubiquitin ligase complex regulating NF-κB activity and apoptosis. Nature *471*, 637–641.

Ito, M., and Cotsarelis, G. (2008). Is the hair follicle necessary for normal wound healing? J. Invest. Dermatol. *128*, 1059–1061.

Ji, S., Zhu, Z., Sun, X., and Fu, X. (2021). Functional hair follicle regeneration: an updated review. Signal Transduct. Target. Ther. 2021 61 *6*, 1–11.

Johnson, J.L., Najor, N.A., and Green, K.J. (2014). Desmosomes: regulators of cellular signaling and adhesion in epidermal health and disease. Cold Spring Harb. Perspect. Med. *4*.

Jung, S.M., Doxsey, W.G., Le, J., Haley, J.A., Mazuecos, L., Luciano, A.K., Li, H., Jang, C., and Guertin, D.A. (2021). In vivo isotope tracing reveals the versatility of glucose as a brown adipose tissue substrate. Cell Rep. *36*, 109459.

Kabashima, K., Honda, T., Ginhoux, F., and Egawa, G. (2018). The immunological anatomy of the skin. Nat. Rev. Immunol. 2018 191 *19*, 19–30.

Kakkar, R., and Lee, R.T. (2008). The IL-33/ST2 pathway: therapeutic target and novel biomarker. Nat Rev Drug Discov *7*, 827–840.

Kalluri, R., and Weinberg, R.A. (2009). The basics of epithelial-mesenchymal transition. J. Clin. Invest. *119*, 1420–1428.

Kashgari, G., Meinecke, L., Gordon, W., Ruiz, B., Yang, J., Ma, A.L., Xie, Y., Ho, H., Plikus, M. V., Nie, Q., et al. (2020). Epithelial Migration and Non-adhesive Periderm Are Required for Digit Separation during Mammalian Development. Dev. Cell *52*, 764-778.e4.

Kienle, K., and Lämmermann, T. (2016). Neutrophil swarming: an essential process of the neutrophil tissue response. Immunol. Rev. *273*, 76–93.

Kim, B.E., and Leung, D.Y.M. (2018). Significance of Skin Barrier Dysfunction in Atopic Dermatitis. Allergy Asthma Immunol Res *10*, 207–215.

Kobayashi, T., Naik, S., and Nagao, K. (2019). Choreographing Immunity in the Skin Epithelial Barrier. Immunity *50*, 552–565.

Koegel, H., Von Tobel, L., Schäfer, M., Alberti, S., Kremmer, E., Mauch, C., Hohl, D., Wang, X.J., Beer, H.D., Bloch, W., et al. (2009). Loss of serum response factor in keratinocytes results in hyperproliferative skin disease in mice. J. Clin. Invest. *119*, 899–910.

Kolarsick, P.A.J., Kolarsick, M.A., and Goodwin, C. (2011). Anatomy and Physiology of the Skin. J. Dermatol. Nurses. Assoc. *3*, 203–213.

Kortekaas Krohn, I., Aerts, J.L., Breckpot, K., Goyvaerts, C., Knol, E., Van Wijk, F., and Gutermuth, J. (2022). T-cell subsets in the skin and their role in inflammatory skin disorders. Allergy *77*, 827–842.

Kunz, B., Przybilla, B., and Vieluf, D. (1991). Atopic eczema, langerhans cells and allergy. Int. Arch. Allergy Immunol. *94*, 194–201.

Kunz, M., Simon, J.C., and Saalbach, A. (2019). Psoriasis: Obesity and Fatty Acids. Front. Immunol. *10*, 1807.

Lambert, A.W., and Weinberg, R.A. (2021). Linking EMT programmes to normal and neoplastic epithelial stem cells. Nat. Rev. Cancer *21*, 325–338.

Lamouille, S., Xu, J., and Derynck, R. (2014). Molecular mechanisms of epithelial-mesenchymal transition. Nat. Rev. Mol. Cell Biol. *15*, 178–196.

Lan, F., Yuan, B., Liu, T., Luo, X., Huang, P., Liu, Y., Dai, L., and Yin, H. (2016). Interleukin-33 facilitates neutrophil recruitment and bacterial clearance in S. aureus-caused peritonitis. Mol. Immunol. *72*, 74–80.

Langmead, B., and Salzberg, S.L. (2012). Fast gapped-read alignment with Bowtie 2. Nat. Methods 2012 94 *9*, 357–359.

Lee, B., Villarreal-Ponce, A., Fallahi, M., Ovadia, J., Sun, P., Yu, Q.C.Q.-C.Q.C., Ito, S., Sinha, S., Nie, Q., and Dai, X. (2014). Transcriptional mechanisms link epithelial plasticity to adhesion and differentiation of epidermal progenitor cells. Dev. Cell *29*, 47–58.

Lehoczky, J.A., and Tabin, C.J. (2015). Lgr6 marks nail stem cells and is required for digit tip regeneration. Proc Natl Acad Sci USA *112*, 13249–13254.

Leung, Y., Kandyba, E., Chen, Y.B., Ruffins, S., Chuong, C.M., and Kobielak, K. (2014). Bifunctional ectodermal stem cells around the nail display dual fate homeostasis and adaptive wounding response toward nail regeneration. Proc Natl Acad Sci USA *111*, 15114–15119.

Li, S., Teegarden, A., Bauer, E.M., Choi, J., Messaddeq, N., Hendrix, D.A., Ganguli-Indra, G., Leid, M., and Indra, A.K. (2017). Transcription Factor CTIP1/ BCL11A Regulates Epidermal Differentiation and Lipid Metabolism During Skin Development. Sci Rep *7*, 13427.

Liakath-Ali, K., Vancollie, V.E., Lelliott, C.J., Speak, A.O., Lafont, D., Protheroe, H.J., Ingvorsen, C., Galli, A., Green, A., Gleeson, D., et al. (2016). Alkaline ceramidase 1 is essential for mammalian skin homeostasis and regulating whole-body energy expenditure. J. Pathol. *239*, 374–383.

Lim, J., and Thiery, J.P. (2012). Epithelial-mesenchymal transitions: Insights from development. Dev. *139*, 3471–3486.

Lin, C., Hindes, A., Burns, C.J., Koppel, A.C., Kiss, A., Yin, Y., Ma, L., Blumenberg, M., Khnykin, D., Jahnsen, F.L., et al. (2013). Serum response factor controls transcriptional network regulating epidermal function and hair follicle morphogenesis. J. Invest. Dermatol. *133*, 608–617.

Liu, B., Tai, Y., Achanta, S., Kaelberer, M.M., Caceres, A.I., Shao, X., Fang, J., and Jordt, S.-E. (2016). IL-33/ST2 signaling excites sensory neurons and mediates itch response in a mouse model of poison ivy contact allergy. Proc. Natl. Acad. Sci. *113*, E7572–E7579.

Liu, N., Matsumura, H., Kato, T., Ichinose, S., Takada, A., Namiki, T., Asakawa, K., Morinaga, H., Mohri, Y., De Arcangelis, A., et al. (2019). Stem cell competition orchestrates skin homeostasis and ageing. Nature *568*, 344–350.

MacLeod, A.S., and Havran, W.L. (2011). Functions of skin-resident γδ T cells. Cell. Mol. Life Sci. *68*, 2399.

Marenholz, I., Esparza-Gordillo, J., Rüschendorf, F., Bauerfeind, A., Strachan, D.P., Spycher, B.D., Baurecht, H., Margaritte-Jeannin, P., Sääf, A., Kerkhof, M., et al. (2015). Meta-analysis identifies seven susceptibility loci involved in the atopic March. Nat. Commun. *6*, 1–8.

Margadant, C., Charafeddine, R.A., and Sonnenberg, A. (2010). Unique and redundant functions of integrins in the epidermis. FASEB J. *24*, 4133–4152.

Marzano, A. V., Ortega-Loayza, A.G., Heath, M., Morse, D., Genovese, G., and Cugno, M. (2019). Mechanisms of Inflammation in Neutrophil-Mediated Skin Diseases. Front. Immunol. *10*, 1059.

Mascré, G., Dekoninck, S., Drogat, B., Youssef, K.K., Brohée, S., Sotiropoulou, P.A., Simons,

B.D., and Blanpain, C. (2012). Distinct contribution of stem and progenitor cells to epidermal maintenance. Nat. 2012 4897415 *489*, 257–262.

Matta, B.M., Lott, J.M., Mathews, L.R., Liu, Q., Rosborough, B.R., Blazar, B.R., and Turnquist, H.R. (2014). IL-33 Is an Unconventional Alarmin That Stimulates IL-2 Secretion by Dendritic Cells To Selectively Expand IL-33R/ST2 + Regulatory T Cells . J. Immunol. *193*, 4010–4020.

McDonald, B., Pittman, K., Menezes, G.B., Hirota, S.A., Slaba, I., Waterhouse, C.C.M., Beck, P.L., Muruve, D.A., and Kubes, P. (2010). Intravascular danger signals guide neutrophils to sites of sterile inflammation. Science (80-.). *330*, 362–366.

Merad, M., Ginhoux, F., and Collin, M. (2008). Origin, homeostasis and function of Langerhans cells and other langerin-expressing dendritic cells. Nat. Rev. Immunol. *8*, 935–947.

Mevel-Ninio, M., Terracol, R., and Kafatos, F.C. (1991). The ovo gene of Drosophila encodes a zinc finger protein required for female germ line development. EMBO J. *10*, 2259.

Miao, H., Hollenbaugh, J.A., Zand, M.S., Holden-Wiltse, J., Mosmann, T.R., Perelson, A.S., Wu, H., and Topham, D.J. (2010). Quantifying the Early Immune Response and Adaptive Immune Response Kinetics in Mice Infected with Influenza A Virus. J. Virol. *84*, 6687–6698.

Miller, A.M., Asquith, D.L., Hueber, A.J., Anderson, L.A., Holmes, W.M., McKenzie, A.N., Xu, D., Sattar, N., McInnes, I.B., and Liew, F.Y. (2010). Interleukin-33 induces protective effects in adipose tissue inflammation during obesity in mice. Circ. Res. *107*, 650–658.

Milora, K.A., Fu, H., Dubaz, O., and Jensen, L.E. (2015). Unprocessed Interleukin-36alpha Regulates Psoriasis-Like Skin Inflammation in Cooperation With Interleukin-1. J Invest Dermatol *135*, 2992–3000.

Murphy, J.E., Robert, C., and Kupper, T.S. (2000). Interleukin-1 and cutaneous inflammation: A crucial link between innate and acquired immunity. J. Invest. Dermatol. *114*, 602–608.

Murphy, M., Kerr, P., and Grant-Kels, J.M. (2007). The histopathologic spectrum of psoriasis. Clin Dermatol *25*, 524–528.

Nair, M., Teng, A., Bilanchone, V., Agrawal, A., Li, B., and Dai, X. (2006). Ovol1 regulates the growth arrest of embryonic epidermal progenitor cells and represses c-myc transcription. J. Cell Biol. *173*, 253–264.

Nair, M., Bilanchone, V., Ortt, K., Sinha, S., and Dai, X. (2007). Ovol1 represses its own transcription by competing with transcription activator c-Myb and by recruiting histone deacetylase activity. Nucleic Acids Res *35*, 1687–1697.

Nakamura, M., and Ishikawa, O. (2008). The localization of label-retaining cells in mouse nails. J Investig Dermatol *128*, 728–730.

Natsuga, K. (2014). Epidermal Barriers (Cold Spring Harbor Laboratory Press).

Neess, D., Kruse, V., Marcher, A.B., Wæde, M.R., Vistisen, J., Møller, P.M., Petersen, R., Brewer, J.R., Ma, T., Colleluori, G., et al. (2021). Epidermal Acyl-CoA-binding protein is indispensable for systemic energy homeostasis. Mol. Metab. *44*, 101144.

Nguyen, A. V., and Soulika, A.M. (2019). The Dynamics of the Skin's Immune System. Int. J. Mol. Sci. *20*.

Nieto, M.A., Huang, R.Y.Y.J.J., Jackson, R.A.A., and Thiery, J.P.P. (2016). Emt: 2016. Cell *166*, 21–45.

Nunan, R., Campbell, J., Mori, R., Pitulescu, M.E., Jiang, W.G., Harding, K.G., Adams, R.H., Nobes, C.D., and Martin, P. (2015). Ephrin-Bs Drive Junctional Downregulation and Actin Stress Fiber Disassembly to Enable Wound Re-epithelialization. Cell Rep. *13*, 1380–1395.

Ohno, T., Oboki, K., Morita, H., Kajiwara, N., Arae, K., Tanaka, S., Ikeda, M., Iikura, M., Akiyama, T., Inoue, J., et al. (2011). Paracrine IL-33 Stimulation Enhances Lipopolysaccharide-Mediated Macrophage Activation. PLoS One *6*.

Oji, V., Eckl, K.M., Aufenvenne, K., Nätebus, M., Tarinski, T., Ackermann, K., Seller, N., Metze, D., Nürnberg, G., Fölster-Holst, R., et al. (2010). Loss of Corneodesmosin Leads to Severe Skin Barrier Defect, Pruritus, and Atopy: Unraveling the Peeling Skin Disease. Am. J. Hum. Genet. *87*, 274.

Okano, J., Kojima, H., Katagi, M., Nakagawa, T., Nakae, Y., Terashima, T., Kurakane, T., Kubota, M., Maegawa, H., and Udagawa, J. (2016). Hyperglycemia Induces Skin Barrier Dysfunctions with Impairment of Epidermal Integrity in Non-Wounded Skin of Type 1 Diabetic Mice. PLoS One *11*, 166215.

Olaru, F., and Jensen, L.E. (2010). Staphylococcus aureus stimulates neutrophil targeting chemokine expression in keratinocytes through an autocrine IL-1alpha signaling loop. J Invest Dermatol *130*, 1866–1876.

Oliveira, C., and Torres, T. (2019). More than skin deep: the systemic nature of atopic dermatitis. Eur J Dermatol.

Pappas, A. (2009). Epidermal surface lipids. Dermatoendocrinol. *1*, 72.

Park, S., Matte-Martone, C., Gonzalez, D.G., Lathrop, E.A., May, D.P., Pineda, C.M., Moore, J.L., Boucher, J.D., Marsh, E., Schmitter-Sánchez, A., et al. (2021). Skin-resident immune cells actively coordinate their distribution with epidermal cells during homeostasis. Nat. Cell Biol. 2021 235 *23*, 476–484.

Park, S.M., Gaur, A.B., Lengyel, E., and Peter, M.E. (2008). The miR-200 family determines the epithelial phenotype of cancer cells by targeting the E-cadherin repressors ZEB1 and

ZEB2. Genes Dev. *22*, 894–907.

Pasparakis, M., Haase, I., and Nestle, F.O. (2014). Mechanisms regulating skin immunity and inflammation. Nat Rev Immunol *14*, 289–301.

Pastille, E., Wasmer, M.H., Adamczyk, A., Vu, V.P., Mager, L.F., Phuong, N.N.T., Palmieri, V., Simillion, C., Hansen, W., Kasper, S., et al. (2019). The IL-33/ST2 pathway shapes the regulatory T cell phenotype to promote intestinal cancer. Mucosal Immunol. *12*, 990–1003.

Pastushenko, I., and Blanpain, C. (2019). EMT Transition States during Tumor Progression and Metastasis. Trends Cell Biol.

Paternoster, L., Standl, M., Chen, C.M., Ramasamy, A., Bøpnnelykke, K., Duijts, L., Ferreira, M.A., Alves, A.C., Thyssen, J.P., Albrecht, E., et al. (2011). Meta-analysis of genome-wide association studies identifies three new risk loci for atopic dermatitis. Nat Genet *44*, 187–192.

Payre, F., Vincent, A., and Carreno, S. (1999). ovo/svb integrates Wingless and DER pathways to control epidermis differentiation. Nature *400*, 271–275.

Peng, G., Mu, Z., Cui, L., Liu, P., Wang, Y., Wu, W., and Han, X. (2017). Anti-IL-33 Antibody Has a Therapeutic Effect in an Atopic Dermatitis Murine Model Induced by 2, 4-Dinitrochlorobenzene. Inflamm. 2017 411 *41*, 154–163.

Pichery, M., Mirey, E., Mercier, P., Lefrancais, E., Dujardin, A., Ortega, N., and Girard, J.-P. (2012). Endogenous IL-33 Is Highly Expressed in Mouse Epithelial Barrier Tissues, Lymphoid Organs, Brain, Embryos, and Inflamed Tissues: In Situ Analysis Using a Novel Il-33–LacZ Gene Trap Reporter Strain . J. Immunol. *188*, 3488–3495.

Pinkus, H., and Mehregan, A.H. (1966). The primary histologic lesion of seborrheic dermatitis and psoriasis. J Invest Dermatol *46*, 109–116.

Plikus, M. V, Gay, D.L., Treffeisen, E., Wang, A., Supapannachart, R.J., and Cotsarelis, G. (2012). Epithelial stem cells and implications for wound repair. Semin. Cell Dev. Biol. *23*, 946–953.

Pradella, D., Naro, C., Sette, C., and Ghigna, C. (2017). EMT and stemness: flexible processes tuned by alternative splicing in development and cancer progression. Mol. Cancer 2017 161 *16*, 1–19.

Proksch, E., Fölster-Holst, R., and Jensen, J.M. (2006). Skin barrier function, epidermal proliferation and differentiation in eczema. J. Dermatol. Sci. *43*, 159–169.

Pulawska-Czub, A., Pieczonka, T.D., Mazurek, P., and Kobielak, K. (2021). The Potential of Nail Mini-Organ Stem Cells in Skin, Nail and Digit Tips Regeneration. Int. J. Mol. Sci. *22*, 1–17.

Rajarathnam, K., Schnoor, M., Richardson, R.M., and Rajagopal, S. (2019). How do chemokines navigate neutrophils to the target site: Dissecting the structural mechanisms and signaling pathways. Cell. Signal. *54*, 69–80.

Ramos-e-Silva, M., and Jacques, C. de M.C. (2012). Epidermal barrier function and systemic diseases. Clin. Dermatol. *30*, 277–279.

Renaud, S.J., Chakraborty, D., Mason, C.W., Rumi, M.A., Vivian, J.L., Soares, M.J., Karim Rumi, M.A., Vivian, J.L., and Soares, M.J. (2015). OVO-like 1 regulates progenitor cell fate in human trophoblast development. Proc Natl Acad Sci U S A *112*, E6175-84.

Rider, P., Carmi, Y., Guttman, O., Braiman, A., Cohen, I., Voronov, E., White, M.R., Dinarello, C.A., and Apte, R.N. (2011). IL-1α and IL-1β Recruit Different Myeloid Cells and Promote Different Stages of Sterile Inflammation. J. Immunol. *187*, 4835–4843.

Rider, P., Carmi, Y., Voronov, E., and Apte, R.N. (2013). Interleukin-1alpha. Semin Immunol

25, 430–438.

Ring, J., Mohrenschlager, M., and Weidinger, S. (2012). Molecular genetics of atopic eczema. Chem Immunol Allergy *96*, 24–29.

Rivera-Gonzalez, G., Shook, B., and Horsley, V. (2014). Adipocytes in skin health and disease. Cold Spring Harb. Perspect. Med. *4*.

Roberson, E.D.O., and Bowcock, A.M. (2010). Psoriasis genetics: Breaking the barrier. Trends Genet. *26*, 415–423.

Rodriguez, C.I., Buchholz, F., Galloway, J., Sequerra, R., Kasper, J., Ayala, R., Stewart, A.F., and Dymecki, S.M. (2000). High-efficiency deleter mice show that FLPe is an alternative to Cre-loxP. Nat Genet *25*, 139–140.

Rognoni, E., and Watt, F.M. (2018). Skin Cell Heterogeneity in Development, Wound Healing, and Cancer. Trends Cell Biol. *28*, 709–722.

Ross, R., and Odland, G. (1968). Human wound repair. II. Inflammatory cells, epithelial-mesenchymal interrelations, and fibrogenesis. J. Cell Biol. *39*, 152–168.

Rousselle, P., Montmasson, M., and Garnier, C. (2019). Extracellular matrix contribution to skin wound re-epithelialization. Matrix Biol. *75–76*, 12–26.

Rübsam, M., Broussard, J.A., Wickström, S.A., Nekrasova, O., Green, K.J., and Niessen, C.M. (2018). Adherens Junctions and Desmosomes Coordinate Mechanics and Signaling to Orchestrate Tissue Morphogenesis and Function: An Evolutionary Perspective. Cold Spring Harb. Perspect. Biol. *10*, a029207.

Ryu, W.I., Lee, H., Kim, J.H., Bae, H.C., Ryu, H.J., and Son, S.W. (2015). IL-33 induces Egr-1-dependent TSLP expression via the MAPK pathways in human keratinocytes. Exp. Dermatol. *24*, 857–863.

Saito, M., Ohyama, M., and Amagai, M. (2015). Exploring the biology of the nail: An intriguing but less-investigated skin appendage. J. Dermatol. Sci. *79*, 187–193.

Sampath, H., Flowers, M.T., Liu, X., Paton, C.M., Sullivan, R., Chu, K., Zhao, M., and Ntambi, J.M. (2009). Skin-specific deletion of stearoyl-CoA desaturase-1 alters skin lipid composition and protects mice from high fat diet-induced obesity. J Biol Chem *284*, 19961–19973.

Sano, S. (2015). Psoriasis as a barrier disease. Dermatologica Sin. *33*, 64–69.

Sawant, K. V., Xu, R., Cox, R., Hawkins, H., Sbrana, E., Kolli, D., Garofalo, R.P., and Rajarathnam, K. (2015). Chemokine CXCL1-Mediated Neutrophil Trafficking in the Lung: Role of CXCR2 Activation. J. Innate Immun. *7*, 647–658.

Saxena, K., Srikrishnan, S., Celia-Terrassa, T., and Jolly, M.K. (2022). OVOL1/2: Drivers of Epithelial Differentiation in Development, Disease, and Reprogramming. Cells Tissues Organs *211*, 183–192.

Schäfer, M., and Werner, S. (2008). Cancer as an overhealing wound: an old hypothesis revisited. Nat. Rev. Mol. Cell Biol. 2008 98 *9*, 628–638.

Schmitz, J., Owyang, A., Oldham, E., Song, Y., Murphy, E., McClanahan, T.K., Zurawski, G., Moshrefi, M., Qin, J., Li, X., et al. (2005). IL-33, an Interleukin-1-like Cytokine that Signals via the IL-1 Receptor-Related Protein ST2 and Induces T Helper Type 2-Associated Cytokines. Immunity *23*, 479–490.

Schmuth, M., Blunder, S., Dubrac, S., Gruber, R., and Moosbrugger-Martinz, V. (2015). Epidermal barrier in hereditary ichthyoses, atopic dermatitis, and psoriasis. J Dtsch Dermatol Ges *13*, 1119–1123.

Segre, J.A. (2006). Epidermal barrier formation and recovery in skin disorders. J Clin Invest

116, 1150–1158.

Segre, J.A., Bauer, C., and Fuchs, E. (1999). Klf4 is a transcription factor required for establishing the barrier function of the skin. Nat Genet *22*, 356–360.

Sehat, M., Talaei, R., Dadgostar, E., Nikoueinejad, H., Akbari, H., and Sehat, M. (2018). Evaluating Serum Levels of IL-33, IL-36, IL-37 and Gene Expression of IL-37 in Patients with Psoriasis Vulgaris.

Sha, Y., Haensel, D., Gutierrez, G., Du, H., Dai, X., and Nie, Q. (2019). Intermediate cell states in epithelial-to-mesenchymal transition.

Shaw, T.J., and Martin, P. (2009). Wound repair at a glance. J. Cell Sci. *122*, 3209–3213.

Siede, J., Fröhlich, A., Datsi, A., Hegazy, A.N., Varga, D. V., Holecska, V., Saito, H., Nakae, S., and Löhning, M. (2016). IL-33 receptor-expressing regulatory t cells are highly activated, Th2 biased and suppress CD4 T Cell proliferation through IL-10 and TGFβ Release. PLoS One *11*.

Simpson, C.L., Patel, D.M., and Green, K.J. (2011). Deconstructing the skin: cytoarchitectural determinants of epidermal morphogenesis. Nat. Rev. Mol. Cell Biol. 2011 129 *12*, 565–580.

Sirvent, S., Vallejo, A.F., Davies, J., Clayton, K., Wu, Z., Woo, J., Riddell, J., Chaudhri, V.K., Stumpf, P., Nazlamova, L.A., et al. (2020). Genomic programming of IRF4-expressing human Langerhans cells. Nat. Commun. *11*, 1–12.

Stone, R.C., Pastar, I., Ojeh, N., Chen, V., Liu, S., Garzon, K.I., and Tomic-Canic, M. (2016). Epithelial-Mesenchymal Transition in Tissue Repair and Fibrosis. Cell Tissue Res. *365*, 495.

Su, Q., and Igyártó, B.Z. (2019). Keratinocytes Share Gene Expression Fingerprint with Epidermal Langerhans Cells via mRNA Transfer. J. Invest. Dermatol. *139*, 2313-2323.e8.

Su, Y., and Richmond, A. (2015). Chemokine Regulation of Neutrophil Infiltration of Skin Wounds. Adv. Wound Care *4*, 631.

Sumida, H., Yanagida, K., Kita, Y., Abe, J., Matsushima, K., Nakamura, M., Ishii, S., Sato, S., and Shimizu, T. (2014). Interplay between CXCR2 and BLT1 facilitates neutrophil infiltration and resultant keratinocyte activation in a murine model of imiquimod-induced psoriasis. J Immunol *192*, 4361–4369.

Sun, P., Vu, R., Dragan, M., Haensel, D., Gutierrez, G., Nguyen, Q., Greenberg, E., Chen, Z., Wu, J., Atwood, S., et al. (2021). OVOL1 Regulates Psoriasis-Like Skin Inflammation and Epidermal Hyperplasia. J. Invest. Dermatol. *141*, 1542–1552.

Swindell, W.R., Johnston, A., Carbajal, S., Han, G., Wohn, C., Lu, J., Xing, X., Nair, R.P., Voorhees, J.J., Elder, J.T., et al. (2011). Genome-wide expression profiling of five mouse models identifies similarities and differences with human psoriasis. PLoS One *6*, e18266.

Swindell, W.R., Michaels, K.A., Sutter, A.J., Diaconu, D., Fritz, Y., Xing, X., Sarkar, M.K., Liang, Y., Tsoi, A., Gudjonsson, J.E., et al. (2017). Imiquimod has strain-dependent effects in mice and does not uniquely model human psoriasis. Genome Med *9*, 24.

Teng, A., Nair, M., Wells, J., Segre, J.A., and Dai, X. (2007). Strain-dependent perinatal lethality of Ovol1-deficient mice and identification of Ovol2 as a downstream target of Ovol1 in skin epidermis. Biochim. Biophys. Acta - Mol. Basis Dis. *1772*, 89–95.

Theoharides, T.C., Zhang, B., Kempuraj, D., Tagen, M., Vasiadi, M., Angelidou, A., Alysandratos, K.D., Kalogeromitros, D., Asadi, S., Stavrianeas, N., et al. (2010). IL-33 augments substance P-induced VEGF secretion from human mast cells and is increased in psoriatic skin. Proc. Natl. Acad. Sci. U. S. A. *107*, 4448–4453.

Thiery, J.P., Acloque, H., Huang, R.Y.J., and Nieto, M.A. (2009). Epithelial-Mesenchymal Transitions in Development and Disease. Cell.

Thomason, H.A., Cooper, N.H., Ansell, D.M., Chiu, M., Merrit, A.J., Hardman, M.J., and Garrod,

D.R. (2012). Direct evidence that PKCα positively regulates wound re-epithelialization: correlation with changes in desmosomal adhesiveness. J. Pathol. *227*, 346–356.

Tigelaar, R.E., Lewis, J.M., and Bergstresser, P.R. (1990). TCR γ δ+ dendritic epidermal T cells as constituents of skin-associated lymphoid tissue. J. Invest. Dermatol. *94*.

Tokunaga, F., Nakagawa, T., Nakahara, M., Saeki, Y., Taniguchi, M., Sakata, S.I., Tanaka, K., Nakano, H., and Iwai, K. (2011). SHARPIN is a component of the NF-κB-activating linear ubiquitin chain assembly complex. Nature *471*, 633–636.

Tsuji, G., Hashimoto-Hachiya, A., Kiyomatsu-Oda, M., Takemura, M., Ohno, F., Ito, T., Morino-Koga, S., Mitoma, C., Nakahara, T., Uchi, H., et al. (2017). Aryl hydrocarbon receptor activation restores filaggrin expression via OVOL1 in atopic dermatitis. Cell Death Dis *8*, e2931.

Tsuji, G., Hashimoto-Hachiya, A., Yen, V.H., Miake, S., Takemura, M., Mitamura, Y., Ito, T., Murata, M., Furue, M., and Nakahara, T. (2020). Aryl Hydrocarbon Receptor Activation Downregulates IL-33 Expression in Keratinocytes via Ovo-Like 1. J. Clin. Med. *9*, 891.

Unezaki, S., Horai, R., Sudo, K., Iwakura, Y., and Ito, S. (2007). Ovol2/Movo, a homologue of Drosophila ovo, is required for angiogenesis, heart formation and placental development in mice. Genes to Cells.

Uribe-Herranz, M., Lian, L.H., Hooper, K.M., Milora, K.A., and Jensen, L.E. (2013). IL-1R1 signaling facilitates Munro's microabscess formation in psoriasiform imiquimod-induced skin inflammation. J Invest Dermatol *133*, 1541–1549.

Vasioukhin, V., Degenstein, L., Wise, B., and Fuchs, E. (1999). The magical touch: Genome targeting in epidermal stem cells induced by tamoxifen application to mouse skin. Proc. Natl. Acad. Sci. *96*, 8551–8556.

Vu, R., Dragan, M., Sun, P., Werner, S., and Dai, X. Epithelial-mesenchymal plasticity and endothelial-mesenchymal transition in cutaneous wound healing. Cold Spring Harb. Perspect. Biol.

Vulcano, M., Albanesi, C., Stoppacciaro, A., Bagnati, R., D'Amico, G., Struyf, S., Transidico, P., Bonecchi, R., Prete, A. Del, Allavena, P., et al. (2001). Dendritic cells as a major source of macrophage-derived chemokine/CCL22 in vitro and in vivo. Eur. J. Immunol. *31*, 812–822.

Wang, F., Chen, S., Liu, H.B., Parent, C.A., and Coulombe, P.A. (2018). Keratin 6 regulates collective keratinocyte migration by altering cell–cell and cell–matrix adhesion. J. Cell Biol. *217*, 4314–4330.

Wang, X., Fujita, M., Prado, R., Tousson, A., Hsu, H.C., Schottelius, A., Kelly, D.R., Yang, P.A., Wu, Q., Chen, J., et al. (2010). Visualizing CD4 T-cell migration into inflamed skin and its inhibition by CCR4/CCR10 blockades using in vivo imaging model. Br. J. Dermatol. *162*, 487.

Watanabe, K., Villarreal-Ponce, A., Sun, P., Salmans, M.L., Fallahi, M., Andersen, B., and Dai, X. (2014). Mammary morphogenesis and regeneration require the inhibition of EMT at terminal end buds by ovol2 transcriptional repressor. Dev. Cell *29*, 59–74.

Watt, F.M. (2002). Role of integrins in regulating epidermal adhesion, growth and differentiation. EMBO J. *21*, 3919–3926.

Wells, J., Lee, B., Cai, A.Q., Karapetyan, A., Lee, W.J., Rugg, E., Sinha, S., Nie, Q., and Dai, X. (2009). Ovol2 suppresses cell cycling and terminal differentiation of keratinocytes by directly repressing c-Myc and Notch1. J Biol Chem *284*, 29125–29135.

Westerberg, R., Tvrdik, P., Undén, A.B., Månsson, J.E., Norlén, L., Jakobsson, A., Holleran, W.H., Elias, P.M., Asadi, A., Flodby, P., et al. (2004). Role for ELOVL3 and fatty acid chain length in development of hair and skin function. J. Biol. Chem. *279*, 5621–5629.

Wikramanayake, T.C., Stojadinovic, O., and Tomic-Canic, M. (2014). Epidermal Differentiation in Barrier Maintenance and Wound Healing. Adv. Wound Care *3*, 272.

Wilson, R.P., Börger, L., Holton, M.D., Scantlebury, D.M., Gómez-Laich, A., Quintana, F., Rosell, F., Graf, P.M., Williams, H., Gunner, R., et al. (2019). Estimates for energy expenditure in free-living animals using acceleration proxies; a reappraisal. J. Anim. Ecol. *89*, 161–172.

Wood, L.C., Jackson, S.M., Elias, P.M., Grunfeld, C., and Feingold, K.R. (1992). Cutaneous barrier perturbation stimulates cytokine production in the epidermis of mice. J Clin Invest *90*, 482–487.

Xiao, T., Yan, Z., Xiao, S., and Xia, Y. (2020). Proinflammatory cytokines regulate epidermal stem cells in wound epithelialization. Stem Cell Res. Ther. *11*, 1–9.

Xiong, Y., and Bosselut, R. (2012). CD4-CD8 differentiation in the thymus: connecting circuits and building memories. Curr. Opin. Immunol. *24*, 139.

Xu, Q., Deng, F., Qin, Y., Zhao, Z., Wu, Z., Xing, Z., Ji, A., and Wang, Q.J. (2016). Long non-coding RNA regulation of epithelial–mesenchymal transition in cancer metastasis. Cell Death Dis. 2016 76 *7*, e2254--e2254.

Yamamoto, H., Hattori, M., Chamulitrat, W., Ohno, Y., and Kihara, A. (2020). Skin permeability barrier formation by the ichthyosis-causative gene FATP4 through formation of the barrier lipid ω-O-acylceramide. Proc. Natl. Acad. Sci. U. S. A. *117*, 2914–2922.

Yan, B., Liu, N., Li, J., Li, J., Zhu, W., Kuang, Y., Chen, X., and Peng, C. (2020). The role of Langerhans cells in epidermal homeostasis and pathogenesis of psoriasis. J. Cell. Mol. Med. *24*, 11646.

Yang, C.Y., Vogt, T.K., Favre, S., Scarpellino, L., Huang, H.Y., Tacchini-Cottier, F., and Luther, S.A. (2014). Trapping of naive lymphocytes triggers rapid growth and remodeling of the

fibroblast network in reactive murine lymph nodes. Proc. Natl. Acad. Sci. U. S. A. *111*, E109–E118.

Yang, G., Seok, J.K., Kang, H.C., Cho, Y.-Y., Lee, H.S., and Lee, J.Y. (2020a). Skin Barrier Abnormalities and Immune Dysfunction in Atopic Dermatitis. Int. J. Mol. Sci. *21*, 2867.

Yang, J., Antin, P., Berx, G., Blanpain, C., Brabletz, T., Bronner, M., Campbell, K., Cano, A., Casanova, J., Christofori, G., et al. (2020b). Guidelines and definitions for research on epithelial–mesenchymal transition. Nat. Rev. Mol. Cell Biol. 2020 216 *21*, 341–352.

Yang, J., Antin, P., Berx, G., Blanpain, C., Brabletz, T., Bronner, M., Campbell, K., Cano, A., Casanova, J., Christofori, G., et al. (2020c). Guidelines and definitions for research on epithelial–mesenchymal transition. Nat. Rev. Mol. Cell Biol.

Yokouchi, M., and Kubo, A. (2018). Maintenance of tight junction barrier integrity in cell turnover and skin diseases. Exp. Dermatol. *27*, 876–883.

Zach-Avec, D., Brolinson, A., Fisher, R.M., Carneheim, C., Csikasz, R.I., Bertrand-Michel, J., Borén, J., Guillou, H., Rudling, M., and Jacobsson, A. (2010). Ablation of the very-long-chain fatty acid elongase ELOVL3 in mice leads to constrained lipid storage and resistance to diet-induced obesity. FASEB J. *24*, 4366–4377.

Zenz, R., Eferl, R., Kenner, L., Florin, L., Hummerich, L., Mehic, D., Scheuch, H., Angel, P., Tschachler, E., and Wagner, E.F. (2005). Psoriasis-like skin disease and arthritis caused by inducible epidermal deletion of Jun proteins. Nature *437*, 369–375.

Zenz, R., Eferl, R., Scheinecker, C., Redlich, K., Smolen, J., Schonthaler, H.B., Kenner, L., Tschachler, E., and Wagner, E.F. (2008). Activator protein 1 (Fos/Jun) functions in inflammatory bone and skin disease. Arthritis Res. Ther. *10*.

Zhang, D.W., Shao, J., Lin, J., Zhang, N., Lu, B.J., Lin, S.C., Dong, M.Q., and Han, J. (2009). RIP3,

an energy metabolism regulator that switches TNF-induced cell death from apoptosis to necrosis. Science *325*, 332–336.

Zhang, X., Yin, M., and Zhang, L. (2019). Keratin 6, 16 and 17—Critical Barrier Alarmin Molecules in Skin Wounds and Psoriasis. Cells *8*, 807.

Zhang, Y., Liu, T., Meyer, C.A., Eeckhoute, J., Johnson, D.S., Bernstein, B.E., Nussbaum, C., Myers, R.M., Brown, M., Li, W., et al. (2008). Model-based analysis of ChIP-Seq (MACS). Genome Biol. *9*, 1–9.

Zheng, T. (2014). The Atopic March: Progression from Atopic Dermatitis to Allergic Rhinitis and Asthma. J. Clin. Cell. Immunol. *05*.

Zubiría, M.G., Giordano, A.P., Gambaro, S.E., Alzamendi, A., Frontini-López, Y.R., Moreno, G., Spinedi, E., and Giovambattista, A. (2020). Dexamethasone primes adipocyte precursor cells for differentiation by enhancing adipogenic competency. Life Sci. *261*, 118363.

APPENDIX 1: Ovol1 and Ovol2 contribution to wound healing.

Incorporates information from published review articles:

Article:

Epithelial-mesenchymal plasticity and endothelial-mesenchymal transition in cutaneous wound healing

Remy Vu*, Morgan Dragan*, Peng Sun, Sabine Werner, and Xing Dai
('*' denotes co-first authors)

Introduction

Chronic wounds are more common among the elderly and wound healing in general is known to slow with age (Gould et al., 2015). Wound healing is a concerted process involving a multitude of cell types (e.g. keratinocytes, fibroblasts, immune cells, endothelial cells) in the wound microenvironment and consists of several overlapping phases that include injury-induced hemostasis and inflammation, new tissue formation fueled by migration and proliferation of different cell types, and finally tissue remodeling (Eming et al., 2014; Shaw and Martin, 2009). Central to the healing process is re-epithelialization, where keratinocytes in wound-edge epidermis and within the injured hair follicles proliferate, migrate, and differentiate in a highly controlled and spatiotemporally orchestrated manner to produce a new epidermis that covers the wound. A long-held view has been that during wound healing, wound peripheral keratinocytes undergo partial and reversible EMT to facilitate migration and re-epithelialization (Arnoux V., Come C., Kusewitt D., 2005; Haensel and Dai, 2018). However, this process is now termed epithelial-mesenchymal plasticity (EMP) to describe the morphological/cellular/molecular events

that occur during wound epidermal cell migration and re-epithelialization that do not require full reversion since keratinocytes still maintain their identity. TFs that inhibit EMT and promote the reverse process, mesenchymal-epithelial transition or MET, have also been identified and these include Ovol1, Ovol2, and Grhl2 (Lee et al., 2014; Nieto et al., 2016; Watanabe et al., 2014).

Ovol2 zinc finger TF has been identified as a master transcriptional suppressor of EMT-associated gene expression, and its major target is core EMT-TF Zeb1 (Lee et al., 2014; Watanabe et al., 2014). Ovol2 is expressed by epidermal cells in the proliferative region but not the migrating front of the wound, and *K14-Cre*-directed *Ovol2* deletion in keratinocytes delays wound healing (Haensel et al., 2019). The migrating front is aberrantly extended in wounds of *Ovol2*-deficient mice, and genetic lineage tracing of epidermal cells reveals dissemination of what appear to be single cells in the wound dermis (Haensel et al., 2019). This latter finding is seemingly consistent with typical EMT-like behavior, i.e., the ability of epithelial cells to breach the basement membrane and to lose all cell-cell contacts (Yang et al., 2020c). This said, such single cells are very rare and whether they adopt a true mesenchymal fate has not been investigated. Live cell imaging of wound explants and cultured hair follicle stem cells (HFSCs) support a requirement of Ovol2 for cohesive and directional migration, and in its absence, cells become mesenchymal-like and migrate at a faster speed than their normal counterparts but with significantly reduced directionality (Haensel et al., 2019). Importantly, such defects are near-completely rescued when *Zeb1* is simultaneously deleted. The demonstrated functional significance of balancing the actions of EMT-inhibiting TF Ovol2 and EMT-TF Zeb1 in achieving directional cell migration of epidermal cells implicates the importance of maintaining an E/M

intermediate state for optimal wound re-epithelialization. In a nut shell, wound-edge keratinocytes not only undergo partial EMT-like changes in order to migrate, they also need to actively prevent adhesion dissolution from going too far so this process becomes more like a full EMT. This may be one of the mechanisms that prevent malignant transformation of these cells in a wound environment that exhibits various tumor-promoting features (Schäfer and Werner, 2008).

While Ovol2 proved to be important for wound healing, Ovol1-defficient mouse, shown to have more of a function in maintaining skin barrier and inflammation, epidermis showed no difference in wound closure in preliminary studies (data not shown) (Dragan et al., 2022; Sun et al., 2021). Since my current thesis work in Chapter 4 shows that Ovol1 and Ovol2 have some unique and redundant functions, we sought to discover if loss of *Ovol1* and *Ovol2* in adulthood removed any compensatory mechanisms that may have prevented Ovol1-deficient mice from displaying a defect in re-epithelialization of cutaneous wounds

Results

Initial time course characterization of epithelialization of wounds in *Ovol1/2* iDKO mice show no visual changes in wound of mice that were treated with TAM at P21 and wounded at P49 showed no obvious delay in wound closure (Appendix Figure 1.1 A). Given that there were no changes to mice at a younger timepoint we next tested if aged *Ovol1/2* iDKO have deficiencies in wounding when keratinocytes are less plastic. We saw no differences in wound closure between *Ovol1/2* iDKO and control littermates that displayed differences in bod weight (Appendix Figure 1.1 B). We also did not observe any differences in vascularization of the wounds between *Ovol1/2* iDKO and control mice (Appendix Figure

1.1 A). When analyzing histology of wounds at 7d after wounding we did not see any changes to reepithelization or to resolution of the wound bed (Appendix Figure 1.1 C). When combining wound closure measurements between the young and aged mice we saw no difference in wound closure (Appendix Figure 1.1 D).

Conclusions

Interestingly, there was no difference seen in this particular experiment between aged *Ovol1/2* iDKO wound closure against the young. In chapter 4, I show that Ovol1 and Ovol2 alters transcriptional networks important for keratinocyte maturation and function leading to the question of whether the *Ovol1/2* iDKO keratinocytes become "exhausted" over time. It appears as that this may not be the case, or if it were, it did not manifest in wounding experiments. It is also curious that loss of Ovol1 and Ovol2 did not cause any changes in wound closure in both aged and young mice since loss of *Ovol2* alone was enough to cause delayed wound healing. It is possible that since Ovol1 and Ovol2 transcriptionally repress one another that there is a cancellation effect where the loss of regulation by Ovol1 or 2 can nullify the function of the other. It is interesting to note that homeostatic *Ovol1/2* iDKO already exhibits EMP-like structural and adhesion qualities (Chapter 4), perhaps priming keratinocytes such that they are pre-transcriptionally activated for epithelial migration. Since Ovol1 and Ovol2 are important for maintaining barrier, it is also possible that in the case of severe trauma, like a wound, other compensatory mechanisms are upregulated to offset for the deficiency. Future work could be done to progressively track the migration the leading edge and proliferative zone of wounded Ovol*1/2* iDKO epidermis to understand whether there are subtle defects or an

definitive explanation as to why *Ovol1/2* iDKO skin heals normal in aged and young mice compared to *Ovol2* SSKO mice.

Additional materials and methods

Wounding

7-week-old (p49, telogen) and 8 MPI mice were anesthetized using isoflurane (Primal Healthcare; NDC-66794-017-25), their backs shaved, and then a 6-mm punch (Integra; 33-36) was used to generate a full-thickness wound on each side of the mouse. Wounds were collected 7 days later for analysis.

Appendix Figure 1.1: Loss of *Ovol1* and *Ovol2* in adulthood does not lead to wound healing defects in young or aged mice.

- **A.** Representative time course images of wounded mice back skin treated with TAM at P21 and wounded at P49.
- **B.** Image of wounded mice back skin (top) and underlying vasculature to the wound (bottom) at day 7 after wounding treated with TAM at P49 and wounded at 8 MPI.
- **C.** H&E images of the whole wounds from mice wounded at 8 MPI at 7d.
- **D.** Combined measurements of young and old mouse wound closure area over time. n=2 pairs.

Data information: Scale bar: 500 μm in C. MPI = Months post injection, d = days post wounding.

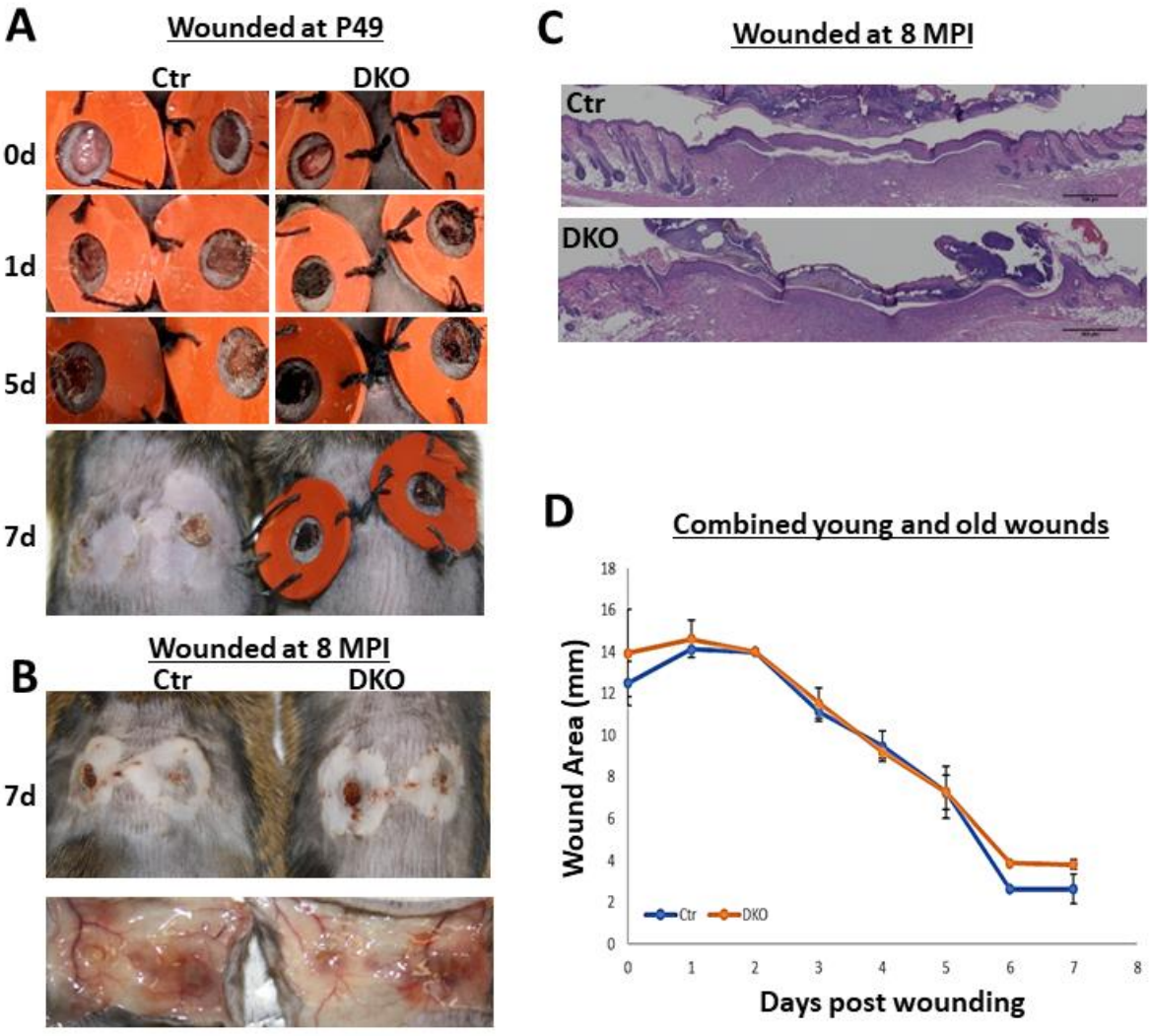

References

Arnoux V., Come C., Kusewitt D., S.P. (2005). Cutaneous Wound Reepithelialization: A Partial and Reversible EMT. In Rise and Fall of Epithelial Phenotype: Concepts OfEpithelial-Mesenchymal T, S. P., ed. pp. 111–134.

Dragan, M., Sun, P., Chen, Z., Ma, X., Vu, R., Shi, Y., Villalta, S.A., and Dai, X. (2022). Epidermis-Intrinsic Transcription Factor Ovol1 Coordinately Regulates Barrier Maintenance and Neutrophil Accumulation in Psoriasis-Like Inflammation. J. Invest. Dermatol. *142*, 583-593.e5.

Eming, S.A., Martin, P., and Tomic-canic, M. (2014). Wound repair and regeneration : Mechanisms , signaling , and translation. Sci. Transl. Med. *6*.

Gould, L., Abadir, P., Brem, H., Carter, M., Conner-Kerr, T., Davidson, J., Dipietro, L., Falanga, V., Fife, C., Gardner, S., et al. (2015). Chronic Wound Repair and Healing in Older Adults: Current Status and Future Research. J. Am. Geriatr. Soc. *63*, 427.

Haensel, D., and Dai, X. (2018). Epithelial-to-mesenchymal transition in cutaneous wound healing: Where we are and where we are heading. Dev. Dyn. *247*, 473–480.

Haensel, D., Sun, P., MacLean, A.L., Ma, X., Zhou, Y., Stemmler, M.P., Brabletz, S., Berx, G., Plikus, M. V, Nie, Q., et al. (2019). An Ovol2-Zeb1 transcriptional circuit regulates epithelial directional migration and proliferation. EMBO Rep. *20*.

Lee, B., Villarreal-Ponce, A., Fallahi, M., Ovadia, J., Sun, P., Yu, Q.C.Q.-C.Q.C., Ito, S., Sinha, S., Nie, Q., and Dai, X. (2014). Transcriptional mechanisms link epithelial plasticity to adhesion and differentiation of epidermal progenitor cells. Dev. Cell *29*, 47–58.

Nieto, M.A., Huang, R.Y.Y.J.J., Jackson, R.A.A., and Thiery, J.P.P. (2016). Emt: 2016. Cell *166*, 21–45.

Schäfer, M., and Werner, S. (2008). Cancer as an overhealing wound: an old hypothesis revisited. Nat. Rev. Mol. Cell Biol. 2008 98 *9*, 628–638.

Shaw, T.J., and Martin, P. (2009). Wound repair at a glance. J. Cell Sci. *122*, 3209–3213.

Sun, P., Vu, R., Dragan, M., Haensel, D., Gutierrez, G., Nguyen, Q., Greenberg, E., Chen, Z., Wu, J., Atwood, S., et al. (2021). OVOL1 Regulates Psoriasis-Like Skin Inflammation and Epidermal Hyperplasia. J. Invest. Dermatol. *141*, 1542–1552.

Watanabe, K., Villarreal-Ponce, A., Sun, P., Salmans, M.L., Fallahi, M., Andersen, B., and Dai, X. (2014). Mammary morphogenesis and regeneration require the inhibition of EMT at terminal end buds by ovol2 transcriptional repressor. Dev. Cell *29*, 59–74.

Yang, J., Antin, P., Berx, G., Blanpain, C., Brabletz, T., Bronner, M., Campbell, K., Cano, A., Casanova, J., Christofori, G., et al. (2020). Guidelines and definitions for research on epithelial–mesenchymal transition. Nat. Rev. Mol. Cell Biol.

APPENDIX 2: Gene expression changes in sorted LCs from iDKO mice.

Introduction

LCs are a tissue resident immune cells residing in the epidermis. In homeostasis when LCs are not cycling to the LN to promote tolerance, they must be adhered to keratinocytes to maintain structure and barrier (Yan et al., 2020). During mild barrier disruption, LCs promote preventative immunity by activating humoral responses and after severe barrier defects, LCs can initiate T cell responses by trafficking to the lymph node to present antigen (Yan et al., 2020). While much research has gone into LC development and response to pathogens, less is known about non-canonical molecular regulation of LC function and the cross-talk between LCs and keratinocytes and how this cross-talk can affect LC activation and migration.

LCs can regulate adhesions with keratinocytes in order to maintain barrier integrity while sampling pathogens near the cornified layer (Yan et al., 2020). When LCs become activated to present LCs to the lymph node, they must also break adhesions with keratinocytes and retract their dendrites before they can migrate (Yan et al., 2020). Interestingly, it has been speculated that loss of contact with epidermal cells drives transcriptional changes in LCs to promote tolerogenic T cell response and immune homeostasis (Sirvent et al., 2020). Evidence also suggests that changes in LC dendrite structure and morphology can change their special patterning in the epidermis (Park et al., 2021). My work in Chapter 4 shows that LCs appear activated in the *Ovol1/2* iDKO mice exhibiting the characteristic rounded morphology and increased expression of MHC II (Figure 4.4A-D) (Van den Bossche and Van Ginderachter, 2013; Yan et al., 2020). Since

Ovol1 and Ovol2 ChIP-seq cross analyzed with *Ovol1/2* iDKO RNA-sequencing data from Chapter 4 showed that Ovol1 and Ovol2 likely regulate genes involved in cytoskeletal structure and adhesion, we wondered whether Ovol1 and Ovol2 could have cell autonomous functions in LCs.

Results

Using the publicly available microarray dataset Gene Skyline by the Immgen database gene (https://www.immgen.org/ImmGenApps.html), we found that LCs express RNA transcripts for *K14, Ovol1,* and *Ovol2* (Appendix Figure 2.A). Since Keratinocytes are known to transfer functional transcripts to LCs via nanotubes, we wondered whether Ovol1 and Ovol2 could be dysregulated in LCs and whether they can regulate LC gene expression. First, we sorted LCs from *Ovol1/2* iDKO mice and littermate controls and performed RT-qPCR on *K14, Ovol1* and *Ovol2* and found them to be downregulated in the *Ovol1/2* iDKO mice compared with control and similar to that of $CD45^-$ cells (namely keratinocytes) sorted from the same tissue (Appendix Figure 2.B-C). We next asked whether Ovol1 and Ovol2 target genes identified by ChIP- and RNA-seq analysis in Chapter 4 were also downregulated. We screened some of the top candidate genes involved in cytoskeletal structure and adhesion on the Gene Skyline database and found that LCs do express a number of the genes that Ovol1 and Ovol2 co-regulate (e.g., *Vim, Dennd5a,* and *Ccl22* among others, not shown) (Appendix Figure 2.D). We then performed RT-qPCR on the top three genes that appeared most highly expressed in LCs from the microarray data on sorted LCs from control and *Ovol1/2* iDKO mice, but only found *Ccl22* to be upregulated in the *Ovol1/2*

DKO sample. Interestingly, *Ccl22* appears to be decreased in CD45$^-$ cells while *Dennd5a* and *Vim* appear to be upregulated.

Discussion

LCs in the epidermis of iDKO mice appear more activated than their control counterparts. We speculated three main hypothesis. 1) It is possible that the reduced adhesive properties of *Ovol1/2*-deficient epidermal cells may be a potential mechanism to drive aberrant activation of LCs. 2) Alternatively, *Ovol1/2*-deficient epidermal cells may alter their expression of inflammatory cytokines that signal to LCs. 3) Lastly, it is possible that Ovol1 and Ovol2 have cell autonomous function in LCs.

These data show that *K14, Ovol1* and *Ovol2* are reduced in the LCs of *Ovol1/2* DKO mice and *Ccl22* appears to be upregulated. It appears that the gene expression changes we observed from RNA-seq of *Ccl22* are mostly driven by LCs. LCs are known to be the most prolific expressors of *Ccl22* and our findings showing that iDKO LCs had higher expression of *Ccl22* compared with control and CD45$^-$ actually expressed lower levels of *Ccl22* is consistent with this (Vulcano et al., 2001). While we did see an elevated expression of *Ccl22*, suggesting a possible function for Ovol1 and Ovol2 within LCs, none of the other top candidates for Ovol1 and Ovol2 showed any change in gene expression. There were other candidate genes not shown here that can be screened to see if there is a LC-Ovol1/Ovol2 specific function in regulating those genes. It is also possible that Ovol1 and Ovol2 have highly specific functions in LCs and only regulate few genes, possibly only inflammatory genes. However, we did not rule out the possibility that the keratinocyte-driven loss of contact with LCs is a trigger for LC activation in and of itself. Much work would need to be

done to 1) prove that Ovol1/2 can regulate expression of *Ccl22* in LCs or 2) to show that loss of contact with neighboring cells can induce transcriptional changes in LCs. Answering these questions would provide new lights to keratinocyte-immune cross talks and how transferring of regulators may be a major function of mediating inflammatory responses.

Appendix Figure 2.1: Transcriptional changes from LCs sorted from *Ovol1* and *Ovol2* iDKO mice.

- **A.** Microarray gene expression data from the designated immune cell subtypes from Gene Skyline from the Immgen database (https://www.immgen.org/ImmGenApps.html) for the indicated genes.
- **B.** RT-qPCR data of the indicated genes from sorted LCs at 52 DPI post TAM injections. n=2 pairs
- **C.** RT-qPCR data of the indicated genes from sorted $CD45^-$ cells at 52 DPI post TAM injections. n=1 pair
- **D.** Microarray gene expression data from the designated immune cell subtypes from Gene Skyline from the Immgen database (https://www.immgen.org/ImmGenApps.html) for the indicated genes.
- **E.** RT-qPCR data of the indicated genes from sorted LCs at 52 DPI post TAM injections. n=2 pairs
- **F.** RT-qPCR data of the indicated genes from sorted $CD45^-$ cells at 52 DPI post TAM injections. n=1 pair

Data information: Scale bar: LCs = Langerhans cells

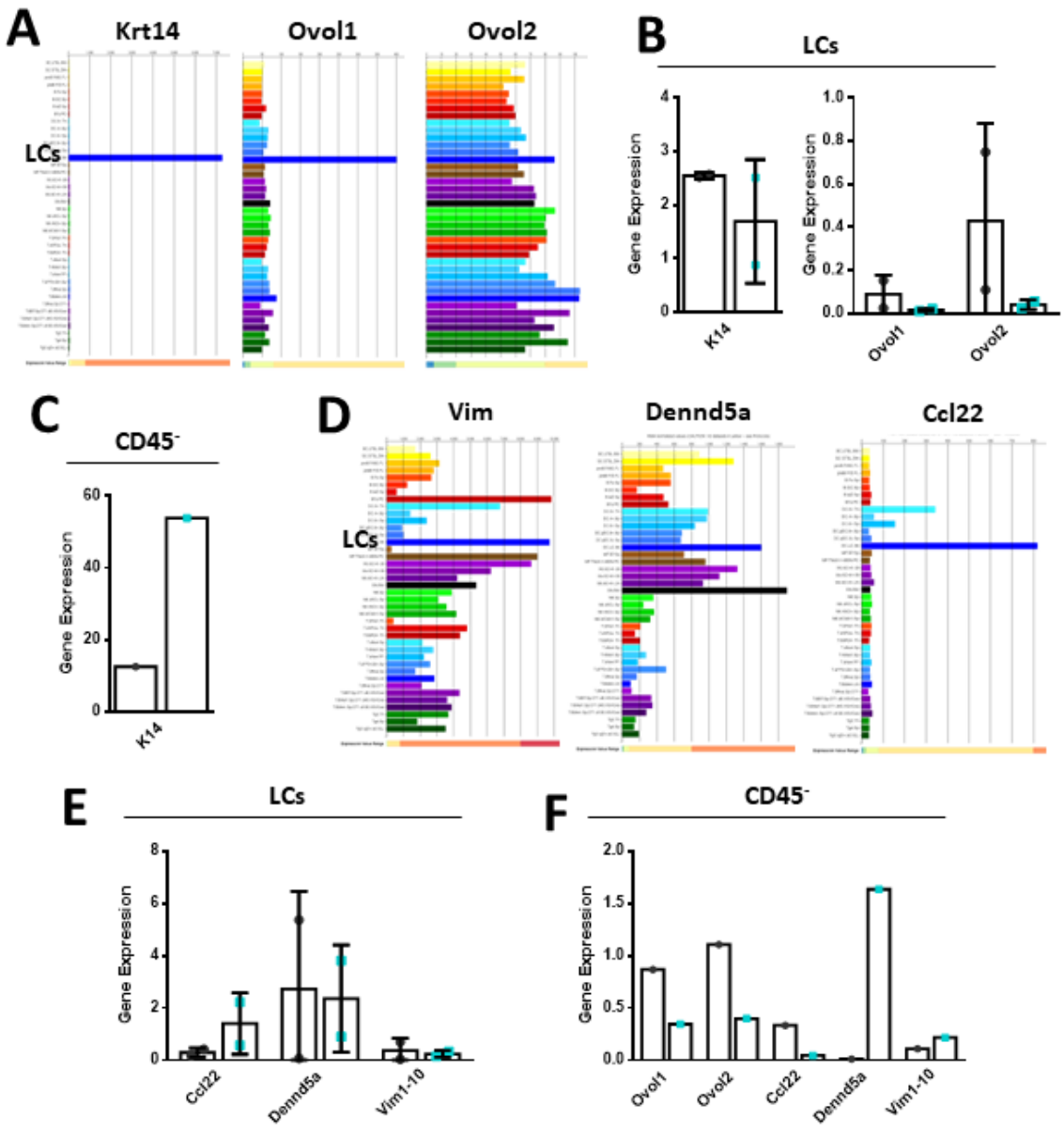
A
Krt14
Ovol1
Ovol2
LCs
B
LCs
Gene Expression
K14
Ovol1
Ovol2
C
CD45-
Gene Expression
K14
D
Vim
Dennd5a
Ccl22
LCs
E
LCs
Gene Expression
Ccl22
Dennd5a
Vim1-10
F
CD45-
Gene Expression
Ovol1
Ovol2
Ccl22
Dennd5a
Vim1-10

References

Van den Bossche, J., and Van Ginderachter, J.A. (2013). E-cadherin: from epithelial glue to immunological regulator. Eur. J. Immunol. *43*, 34–37.

Park, S., Matte-Martone, C., Gonzalez, D.G., Lathrop, E.A., May, D.P., Pineda, C.M., Moore, J.L., Boucher, J.D., Marsh, E., Schmitter-Sánchez, A., et al. (2021). Skin-resident immune cells actively coordinate their distribution with epidermal cells during homeostasis. Nat. Cell Biol. 2021 235 *23*, 476–484.

Sirvent, S., Vallejo, A.F., Davies, J., Clayton, K., Wu, Z., Woo, J., Riddell, J., Chaudhri, V.K., Stumpf, P., Nazlamova, L.A., et al. (2020). Genomic programming of IRF4-expressing human Langerhans cells. Nat. Commun. *11*, 1–12.

Vulcano, M., Albanesi, C., Stoppacciaro, A., Bagnati, R., D'Amico, G., Struyf, S., Transidico, P., Bonecchi, R., Prete, A. Del, Allavena, P., et al. (2001). Dendritic cells as a major source of macrophage-derived chemokine/CCL22 in vitro and in vivo. Eur. J. Immunol. *31*, 812–822.

Yan, B., Liu, N., Li, J., Li, J., Zhu, W., Kuang, Y., Chen, X., and Peng, C. (2020). The role of Langerhans cells in epidermal homeostasis and pathogenesis of psoriasis. J. Cell. Mol. Med. *24*, 11646.

APPENDIX C: The Role of Ovol1 during *Pseudomonas aeruginosa* infection of the Corneas

(In collaboration with Dr. Bridget Ratitong and Dr. Eric Pearlman.)

Introduction

Microbial keratitis, or infection of the cornea, is one of the leading causes of blindness worldwide. In immunocompromised individuals, the infection could lead to fatal disseminated disease if left untreated (Ratitong and Pearlman 2021). Risk factors include ocular trauma and contact lens use that allow opportunistic pathogens such as *Pseudomonas aeruginosa* to breach the corneal epithelial barrier. Treatment for microbial keratitis include antimicrobial agents followed by corticosteroids to suppress inflammation. However, corticosteroids globally reduce immunity and could potentially allow rapid growth of bacteria or fungi in the absence of an immune response. Thus, understanding the molecular mechanisms governing corneal barrier maintenance and regulation of inflammation will provide a more targeted treatment for the disease.

The cornea consists of a stratified corneal epithelial cell barrier, the corneal stroma, and a singular layer of endothelium. The corneal stroma is primarily composed of extracellular collagen matrix and is avascular to maintain transparency (Blackburn et al. 2019). Thus, the cornea has relatively few resident immune cells, and upon ocular trauma is highly susceptible to infections. Previous studies revealed that the transcription factor Ovol2, an inhibitor of epithelial-to-mesenchymal transition (Lee et al., 2014), maintains the cell identity of corneal epithelial cells through repressing mesenchymal gene expression

(Kitazawa et al 2016; Chung et al. 2019). However, its homolog Ovol1 has not been studied in the cornea despite being expressed in the corneal epithelial layer and the limbus and conjunctiva of the eye.

Ovol1 is a transcription factor present in stratified squamous keratinized epithelium, such as the skin. Embryonically, Ovol1 is shown to repress proliferation of epidermal keratinocytes (Nair et al 2006). Using adult *Ovol1*$^{fl/-}$; K14-Cre$^{+/-}$ (SSKO) mice, that Ovol1 helps maintain skin barrier function upon external challenges that induce inflammation (Dragan et al., 2021). Moreover, in psoriatic-like skin inflammation, Ovol1 can regulate an inflammatory response, namely neutrophil recruitment, through directly repressing expression of *Cxcl1* and indirectly reducing expression of *Il1a* (Sun et al 2021, Dragan et al 2021). Ocular trauma is the most common risk factor for infection of the corneas (microbial keratitis) which is the second major cause of permanent blindness worldwide. Despite advances in the field, there is still a need for better and more targeted treatment for keratitis. Understanding the molecular regulation behind corneal epithelial cell barrier maintenance and exploring the role Ovol1 has in the corneal-immune cell cross-talks could provide potential targets for better therapeutics.

Results

The function of Ovol1 in the cornea has not been explored. Preliminary data suggests that corneal progenitor cells located in the conjunctiva and limbus express K14 (Appendix Figure 3A). Moreover, expression levels of human OVOL1 (GDS2682/206604) and mouse Ovol1 (GDS2682/206604) from the Gene Expression Omnibus show the

presence of Ovol1 transcripts in cornea of mice and humans, and also in the conjunctiva of humans (Appendix Figure 3B-C). Using RNA-scope for *Ovol1* and immunofluorescent staining of K14, expression of Ovol1 is found to be predominantly at the transition from the corneal region to the limbus ($K14^{+}$) where the progenitor cells reside (Appendix Figure 3D-E). In order to understand the function of Ovol1 in corneas after bacterial infection, we scratched and infected littermate control mice and $Ovol1^{fl/-}$;K14-$Cre^{+/-}$ (SSKO) mice GFP-labeled *P. aeruginosa* (PAO1) for either 28 or 48 hours and measured the bacterial burden (Appendix Figure 3F). 28 hours post infection (hpi) we found that Ovol1 SSKO mice had decreased bacterial burden compared with controls (Appendix Figure 3G). However, 48 hpi we saw both increased keratitis and bacterial burden in light fluorescence images of GFP and by colony counting of plated bacteria from the corneas (Appendix Figure 3H-I). Given this data, we hypothesize that Ovol1 deficiency leads to decreased corneal epithelial cell differentiation, and therefore impaired healing of the ocular surface and reduced bacterial killing during infection.

Discussion

Preliminary data shows that corneal progenitor cells located in the conjunctiva and limbus express K14 and corneal cells between the cornea and limbus express Ovol1 (Appendix Figure 3A-E). We show that K14-driven *Ovol1* deletion leads to initially (28 hpi) less bacterial burden with a higher bacterial inoculum, but after 48 hpi of normal bacterial inoculum, we observe more severe keratitis after infection (Appendix Figure 3F-I). We hypothesize that Ovol1 helps maintain corneal barrier function and facilitates corneal

epithelial cell differentiation. Given that Ovol1 has known function in regulating neutrophil recruitment and cytokine expression in both a direct and indirect manner within skin epithelium, we also hypothesize that Ovol1 may have site-specific immune regulatory function in the corneal epithelium as well (Sun et al. 2020; Dragan et al. 2021). Existing ChIP-sequencing of Ovol1 done in skin can be used as a screen for potential targets. Future studies will need to test the function of Ovol1 in corneas so *in vitro* iRNA knock down of Ovol1 in corneal cell lines can provide insights into the relevance and function of Ovol1 in the eye. Moreover, corneal scratch assays and single cell RNA-seq can provide insights into the molecular regulation of Ovol1 in homeostasis and after damage when eye barrier needs to be repaired. We hypothesize that the loss of Ovol1 leaves the cornea susceptible to barrier defects especially after ocular trauma. Therefore, we anticipate that siRNA KD of *Ovo1* in corneal epithelial cell cultures will result in reduced cellular adherence and impaired corneal stratification. Further, we anticipate that infection of these cell lines will exacerbate barrier defects and transiently delay healing. Since loss of *Ovol1* can cause subtle phenotypes to emerge when unstimulated, one way to combat this is to induce ocular trauma by scratching the cornea. *In vivo,* we expect the scratches to reveal barrier defects in *Ovol1* SSKO mice with a potential delay in healing. We expect to see increased pro-inflammatory cytokines in SSKO mice along with corneal epithelial cell death and delayed epithelial differentiation. The defects caused by Ovol1-deficient corneal epithelial cells are expected to delay bacterial clearance. Finally, we expect that scRNA-seq analysis will reveal a delay in transition from the basal states to the differentiated states for corneal epithelial cells. We also expect that CellChat will reveal a shift in communication between epithelial cells and the “preferred” immune cell response in the infected WT control and we

would observe an “altered” cellular response where there is a change in recruited immune cell composition in the infected SSKO mice.

Additional Materials and Methods

Bacterial strains and culture conditions

P. aeruginosa ExoS-expressing strains PAO1 and PAO1-GFP were obtained from Dr. A. Rietsch (Case Western Reserve University). Bacteria were grown to midlog phase (~1×10^8 bacteria/ml) in high-salt Luria–Bertoni broth, which enhances expression of the type III secretion system (T3SS) at 37°C with 5% CO_2, 200 rpm. Bacteria were then washed and resuspended in sterile PBS to 5×10^4 bacteria/2 μl for all in vivo infections.

Murine model of Pseudomonas keratitis

Corneal epithelial abrasion of 3 × 10 mm was performed using a sterile 30-gauge needle followed by topical infection of 5×10^4 PAO1 or PAO1-GFP in 2 μl PBS as described previously (**5**). CFU was quantified at 2 hpi to verify the inoculum for each experiment. At 24, 28, or 48 hpi, mice were euthanized, and corneal opacity and GFP fluorescence were imaged and quantified.

CFU quantification

At 2 (inoculum), 24, 48, or 72 hpi, whole eyes were collected and homogenized in 1 ml PBS. Serial log dilutions of homogenate were plated on LB plates and incubated at 37°C with 5% CO_2 overnight. Colonies were counted manually, and CFUs were calculated as: (number of colonies × dilution factor × 100 [10 μl of the 1 ml was used for plating and dilution]).

Figure 1: Ovol1 SSKO corneas have increased bacterial burden during Pseudomonas keratitis.

A. Immunofluorescent staining of uninfected, WT eyes for K14 (green) and DAPI. Scale bars: 500um (top, whole eye), 50um (bottom, conjunctiva).
B. Expression levels of human GDS2682/206604 *OVOL1* from the Gene Expression Omnibus. N=3.
C. Expression levels of mouse GDS2682/206604 *Ovol1* from the Gene Expression Omnibus. N=4
D. RNA-scope immunofluorescent images of noninfected (top) and 24-hpi (bottom) eyes focusing on the limbus to cornea region for the indicated markers.
E. Zoom in of the cornea from (D) on the Ovol1$^+$ region where the cornea transitions to the limbus.
F. Diagram depicting the treatment strategy for corneal eye infections of SSKO mice.
G. Colony formation units (CFUs) of bacteria counted from infected WT and Ovol1 SSKO eyes 28-hpi but with 300,000 units of *P. Aeruginosa*. N=4.
H. Colony formation units (CFUs) of bacteria counted from infected WT and Ovol1 SSKO eyes 48-hpi. For T=2 n=11, for Control n=13, and for SSKO, n=6.
I. Images of corneal opacity (top) and GFP-labeled PAO1 48-hpi of the indicated genotypes.

Data information: For statistical analysis in (B-C, and G), we used an unpaired two-tailed Student's t-test. For statistical analysis in H, we used one-way Anova. *** $p<0.005$; ** $p<0.01$; * $p<0.05$. Errors bars are represented as ± SD.

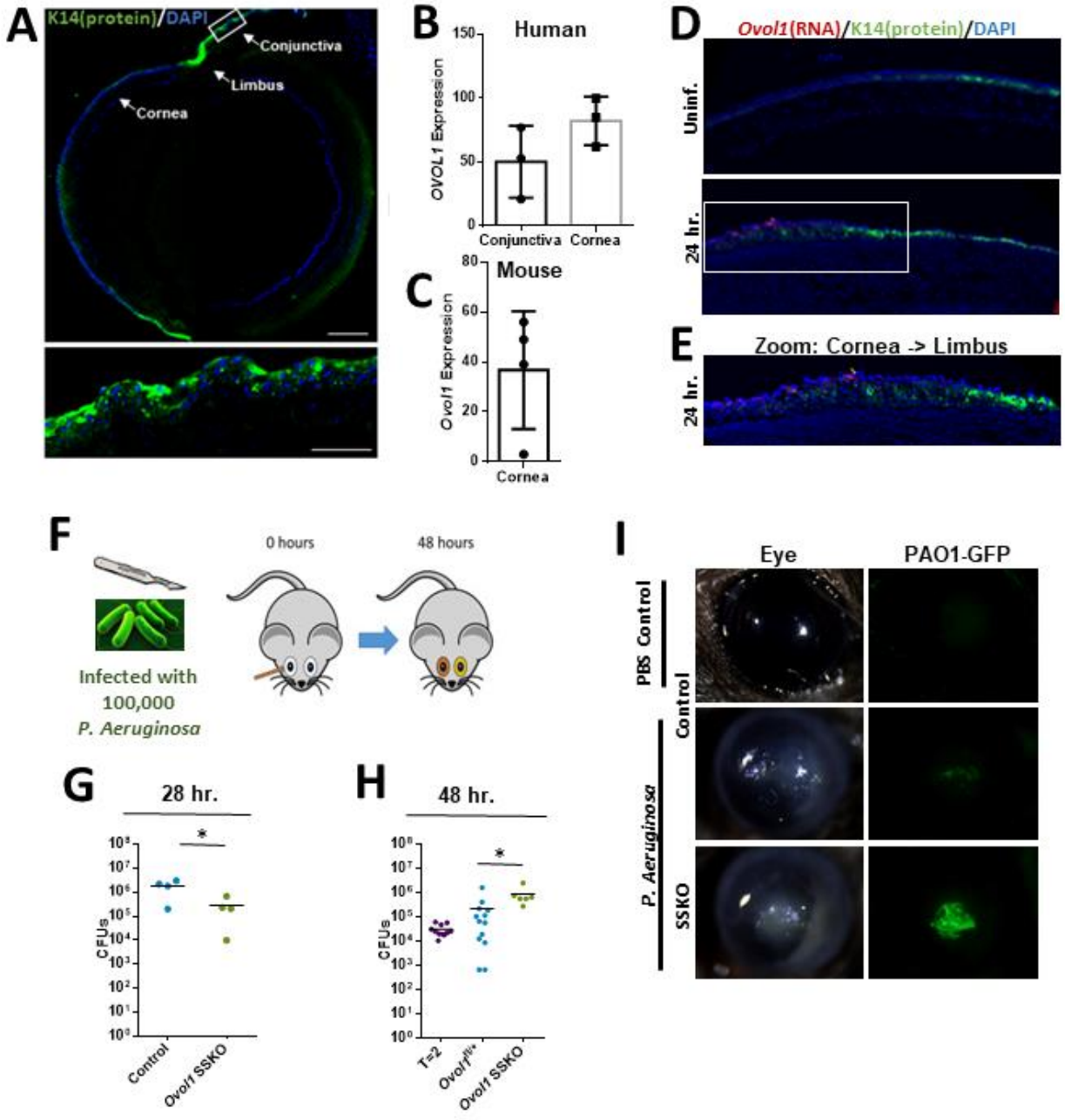
A
K14(protein)/DAPI
Conjunctiva
Limbus
Cornea
B
Human
OVOL1 Expression
Conjunctiva
Cornea
C
Mouse
Ovol1 Expression
Cornea
D
Ovol1(RNA)/K14(protein)/DAPI
Uninf.
24 hr.
E
Zoom: Cornea -> Limbus
24 hr.
F
0 hours
48 hours
Infected with
100,000
P. Aeruginosa
G
28 hr.
CFUs
Control
Ovol1 SSKO
H
48 hr.
CFUs
T=2
Ovol1fl/+
Ovol1 SSKO
I
Eye
PAO1-GFP
PBS Control
Control
P. Aeruginosa
SSKO

References:

Blackburn, B., Jenkins, M., Rollins, A., & Dupps, W. A Review of Structural and Biomechanical Changes in the Cornea in Aging, Disease, and Photochemical Crosslinking. Frontiers in Bioengineering and Biotechnology. 2019 https://doi.org/10.3389/fbioe.2019.00066

Chung, D. D., Zhang, W., Jatavallabhula, K., Barrington, A., Jung, J., & Aldave, A. J. (2019). Alterations in GRHL2-OVOL2-ZEB1 axis and aberrant activation of Wnt signaling lead to altered gene transcription in posterior polymorphous corneal dystrophy. *Experimental eye research*, *188*, 107696. https://doi.org/10.1016/j.exer.2019.107696

Dragan, M., Sun, P., Chen, Z., Ma, X., Vu, R., Shi, Y., Villalta, S. A., & Dai, X. (2021). Epidermis-Intrinsic Transcription Factor Ovol1 Coordinately Regulates Barrier Maintenance and Neutrophil Accumulation in Psoriasis-Like Inflammation. *The Journal of investigative dermatology*, S0022-202X(21)02089-3. Advance online publication. https://doi.org/10.1016/j.jid.2021.08.397

Kitazawa, K., Hikichi, T., Nakamura, T., Mitsunaga, K., Tanaka, A., Nakamura, M., Yamakawa, T., Furukawa, S., Takasaka, M., Goshima, N., Watanabe, A., Okita, K., Kawasaki, S., Ueno, M., Kinoshita, S., & Masui, S. (2016). OVOL2 Maintains the Transcriptional Program of Human Corneal Epithelium by Suppressing Epithelial-to-Mesenchymal Transition. *Cell reports*, *15*(6), 1359–1368. https://doi.org/10.1016/j.celrep.2016.04.020

Lee, B., Villarreal-Ponce, A., Fallahi, M., Ovadia, J., Sun, P., Yu, Q. C., Ito, S., Sinha, S., Nie, Q., & Dai, X. (2014). Transcriptional mechanisms link epithelial plasticity to adhesion and differentiation of epidermal progenitor cells. Developmental cell, 29(1), 47–58. https://doi.org/10.1016/j.devcel.2014.03.005

Movahedan, A., Afsharkhamseh, N., Sagha, H. M., Shah, J. R., Milani, B. Y., Milani, F. Y., Logothetis, H. D., Chan, C. C., & Djalilian, A. R. (2013). Loss of Notch1 disrupts the barrier repair in the corneal epithelium. *PloS one*, *8*(7), e69113. https://doi.org/10.1371/journal.pone.0069113

Nair, M., Teng, A., Bilanchone, V., Agrawal, A., Li, B., & Dai, X. (2006). Ovol1 regulates the growth arrest of embryonic epidermal progenitor cells and represses c-myc transcription. *The Journal of cell biology*, *173*(2), 253–264. https://doi.org/10.1083/jcb.200508196

Park, M., Richardson, A., Pandzic, E., Lobo, E. P., Whan, R., Watson, S. L., Lyons, J. G., Wakefield, D., & Di Girolamo, N. (2019). Visualizing the Contribution of Keratin-14+ Limbal Epithelial Precursors in Corneal Wound Healing. *Stem cell reports*, *12*(1), 14–28. https://doi.org/10.1016/j.stemcr.2018.11.014

Ratitong B, Pearlman E. Pathogenic Aspergillus and Fusarium as important causes of blinding corneal infections - the role of neutrophils in fungal killing, tissue damage and cytokine production. Curr Opin Microbiol. 2021 Oct;63:195-203. doi: 10.1016/j.mib.2021.07.018. Epub 2021 Aug 19. PMID: 34419783.

Sun, P., Vu, R., Dragan, M., Haensel, D., Gutierrez, G., Nguyen, Q., Greenberg, E., Chen, Z., Wu, J., Atwood, S., Pearlman, E., Shi, Y., Han, W., Kessenbrock, K., & Dai, X. (2021). OVOL1

Regulates Psoriasis-Like Skin Inflammation and Epidermal Hyperplasia. *The Journal of investigative dermatology*, *141*(6), 1542–1552. https://doi.org/10.1016/j.jid.2020.10.025

Yu, Q., Biswas, S., Ma, G., Zhao, P., Li, B., & Li, J. (2021). Canonical NF-κB signaling maintains corneal epithelial integrity and prevents corneal aging via retinoic acid. eLife, 10, e67315. https://doi.org/10.7554/eLife.67315